INFORMATION TO USERS

This manuscript has been reproduced from the microfilm master. UMI films the text directly from the original or copy submitted. Thus, some thesis and dissertation copies are in typewriter face, while others may be from any type of computer printer.

The quality of this reproduction is dependent upon the quality of the copy submitted. Broken or indistinct print, colored or poor quality illustrations and photographs, print bleedthrough, substandard margins, and improper alignment can adversely affect reproduction.

In the unlikely event that the author did not send UMI a complete manuscript and there are missing pages, these will be noted. Also, if unauthorized copyright material had to be removed, a note will indicate the deletion.

Oversize materials (e.g., maps, drawings, charts) are reproduced by sectioning the original, beginning at the upper left-hand corner and continuing from left to right in equal sections with small overlaps.

ProQuest Information and Learning
300 North Zeeb Road, Ann Arbor, MI 48106-1346 USA
800-521-0600

Development and application of thermal vaporization sample introduction techniques with demountable sample supports for inductively coupled plasma spectrometry

Michael E. Rybak

A thesis submitted to
the Faculty of Graduate Studies and Research
in partial fulfillment of
the requirements of the degree
Doctor of Philosophy

October, 2000

Department of Chemistry
McGill University
Montréal, Québec, Canada

To my parents, Edward and Jean,
for their encouragement and support,
and to my wife, Adrienne,
whose love will forever be my inspiration.

Foreword

The following text has been reproduced from the "Guidelines for Thesis Preparation", Faculty of Graduate Studies and Research, McGill University, and is included in order to inform the external reader of Faculty Regulations:

> *As an alternative to the traditional thesis format, the dissertation can consist of a collection of papers that have a cohesive, unitary character making them a report of a single program of research. The structure for the manuscript-based thesis must conform to the following:*
>
> *Candidates have the option of including, as part of the thesis, the text of one or more papers submitted, or to be submitted, for publication, or the clearly-duplicated text (not the reprints) of one or more published papers. These texts must conform to the "Guidelines for Thesis Preparation" with respect to font size, line spacing and margin sizes and must be bound together as an integral part of the thesis. (Reprints of published papers can be included in the appendices at the end of the thesis.)*
>
> *The thesis must be more than a collection of manuscripts. All components must be integrated into a cohesive unit with a logical progression from one chapter to the next. In order to ensure that the thesis*

has continuity, connecting texts that provide logical bridges between the different papers are mandatory.

The thesis must conform to all other requirements of the "Guidelines for Thesis Preparation" in addition to the manuscripts. The thesis must include the following: (a) a table of contents; (b) an abstract in English and French; (c) an introduction which clearly states the rational and objectives of the research; (d) a comprehensive review of the literature (in addition to that covered in the introduction to each paper); (e) a final conclusion and summary.

As manuscripts for publication are frequently very concise documents, where appropriate, additional material must be provided (e.g., in appendices) in sufficient detail to allow a clear and precise judgement to be made of the importance and originality of the research reported in the thesis.

In general, when co-authored papers are included in a thesis the candidate must have made a substantial contribution to all papers included in the thesis. In addition, the candidate is required to make an explicit statement in the thesis as to who contributed to such work and to what extent. This statement should appear in a single section entitled "Contributions of Authors" as a preface to the thesis. The supervisor must attest to the accuracy of this statement at the doctoral oral defense. Since the task of the examiners is made more difficult in these cases, it is in the

candidate's interest to clearly specify the responsibilities of all the authors of the co-authored papers.

Abstract

Novel approaches to thermal vaporization sample introduction for inductively coupled plasma (ICP) spectrometry using techniques with demountable sample supports are presented and compared. Developments and applications are presented for two sample introduction arrangements that use interchangeable sample probes in contact-free heating environments: direct sample insertion (DSI), and induction heating–electrothermal vaporization (IH–ETV). For the well-established technique of DSI, studies focused on the development and application of a pyrolytically coated graphite sample support, a feature common to conventional ETV systems. A process for coating sample probes in the ICP discharge was developed, and improvements were seen in both the reproducibility of the volatilization event and the appearance of the transient emission signals with ICP–optical emission spectrometry (OES) when a coated probe was used over an uncoated one. The pyrolytically coated sample probe was successfully used for the direct determination of several metals in wood pulps by ICP–OES, and was found not only to improve the appearance of the temporal signals, but also demonstrated a heightened resistance to chemical attack. For the prototypical IH–ETV system, a general study was first conducted to establish performance attributes and benchmarks such as heating characteristics, transport efficiency, and ICP–OES detection limits using several mixed carrier gases. The IH–ETV arrangement was found to be capable of rapid heating rates and precise, reproducible temperature control suitable for a thermal vaporization sample introduction technique. Of all the gas mixtures studied, the incorporation of 15% (v/v) SF_6 into the Ar carrier flow resulted in the best overall conditions for the vaporization, transport and detection of analytes by ICP–OES. These conditions were

successfully used for the determination of various metals in soil and sediment samples by ICP-OES using IH–ETV sample introduction. Additionally, a novel arrangement that uses gas sampling bags for trapping and dissoluting analyte was developed and validated for the purposes of determining IH–ETV transport efficiency. This closed-system trapping method, which can be used with any ETV system, generally performed as well as the reference method and was simpler to carry out. Based on the examination and comparison of the above experiences with DSI and IH–ETV, the utility of demountable sample support arrangements for thermal sample introduction are evaluated and recommendations for future instrumentation and methodologies are made.

Résumé

De nouvelles approches d'introduction d'échantillons par vaporisation thermique pour la spectroscopie avec un plasma à couplage inductif (ICP) employant des techniques avec supports d'échantillons démontables sont présentées et comparées. Des progrès et applications sont décrits pour deux dispositifs d'insertion d'échantillons qui utilisent des sondes d'échantillons interchangeables dans des environnements de chauffage sans contact: insertion d'échantillon directe (DSI) et chauffage inductif–vaporisation électrothermique (IH-ETV). Pour la méthode bien établie de DSI, les études ont misé concentrées sur le développement et l'application d'un support de graphite traité pyrolytiquement (par pyrolyse), un trait commun des systèmes ETV. Une méthode pour traiter les sondes d'échantillons dans la décharge de l'ICP fut développée, et des améliorations furent observées dans la reproductibilité de l'évènement de volatilisation et dans l'apparence de signaux d'émission transitoires avec un plasma couplé à un spectromètre d'émission optique (ICP-OES) lorsqu'une sonde traitée plutôt que non-traitée fut employée. La sonde traitée pyrolitiquement fut utilisée avec succès pour déterminer directement plusieurs métaux dans la pâte à papier par ICP-OES. Cette sonde montra une résistance accrue envers une attaque chimique en plus d'améliorer l'apparence des signaux temporels. Pour le système prototype d'IH-ETV, une étude générale a d'abord été effectuée pour établir ses performances et paramètres de base tels que les caractéristiques de chauffage, l'efficacité de transport et limites de détection par ICP-OES employant plusieurs mélanges de gaz porteurs. Il a été démontré que le dispositif IH-ETV pouvait être chauffé rapidement et que sa température pouvait être contrôlée d'une manière précise et reproductible, favorisant une méthode d'insertion d'échantillon par

vaporisation thermique. Parmi les mélanges étudiés, l'incorporation de 15% (v/v) de SF_6 dans le courant de gaz porteur Ar donna les meilleures conditions générales de vaporisation, de transport et de détection d'analytes par ICP-OES. Ces conditions furent utilisées avec succès pour déterminer divers métaux dans des échantillons de terre et de sédiment par ICP-OES employant l'insertion d'échantillon par IH-ETV. Par ailleurs, un nouveau dispositif utilisant des sacs d'échantillonnage de gaz pour piéger et dissoudre l'analyte a été développé et validé pour la détermination de l'efficacité de transport par IH-ETV. Cette méthode de piégeage dans un système fermé, qui peut être utilisée par tous les systèmes ETV, est équivalente à la méthode de référence, et est plus facile à exécuter. En examinant et comparant les expériences ci-dessus avec DSI et IH-ETV, l'utilité du dispositif de support d'échantillon démontable pour l'introduction thermique d'échantillons est évaluée et des recommandations pour instruments futurs et méthodologies sont présentées.

Contributions to original knowledge

1. A process for generating pyrolytically coated graphite DSI sample supports in an ICP discharge was demonstrated. The pyrolytic coating was shown to improve the appearance and reproducibility of transient emission signals obtained with ICP–OES, and to reduce the rate at which the graphite was damaged by chemical attack.

2. A method for the direct determination of metals in wood pulp samples using DSI–ICP–OES was developed and demonstrated. Major constituents (Mg, Mn) were determined quantitatively and minor constituents (Cu, Fe, Zn) semi-quantitatively with liquid external standards. Poor precision was observed in some cases, but was improved by homogenizing the pulp samples through air fluffing.

3. An ETV system that uses a demountable sample support in an induction heating arrangement was evaluated as a means of ICP sample introduction. The heating of the vaporization surface was sufficiently rapid and could be adequately controlled by induction heating. The incorporation of SF_6 into the argon atmosphere of the IH–ETV was found to improve the vaporization, transport and detection of analytes by ICP–OES, as well as prevent electrical discharging around the sample support due to the induction field.

4. A method for the direct determination of metals in soils and sediments using IH–ETV–ICP–OES was developed and demonstrated. Elements were determined quantitatively both by aqueous standard additions and by external standardization with certified reference materials.

5. A method that uses gas-sampling bags to trap and dissolve analyte in a single step was developed and validated for the determination of transport efficiency for any ETV system. The method is immediately applicable to ETV–ICP–OES systems based on its detection limits; incorporation of a preconcentration step can extend its use to ETV–ICP–MS.

Contributions of authors

The experiments described in **Chapter 2** and **Chapters 4–6** were conceived, designed, conducted and interpreted by the author under the direction and guidance of Prof. Eric Salin of McGill University. The work described in **Chapters 2 and 6** has been published and appears as the following respective manuscripts:

> "Pyrolytically coated graphite direct sample insertion probe for inductively coupled plasma spectrometry", Michael E. Rybak and Eric D. Salin, *Journal of Analytical Atomic Spectrometry*, 1998, **13**, 707.
>
> "Closed-system trapping method for the direct determination of transport efficiency in electrothermal vaporization sample introduction", Michael E. Rybak and Eric D. Salin, *Journal of Analytical Atomic Spectrometry*, 2000, **15**, 883.

At the time of the final thesis deposition, the work that appears in **Chapters 4 and 5** has been submitted for publication in the serials *Spectrochimica Acta Part B: Atomic Spectroscopy* and *Applied Spectroscopy*, respectively.

Experiments described in **Chapter 3** involved the collaboration of the author and Prof.. Salin with Dr. Kevin Thurbide, then a researcher at the Pulp and Paper Research Centre of McGill University, and Panos Hatsis, a summer student under his direction. Experiments described in Chapter 3 were conceived and designed by the author and carried out either by Mr. Hatsis under the immediate supervision of the author, or by the author himself. Prof. Salin and Dr. Thurbide were available throughout the experiments and contributed helpful discussion and guidance related to their respective areas of

expertise. The contents of this chapter have been published and appear as the following manuscript:

> "Rapid determination of Cu, Fe, Mg, Mn and Zn in wood pulp by direct sample insertion–inductively coupled plasma–optical emission spectrometry using a pyrolytically coated graphite sample probe", Michael E. Rybak, Panos Hatsis, Kevin Thurbide, and Eric D. Salin, *Journal of Analytical Atomic Spectrometry*, 1999, **14**, 1715.

All co-authors and publishers of the aforementioned manuscripts have granted release of copyright for their reproduction in this thesis.

Acknowledgements

I am indebted to many people for their significant contributions over the course of my studies at McGill, and I would like to extend my sincerest thanks to the following:

- to Eric Salin, my research supervisor, for his helpful advice and guidance, as well as his thoughtful encouragement and much-appreciated patience throughout my tenure as a member of his laboratory;
- to Doug Goltz and Cameron Skinner, who, by selflessly offering their time in the laboratory, helped me rapidly acquire much of the initial knowledge and expertise that I needed to successfully carry out my research;
- to Kevin Thurbide, for the opportunity to perform collaborative research with the Pulp and Paper Research Centre at McGill University; and to Panos Hatsis, who was not only a resourceful and hard-working summer student, but also a good friend;
- to Bill Bastien and Alfred Kluck (machining), Rick Rossi (electronics) and Georges Kopp (glassblowing) of the Department of Chemistry, whose respective services and expertise proved invaluable in materializing the instrumentation used in my research;
- to Fonds pour la Formation de Chercherus et l'Aide à la Recherche (FCAR) for scholarship support;
- to all my friends in the department, to whom I wish the best of success in their future endeavors;
- and to my loving parents, Edward and Jean, and my beautiful wife, Adrienne, whose unwavering support, encouragement and love are the three reasons why these very words can be read today.

Table of contents

List of tables

List of figures

Chapter 1

General introduction and literature review

One of the most basic missions encountered in analytical chemistry is the determination of elemental composition. The elemental composition of a sample is often an essential piece of information in assessing its impact on processes ranging from those that naturally occur in the environment to the most advanced activities found in industry. From the need to ensure the quality of the materials used in the manufacturing of high-performance semiconductors, ceramics and alloys, to the need to ensure the quality of our soil, water and air for our well-being and that of the planet; the world has never been in greater demand of sensitive, precise, and accurate methods of elemental analysis that are both practical and cost-effective. A great portion of this need is currently being met by using techniques that are based on the inductively coupled plasma (ICP). The ICP is an atmospheric pressure partially ionized gas discharge that can be used to break down sample matrices, dissociate molecular species, and provide sufficient energy to electronically excite and ionize the incipient free atoms. These excitation and ionization processes are usually incorporated into one of two spectrochemical encoding schemes: emission resulting from electronic excitation processes can be used for the purposes of atomic optical emission spectrometry (OES); or the ion population can be sampled as an ion source for atomic mass spectrometry (MS).

With the ability to excite and ionize a great number of elements in a relatively inert environment, the ICP presents itself as somewhat of a panacea for elemental determinations.[1] Practically every naturally occurring element of the periodic table has been detected, monitored or determined in some capacity using ICP–OES or ICP–MS, and at least 70 of these elements can be accurately quantified with either technique on a routine basis. The ranges of detection for ICP–OES and ICP–MS are also complementary, with the former serving the role for major, minor and trace constituent determinations, and the latter answering the call to the trace and micro-trace level. Improved instrumentation begets improved analyses, and steady advances in optical, electronic, mechanical and computer engineering have lead to the development of ICP–OES and ICP–MS instruments that are not only increasingly powerful in terms of the quality and quantity of information they can gather, but are also increasingly simple to use.[2]

In spite of all the qualities that the ICP possesses and regardless of advances that can be made in instrumentation, one of the oldest adages of analytical chemistry will always remain true: the analysis can only be as good as the sample.[3] The scope of this maxim is prodigious, and includes not only preparative actions such as sample procurement and physical/chemical pretreatment, but also transferential actions such as the introduction of the sample to the instrument. Often overlooked, the means by which the sample is transferred to the spectrochemical encoding process will unquestionably have a direct bearing on the overall performance of the technique. To ensure that an instrumental technique is realizing its full potential, its sample introduction system should be a simple, robust interface that is capable of delivering a representative portion of the sample to the encoding process in an efficient and reproducible manner with minimal

system perturbation and interference introduction. This may seem straightforward enough; however, a mutual exclusivity often exists amongst these qualities with many sample introduction arrangements.[3] A classic example of this occurs with the most common method of sample introduction for ICPs—pneumatic nebulization. It is a convenient technique that is capable of excellent precision (typically 1% relative standard deviation (RSD)) for steady-state sample introduction, but the aerosol discriminating processes that are necessary to achieve such precision result in a net sample introduction efficiency of only about 1%.

Realities such as this have led to the proliferation of numerous alternate sample introduction techniques for the ICP. These techniques, which are based on a variety of ablation, nebulization and vaporization mechanisms, all essentially have the same goal: to strike a compromise that best suits the needs of the analyst. Thermal vaporization methods, which are the focus of this study, comprise one such category of alternate sample introduction techniques. In broad terms, thermal vaporization refers to any technique in which a heated sample support is used to vaporize analytes into a cloud of atoms and molecules that can then be introduced into the plasma. Sample introduction techniques based on thermal vaporization phenomena are generally known and appreciated for their versatility, as they can readily handle both solids and liquid samples, are able to separate and speciate analytes by differential volatilization, and have minimal sample aliquot requirements.

The goal of this study was to develop and apply thermal vaporization techniques in which the sample support was rapidly demountable and interchangeable, and from these experiences, determine the value of such a feature from an experimental standpoint along with which thermal vaporization technique would be the best approach for

achieving this. The literature review that follows serves as an introduction to the ICP and its spectrometric applications, and presents a general survey of the common sample introduction techniques that have been used with ICP-based spectrometry, with greater detail being paid to thermal sample introduction. While certainly not comprehensive, an effort has been made to highlight seminal achievements and present general reviews wherever possible.

1.1 Inductively coupled plasmas

Although the first attempts at using ICPs as energy sources for atomic spectroscopy/ spectrometry were made in the mid 1960s,[4,5] the origins of the ICP can be traced back to the turn of the 20th century, when pioneering efforts were made at generating plasma discharges by inductively heating gases under low pressure.[6,7,8] It was not until 1947, however, that a closed, atmospheric pressure plasma generated by radio-frequency (RF) induction heating was described,[9] and only in 1961 did the closest precursor to the ICP—an open torch, atmospheric pressure, flowing gas plasma for the purposes of growing crystals—appear in the literature.[10,11] It was this design that was first used by Greenfield *et al.* for spectrochemical purposes,[4] and although subsequent torch and coil design modifications were made by both Greenfield[12,13] and Fassel,[14,15] the current design for conventional ICP instrumentation has remained essentially unchanged from that proposed 25 years ago by Fassel.[16]

An ICP system consists of two basic components: a load coil connected to an RF-generator and a quartz torch. The generator is typically a variable power (1–3 kW maximum) oscillator that produces an alternating current at a nominal frequency of either 27.12 or 40.68 MHz and is attached to a copper, water-cooled, 3-turn load coil. The

torch, which is encircled at its uppermost portion by the load coil, is comprised of three concentric quartz tubes of which the outermost two facilitate the introduction of argon in a series of different flows to support the plasma discharge. The innermost tube serves as a means of introducing analyte into the center of the ICP as either a vapor or an aerosol entrained in an argon flow. When an RF-current is applied to the load coil, an oscillating magnetic field results that is aligned axially inside the torch and encircles the turns of the load coil in an elliptical path. By "seeding" the argon with electrons from a spark discharge, the alternating magnetic field can induce an annular Eddy current in the argon flow of the torch. As these electrons are accelerated in the Eddy current, inelastic collisions with argon atoms occur, resulting in collisional ionization. The liberated electrons and incipient argon ions from the collisional ionization process will now be accelerated in the Eddy current and additional collisions and ionization occurs. A cascade effect continues until the rate at which electrons are being ejected from the argon atoms equal the rate at which recombination occurs, at which point a stable, annular ICP discharge is formed.

The atmospheric pressure Ar–ICP possesses many of the characteristics that are desirable in an energy source for atomic spectrometry. The toroidal shape of the ICP discharge provides a natural channel of low resistance through which sample can be introduced, and allows for a relatively long analyte residence time in the plasma (2–3 ms). Combined with relatively high gas temperatures (4500–8000 K) and electron temperatures (8000–10000K), the argon ICP provides highly efficient vaporization, atomization, excitation and ionization capabilities when compared to other atomic spectrometry energy sources such as combustion flames.[17] Once free atoms and ions are formed, they are in an environment that is chemically inert, and the relatively high

electron number density of the plasma ($1–3 \times 10^{15}$ cm^{-3}) ensures that ionization effects are minimal.[18] The plasma, however, is a dynamic gaseous environment that is not in chemical or physical equilibrium, but for the better part does meet the requirements of local thermodynamic equilibrium (LTE)[19,20]

The atmospheric pressure argon ICP is the most common type of ICP discharge used as an excitation source for atomic optical emission spectrometry (OES) or as an ionization source for atomic mass spectrometry (MS). There do exist variants of the ICP that, although not as widely used, have found some use unique applications. These include reduced pressure ICPs which can be used as tuneable ion sources for ICP–MS that are capable of generating both atomic and molecular ions,[21,22] and helium–ICPs for determining halogens and chalcogens by OES[23] or MS.[24,25]

1.2 Spectrometric methods

1.2.1 Optical emission spectrometry

The ICP was first used as an excitation source for emission spectrometry,[4,5] and since the appearance of the first commercial instruments in the mid-1970s, ICP–OES has developed into the predominant tool for elemental analyses. The ICP–OES technique is based on the simple premise that electronically excited ions or atoms will emit light of characteristic wavelengths upon relaxation and that the intensity of the light observed is proportional to the ion or atom concentration. Radiation emitted from this process in the plasma is collected by a solid angle optical element and focused onto the entrance aperture of a spectrometer. Inside the spectrometer, a high-resolution diffraction grating is used to spatially separate the analyte emission lines, of which a narrow spectral bandpass is focused onto a detector.

Common spectrometer arrangements used in ICP–OES include scanning arrangements, such as the Czerny-Turner or Ebert mounting with a planar diffraction grating; and direct reading arrangements such as the Pachen-Runge mounting on a Rowland circle with a concave grating, or the Czerny-Turner type mount with an echelle grating and a cross dispersion element. All have multi-element (*i.e.*, multi-wavelength) capabilities, however, only the Pachen-Runge and echelle spectrometers are capable of simultaneous multi-element determinations. Detection in modern ICP–OES instruments has been achieved in the past predominantly by the use of photomultiplier tubes (PMTs); however, the rapid recent development of array-based charge-transfer devices (CTDs) such as charge-coupled devices (CCDs) and charge-injection devices (CIDs) has led to their recent proliferation in ICP–OES instruments.[26] This is especially true in echelle-based ICP–OES arrangements, due to the natural compatibility of the two-dimensional image generated by these systems with the two-dimensional pixel arrangement of a CTD array.

Some of the attributes that make ICP–OES an attractive technique include the ability to monitor multiple wavelengths simultaneously and limits of detection (LODs) that are of the ng ml^{-1} range (when using solution nebulization). Difficulties encountered in ICP–OES are mostly of spectroscopic origin, the most significant being spectral overlap from atomic lines and molecular band species,[27] fluctuations in the background continuum emission due to the sample matrix and stray light contributions.[28] Although optical arrangements for ICP–OES have traditionally viewed the emission region radially (*i.e.*, side on), recent attention has been paid to the concept of axial viewing (*i.e.* downward).[29,30] The greater signal-to-background ratio (SBR) that results from viewing the plasma axially through the relatively "dark" center of the annulus results in detection

limits that are typically 3–10 × lower.[31] Axial viewing is more prone to matrix effects (*i.e.*, spurious signal enhancements or suppressions that are chemically or physically induced by sample concomitants) originating in the tail of the plasma discharge, and necessitates the use of a "shear gas" flow to skim off this region.

Besides OES, other optical spectrometric schemes, such as atomic fluorescence spectrometry (AFS)[32,33] and atomic absorption spectrometry (AAS)[34,35,36] have been coupled with ICP excitation. Although the ICP–AFS and ICP–AAS techniques do show better spectral selectivity over ICP–OES, their relatively poor analyte sensitivities and/or lack of multi-element analysis capabilities have limited their widespread use.

1.2.2 Mass spectrometry

The concept of using an ICP as an ion source can be traced back to studies from the 1960s and 1970s in which atmospheric pressure flames were sampled into quadrupole mass spectrometers.[37] The concept of using a plasma as an ion source was first explored by Gray in the mid-1970s,[38,39] and in 1980 the first successful interfacing of an Ar–ICP to a mass spectrometer was accomplished.[40] From the pioneering work in ICP–MS done by groups in Canada,[41] the UK,[42,43] and the USA,[40,44] ICP–MS has quickly grown to become the most sensitive method for determining trace elements on a routine basis.

In ICP–MS, a portion of the ionic sample population generated in the ICP is extracted axially from the plasma environment into a mass spectrometer by means of two narrow cone orifices (ca. 1 mm dia. each) that lead into two increasingly higher vacuum regions (1–0.1 Torr and 10^{-5}–10^{-7} Torr, respectively). As the ions pass from the atmospheric pressure environment of the ICP through the sampling cone into the first vacuum region, a supersonic jet surrounded by a shock wave is formed.[45] The central

portion of this jet then passes through a skimmer cone into the second vacuum region, where a series of positively biased electrostatic lenses focus the positive ions into a beam before finally entering the mass analyzer. The most commonly used mass analyzer in ICP–MS is the linear quadrupole, due in part to its ease of use, rapid scanning capabilities and low manufacturing costs. On the downside, quadrupole-based ICP–MS systems are typically only capable of nominal mass resolution, frequently resulting in peak overlaps due to the many species generated in the plasma. Resolution of about 50000 has been achieved in ICP–MS by employing high-resolution double-focussing magnetic/electrostatic mass analyzers,[46] however, ion transmission, and consequentially, detection limits are poorer. Other mass analyzers that have been interfaced to ICP sources with their own unique merits include time-of-flight (TOF)[47] mass analyzers and multiple-collector[48,49] MS arrangements.

Compared with ICP–OES, ICP–MS demonstrates far better sensitivity with detection limits that are typically 2–3 orders of magnitude lower, has a far simpler spectrum with no fundamental background continuum, and is capable of isotopic determinations and isotope dilution analysis. Problems encountered with ICP–MS originate from two general categories of interferences: spectral overlaps due to atomic species present in the sample or molecular adducts that form in the interface region;[50,51] and coulombic repulsion matrix effects in the ion beam due to high concomitant levels.[52,53]

1.3 Nebulization

Probably the most simple and straightforward amongst the sample introduction techniques, nebulization is a concept that was translated directly into ICP spectrometry

from flame spectrometry. In spite of the fact that it may involve a time-consuming digestion/dissolution step, a sample in liquid form is attractive to the analyst. The liquid form is homogeneous, allows for quantitative additions and dilutions and can often be directly compared with liquid standards.

1.3.1 Pneumatic nebulization

Pneumatic nebulization is the most commonly used method of sample introduction in ICP spectrometry. Although many variants exist, pneumatic nebulizers can be broadly classified as either concentric or cross-flow types. Concentric nebulizers consist of a solution capillary surrounded by a gas annulus that draws the solution out and creates a nebulous stream *via* the Venturi effect.[54] Cross-flow arrangements use the same pressure reduction process to draw and nebulize the solution, however, they do so by using a solution capillary whose output intersects at a right-angle with a gas capillary.[55,56]

Pneumatic nebulizers by their nature generate a wide range of droplet sizes. The generation of relatively large (upwards of 100 μm dia.) droplets is undesirable, as they undergo inefficient/incomplete desolvation, volatilization and atomization processes in the plasma, in addition to exhibiting low transport efficiency. As a result, the arrangement for pneumatic nebulization sample introduction usually incorporates a spray chamber immediately after the nebulizer.[57] A spray chamber is a cavity that is designed to act as a size discrimination device, allowing only fine droplets (< 10 μm dia.) from the aerosol to reach the plasma. Two of the most common designs used are the Scott spray chamber,[58] which uses a double-pass barrel-like structure to remove large aerosol droplets by deposition on the spray chamber walls; or a cyclonic/conical spray chamber,[59] which

produces a fine aerosol by using a tangential inlet to generate a mixture of centrifugal and collisional effects in a conical cavity.

The performance of concentric and cross-flow nebulizers are quite similar, with the cross-flow being less prone to clogging from samples containing high amounts of dissolved solids, and the concentric exhibiting slightly better transport efficiency.[60,61] Similar performance is also seen with Scott and cyclonic/conical spray chambers, with the latter typically exhibiting slightly higher transport efficiency at the cost of a slightly coarser aerosol.[62] In general, precision on the order of 1% RSD and sample transport efficiency on the order of 1% has been observed with most conventional nebulizer/spray chamber combinations.[60]

In addition to the traditional concentric and cross-flow types, a variety of specialized pneumatic nebulizers have been developed to meet particular analysis needs. Variations of the cross-flow type nebulizer, such as the V-groove, Babington, Légère,[63] and Hildebrand (grid)[64] nebulizers have been designed to accommodate solutions with high amounts of dissolved solids or slurries[65,66] that would normally present clogging problems with conventional concentric and cross-flow nebulizers. The intefacing of techniques such as high-performance liquid chromatography (HPLC), capillary electrophoresis (CE) and flow injection analysis (FIA) with ICP–OES and ICP–MS has been improved by the development of low sample consumption nebulizers. These include: direct injection nebulizers (DINs);[67] high-efficiency nebulizers (HENs)[68] and direct injection HENs (DIHENs), microconcentric nebulizer (MCNs), oscillating capillary nebulizers (OCNs), jet-impact[69] and glass frit nebulizers.[70] The DIN and DIHEN are of particular interest as their configuration replaces the injector tube of the ICP torch with the nebulizer itself, eliminating the need for a spray chamber.

1.3.2 Ultrasonic nebulization

One of the problems with pneumatic nebulization is that the aerosol formation process is directly dependent on the nebulizer gas flow rate, which can lead to compromises in nebulization efficiency arising from the need to satisfy flow rate requirements in the ICP. This has lead to the development of aerosol generating techniques, such as ultrasonic nebulization (USN), that do not rely on pneumatic phenomena for aerosol generation. In USN, a sample is usually delivered *via* a capillary onto a surface coupled to a piezoelectric transducer. The high frequency oscillations (typically 1–1.5 MHz) of the transducer generate a series of waves on the solution surface leading to the ejection of aerosol droplets. The piezoelectrically-coupled surface can either be positioned horizontally in a vertical spray chamber,[5] or, as is more commonly the case, vertically in a horizontal spray chamber.[71,72] The advantage of the latter is that excess solution delivered to the nebulizing surface flows off the piezoelectrically-coupled plate into the bottom of the spray chamber and is eventually drained.

In addition to having an aerosol forming process that is independent of nebulizer gas flow, USN generates smaller droplets on average when compared to conventional pneumatic nebulization. Sample transport efficiency is also considerably better (10–20%) at relatively high flow rates (1–3 ml min^{-1}),[73] and detection limits are usually a factor of 10–20 lower.[72] As a consequence of the high sample transport realized, solvent transport is also high, necessitating the incorporation of a desolvation apparatus downstream from the USN spray-chamber so as to prevent excessive plasma loading and cooling. Ultrasonic nebulization typically has problems with samples that are either viscous or have high amounts of dissolved solids[72] and relatively long washout times.

1.4 Ablation

The development of the ICP into a source for atomic spectrometry was largely facilitated by the use of nebulization for sample introduction, resulting in the accruement of ICP–OES and ICP–MS into techniques that are bent towards the analysis of liquids; however, a vast majority of the samples whose composition can be determined by ICP–spectrometry occur as solids, not liquids. Slurry nebulization[65,66] does present a strategy by which solids can be introduced into ICPs with modified nebulization arrangements, but requires a uniform distribution of small particles and may not be appropriate for all samples. This has necessitated the development of digestion and dissolution procedures that use acids, bases and oxidizing agents,[74] and fusions and sinters[75] in the case of geological samples. These digestion techniques are well characterized and widely used, and the advent of microwave-assisted digestion methods[76] has improved the ease and reliability with which they can be conducted and reduced concerns regarding contamination. The conversion of a solid sample to liquid format, however, does present an inconvenience (increased handling and time requirements), provides the potential for error and inevitably result in sample dilution. This has led to the development of ICP sample introduction techniques that allow solid samples to be introduced without the need for digestion and/or dissolution.

One such means of directly introducing solids is by ablation. The word "ablation" is of Latin origin, and refers to the action of 'carrying away', with no inference of the mechanism by which the process occurs. In general, ablation sample introduction techniques rely on a focused external force to erode a solid sample at a specific point. This process creates a plume of vaporized material and particles, which is then entrained

into a gaseous flow and introduced into the ICP. Forces that are most commonly used to impart ablation are either radiative (laser ablation) or electrical (arc/spark ablation).

1.4.1 Laser ablation

In laser ablation (LA), a laser equipped with a series of positioning and focusing optics is directed at a sample on a translational platform inside a quartz-windowed chamber equipped with an inlet for the carrier gas flow and an outlet for transport of the ablation plume to the ICP. Typically, an energy density $\geq 10^7$ W cm^{-2} is developed by the laser at the sample surface on a spot size of 10–20 μm in diameter is used to impart ablation. The optics of the LA system usually incorporate some type of ocular device, such as a binocular microscope or a CCD camera and monitor, through which the spatial aspect of the LA sampling process can be monitored and controlled. Types of lasers used in LA include ruby, Nd:YAG, excimer, CO_2, and nitrogen lasers, with the frequency-quadrupled (266 nm) Nd:YAG laser being the most widely used source at present. Laser ablation was first coupled as a solid sample introduction technique with ICP–OES,[77,78] however, the majority of LA studies at present are presently conducted with ICP–MS.[79]

Lasers, depending on the power and wavelength used, have the ability to ablatively sample a wide variety of materials, irrespective of their organic or inorganic nature, electrically conductive or insulative properties, or whether they are presented in a solid or powdered form. With the ability to focus the laser beam on a relatively small spot size, small, localized areas of a sample can be analyzed, allowing for spatially resolved determinations. Sample preparation is minimal, which has the added effect of reducing interferences when LA is paired with ICP–MS. The main difficulty in LA is how to calibrate for the purposes of quantitaion. The only truly reliable way in which this

can be done is by sampling matrix-matched standard reference materials (SRMs). Internal standardization is also frequently needed in LA[77,80,81] to compensate for variations in laser output between shots and transport losses, which necessitates the identification of a homogeneously-distributed constituent that would be suitable for this purpose in a naturally-occurring sample. A "solid–liquid" calibration methodology for LA,[82] in which the flow from the ablation chamber and a solution nebulization arrangement for standard introduction are combined prior to entry into the ICP, has been reported. It has, however, several drawbacks, such as re-introducing polyatomic oxide interferences in ICP–MS that would not be present with LA alone and a decrease in analyte sensitivity due to dilution in the gas flow.[83]

1.4.2 Arc/Spark ablation

Less prevalent as a solid sampling technique when compared to laser ablation, arc ablation and spark ablation (SA) work on a similar principle of particle and vapor plume generation, except that a high-energy electrical discharge is used for purposes vaporizing, sputtering and eroding the sample.

The apparatuses used for spark ablation sample introduction are based on that developed for the purposes of spark–OES.[84] In SA–ICP–OES[85] and SA–ICP–MS,[86,87] an intermittent (1μs–1ms), high-voltage (1–10 kV) low-current (1–10 mA) discharge is formed between a tungsten-tipped electrode and a sample grounded to a Petrey table. In contrast, arc–ICP–OES[88] and arc–ICP–MS[89] uses a continuous (on the order of minutes), high direct current (~10 A) low voltage (10–50 V) discharge that is formed between the cathodic, grounded sample, and a hollow anode that is flushed with argon. In both cases,

the material ablated from the sample is entrained in the argon flow and is carried into either an ICP–OES or ICP–MS.

The strongest asset that arc/spark ablation has when compared to LA is that the matrix from which the analyte is sampled has little if any effect on the sensitivity (*i.e.*, slope of the calibration curve) observed,[88] greatly reducing the need for exact matrix matching. By having to rely on an electrical discharge for ablation, however, arc and spark ablation can only be performed on samples which are either electrically conductive unless a conductive modifier is added. Furthermore, it is not possible to perform highly spatially resolved analyses like those possible with LA, limiting the technique to the analysis of homogeneous materials.

1.5 Vaporization

1.5.1 Chemical vaporization

Chemical vaporization refers to a class of sample introduction techniques in which a volatile form of the analyte is generated by means of a chemical reaction and is introduced into the Ar sample flow of the ICP. The analyte vapor can then be introduced either directly into the ICP as it is formed (continuous generation) or can be collected and introduced afterward (batch generation). These techniques have the advantages of high analyte transport efficiency (approaching 100%) and separating the analyte from its matrix. Of the chemical vaporization techniques interfaced with ICP spectrometries, hydride generation (HG) is the most popular. In hydride generation, advantage is taken of the ability of certain group IVA (Ge, Pb, Sn), VA (As, Bi) and VIA (Se, Te) elements to form volatile hydrides by means of chemical reduction in acidic media. The use of sodium tetrahydroborate ($NaBH_4$) and HCl to accomplish this was first proposed for

atomic absorption spectrometry,[90] and although other reducing agents and acids have been demonstrated suitable for HG, this combination is still the most widely used throughout atomic spectroscopy. Hydride generation has been interfaced with ICP–OES[91,92,93,94] and ICP–MS,[95,96,97] in both continuous generation[91,92,95,96] and batch generation[93,94,97] arrangements.

In addition to HG, examples exist of other more element-specific chemical vaporization processes that have been used with ICP spectrometry. Examples include the introduction of mercury as an atomic vapor into both ICP–OES[98] and ICP–MS[99] by using the cold-vapor (CV) technique first developed for AAS,[100] and the determination of osmium isotope ratio measurements with ICP–MS by introducing the analyte into the argon stream as volatile OsO_4.[101]

1.5.2 Thermal vaporization

Thermal vaporization refers to a category of sample introduction techniques in which analytes are vaporized from a sample using a heated sample support. The vaporized plume of gas-phase and/or particulate matter that is generated by this process is then swept by a carrier gas flow into the ICP. These methods are arguably the most versatile class of sample introduction techniques available to the ICP. For example, unlike most other sample introduction techniques, those that are based on thermal vaporization are equally capable of introducing both solids and liquids, with a minimal amount of sample preparation being required in each case. Furthermore, the dependence of the vaporization characteristics of an analyte upon its elemental and molecular form presents some unique analysis possibilities. Examples of this include parsing the vaporization of interfering analytes and matrix constituents from that of the analyte of interest, and determining the

oxidation states of the analytes based on their differential vaporization characteristics. Thermal sample introduction methods are also relatively parsimonious in terms of the amount of sample material that they require. Where nebulization and ablation techniques typically require samples of the order of several milliliters or grams, respectively, thermal vaporization methods generally require only microliter or milligram sample aliquots. The two most common methods of thermal sample introduction that are used with ICP-based spectrometries are direct sample insertion (DSI), and electrothermal vaporization (ETV).

1.5.2.1 Direct sample insertion

The notion of "inserting" samples directly into an atomic spectrometry source can be traced back to the work of Delves,[102] who designed a sample introduction technique for flame–AAS in which a sample was thermally atomized from a Ta cup by inserting it directly above the combustion flame. The closest precursor to a sample being directly inserted into an ICP is most likely the device described by Kleinmann and Svoboda,[103] who used a Joule heated graphite support placed at a height even with the lowest turn of an ICP load coil to vaporize and introduce samples into a plasma for spectrometric determination. Direct sample insertion as it is known today was first described by Salin and Horlick[104] in 1979, with a similar arrangement by Sommer and Ohls[105] referred to as SET (sample elevator technique) being described shortly thereafter. In its most conventional configuration, DSI entails the axial elevation of a sample directly into the center channel of the annular ICP discharge by means of a sample-carrying probe made of a high melting point material such as graphite, Mo, Ta, or W. The sample support material is heated by the plasma upon insertion, resulting in the vaporization of the sample into the ICP. A quartz rod attached to a drive/guide mechanism supports the

sample probe, and insertion into the plasma is made possible by using an ICP torch with no sample injector tube.

When compared to other sample introduction methods, DSI is the only ICP technique that, in theory, achieves 100% sample transport efficiency, as the sample is physically elevated into the plasma. The end result are detection limits that are typically a factor of 10–100 better than their solution nebulization counterpart with either ICP–OES or ICP–MS.[106] Provided that their geometry and composition are physically and chemically compliant with the plasma environment, sample supports of any design can be used in DSI. The interchangeable nature of the DSI probe also permits "batch" preparation of multiple samples at a time, and concerns of residual memory effects can be reduced if the probes are only used once. Both solids and liquids can be introduced using DSI, however, the loading capabilities of the plasma usually limits DSI to the introduction of relatively small samples that must not only be dry, but also pyrolyzed of any organic material. This can be achieved by inductively heating the DSI probe in the ICP load coil prior to plasma ignition,[110] by proximal positioning of the probe underneath the plasma discharge prior to full insertion,[107,108] or by other means off-line.[104,112]

1.5.2.1.1 Instrumentation and sample supports

Although the DSI process can be performed manually,[104] most systems use some form of automated drive mechanism that allows all aspects of the insertion process (*i.e.*, depth, rate, time) to be precisely and reproducibly controlled. This has included pneumatically driven arrangments,[105,107] belt-driven[108,109,110] and lead screw-driven[111,112,113] arrangements controlled by stepper/servo motors, and systems that combine both pneumatic and mechanical aspects.[114,115] The DSI systems used in ICP–OES and ICP–

MS are quite similar, with the most notable difference being that DSI–ICP–OES systems are typically vertically-operated and DSI–ICP–MS systems are exclusively horizontally-operated due to the respective vertical and horizontal alignment of the ICP torch in each case. The horizontal mounting of DSI–ICP–MS usually places some restrictions on the types of samples and probes that can be used and may require additional sample preparation.[112,116,117]

Graphite is widely accepted as the most generally suitable material for DSI sample probe construction; it is relatively inexpensive, can be easily machined into various shapes, has good heating characteristics, exhibits relatively inert behavior in the plasma, and contributes little to the spectra of both ICP–OES and ICP–MS.[118] The first DSI studies used graphite cup electrodes native to DC–arc spectrometry as sample supports.[104,105] From a design standpoint, the graphite cup is the most versatile sample support for DSI, as it is equally capable of delivering both solid and liquid samples to the ICP and is capable of handling a considerable range of sample capacities. Additionally, when graphite cups are made such that they have a long, undercut design that minimizes the physical mass of the inserted portion, they typically exhibit the most efficient heating rates and attain the highest final temperatures upon insertion when compared to other graphite probe designs.[119,120,121]

In addition to graphite, metals with high-melting points such as Mo, Ta and W have been used to comprise either part of or the entire DSI sample probe. Of the different support geometries used, the wire loop is the simplest to construct and use, and also provides the most rapid volatilization event of all DSI probe material/design combinations, often resulting in peak evolution times less than 1 s.[109] Wire loops, however, are poorly suited for samples other than liquids, unless they are shaped such that

they can cradle a pelletized solid.[116,122] Metal cups have also been used as DSI supports, but are more difficult to construct, with the end result often being the use of a metallic cup on a graphite support.[113,120] Though metallic supports do not impart refractory carbide effects, the metal vaporization surface may result in some interferences, such as the formation of metal oxides.[109]

1.5.2.1.2 Transport efficiency

Transport efficiency is defined as the net amount of analyte or sample that successfully reaches the plasma source in an ICP system and is often expressed as a percent of the gross amount of analyte or sample initially presented to the sample introduction system. Transport efficiency, however, is not a straightforward issue in DSI. Granted, the physical elevation of a sample into the ICP by DSI implies 100% transport efficiency, but this is only true if 100% of the sample is actually vaporized from the sample support and made available to the atomization, excitation, and ionization processes of the plasma. The issue of transport efficiency in DSI then effectively becomes one of volatilization efficiency, with the incomplete volatilization of analytes due to the presence or formation of non-volatile compounds being the principal determining factor. Inferences as to transport efficiency have been made by examining sample supports following vaporization events with radiotracer techniques[123] and x-ray fluorescence (XRF),[124] and incomplete volatilization can often be detected by re-inserting the sample probe.

Without resorting to chemical modification, analyte volatilization can be improved by enhancing the heating characteristics in the plasma. In addition to the sample probe design considerations mentioned previously, improved heating of the sample support be accomplished by using a mixed-gas plasma.[114,125] Gases that are better

thermal conductors than Ar (such as He, H_2, N_2 and O_2) can be mixed into the various flows of an Ar–ICP as a means of improving the heat transfer characteristics of the discharge. When 1–6% O_2 is introduced into the outer and immediate flows of the ICP, improvements in the vaporization of elements of moderate- to high-volatility are seen.[114] When the mixture is increased to 20% O_2, the complete volatilization of refractory compounds such as V is possible, however, these conditions will also result in complete consumption of the graphite sample support.[125]

1.5.2.1.3 Matrix effects and chemical modification

The picture that exists in terms of the effect of the sample matrix on the signal observed with DSI is a mixed one. In general, though, the presence of different sample concomitants has been found to greatly affect the temporal behavior (*i.e.*, appearance time, evolution time, peak shape) of the DSI signal; however, the area of the transient signal usually remains unchanged. This has been observed to some extent with both liquid[109,126,127] and solid samples,[114,128,129] although some exceptions do exist.[130] In addition to sample concomitants, the composition of the sample support also plays a role in terms of the matrix effects observed in DSI, the most notable example being the formation of refractory carbides with graphite probes.[124,128]

The use of chemical modification as a means of selectively enhancing or suppressing the vaporization of analytes or concomitants is a practice that has been extensively used in electrothermal- (ET)–AAS.[131] In the case of DSI, chemical modification has been used almost exclusively to enhance the volatility of analytes that form refractory carbides in graphite probes, with the most common approach using halogen-containing compounds to form volatile metal halides.[132] Halogenation has been

attempted in DSI using solid modifiers such as group IA (KCl, KF, NaCl, NaF, LiF) and IIA ($BaCl_2$, BaF_2) salts, as well as NH_4Cl, AgCl, SrF_2 and polytetrafluorethlene (PTFE).[123,124,133,134]

The addition of a relatively large amount of a solid modifier to a sample is not entirely straightforward, as they tend to vaporize rapidly and may act as a source of sample contamination. Gaseous modifiers, on the other hand, are commonly available in highly pure forms, and can be made available either throughout the entire sample introduction cycle, or at specific intervals. Gaseous halogenating reagents such as CF_2Cl_2 (Freon-12*),[110,121,135] CHF_3 (Freon-23*)[136] and SF_6[137] have been used in DSI to assist in the volatilization of refractory carbide-forming elements by introducing them into the Ar flow of the ICP in low proportion (0.1–1% (v/v)). In most cases, the gaseous modifier is simply mixed into the auxiliary Ar flow; however, the development of hollow-stemmed probes has made it possible to introduce the modifier directly into the sample cup.[110,121] This approach has the advantage of concentrating the introduction of the gaseous modifier to where the sample is deposited.

1.5.2.1.4 Analytical performance and applications

Direct sample insertion is typically capable of a linear dynamic range of 3–5 orders of magnitude when using the integrated area of the transient signal as the dependent calibration variable.[106] The precision associated with DSI is generally of the order of 2–10% for easily-volatilized analytes in clean aqueous sample matrices based on the relative standard deviation (RSD) of the integrated peak area,[106] and can be as low as 1–2% with automated systems.[109] When solid samples are vaporized, the precision degrades

* "Freon" is a registered trademark of the DuPont Corporation.

somewhat to values typically around 10–15% RSD, and can be as high as 30–50% RSD.[106] The degree to which the precision observed with solids depreciates is dictated by factors such as the ease and reproducibility with which the analytes can be vaporized from the matrix, as well as sample homogeneity and weighing errors, although the issues of homogeneity and weighing have been addressed in part by the use of slurry sample deposition.[137] Slight errors in positioning and re-mounting the sample support,[109] as well as variation in the physical placement of the sample in the probe can also contribute towards the observed precision. Detection limits are typically of the range of 1–1000 pg (absolute) for DSI–ICP–OES[106] and 10–1000 fg (absolute) for DSI–ICP–MS.[138,139]

Direct sample insertion has been used for the straightforward analysis of many solid and liquid sample types. A short list of these includes environmental samples such as river water,[139] agricultural samples such as solid[108] and digested[126] plant material, geological samples such as solid[124,140,141] and digested[127] metals, metal oxides and ores, sediments,[122,130,137] and biological samples such as human hair.[142] A recent literature review by Sing[106] gives a thorough summary of these and other sample types determined by DSI-based ICP spectrometries.

In addition to the simple analysis of solid and liquid samples, preconcentration approaches have also been used in DSI as a means of determining analytes whose concentration would otherwise fall short of the quantitation capabilities of the technique. This has been accomplished *in situ* by repeatedly depositing and drying liquid samples,[109] by spray deposition on an inductively heated sample support,[117,143] and by using probes which have extractive capabilities either from the use of activated charcoal in their construction,[144] or by their use in an electrochemical plating arrangement.[145,146] *Ex situ* preconcentration schemes, in which analytes are preconcentrated onto an external

substrate which is then inserted into the plasma, have also been developed using various resins.[147,148,149]

1.5.2.2 Electrothermal vaporization

The concept of using electrothermal vaporization (ETV) in analytical spectrometry was first explored in the 1900s by King[150,151] who used a tubular graphite furnace as both a vaporization and excitation source for generating emission spectra. Some 50 years later, tube furnaces were developed as an atomization source for ET–AAS,[152,153] a technique whose detection limits to this day still rival those of solution nebulization ICP–MS. Nixon *et al.*[154] reported the first coupling of an eletrothermal vaporization sample introduction system with an ICP source in 1974. Ironically, although modified graphite ET–AAS furnaces account for a large portion of the ETV devices used today with ICP sources, the device used by Nixon *et al.* was not a tube furnace at all—it consisted of a Ta filament contained in a flow-through cell.[154]

Electrothermal vaporization is similar to DSI, in that it involves the generation of a dry aerosol or vapor from a discrete solid or liquid sample deposited on a heated sample support. Methodological similarities end there, though, as both the nature and location of the heating is markedly different from that involved in DSI. In ETV, a sample is vaporized from a Joule heated surface into a chamber, generating a mixed aerosol of particulate and/or gas-phase matter. This aerosol is then entrained into a carrier gas flow and transported to the ICP. Electrothermal vaporization shares much of the same qualities as DSI, namely the ability to handle both solids and liquids with minimal sample treatment, and requiring only miniscule sample amounts. Additionally, the ability to generate complex, reproducible heating programs makes the drying and pyrolysis of

samples a much simpler and more reliable process in ETV than in DSI, often permitting the convenient temporal separation of analyte and matrix vaporization. The location of the analyte vaporization event *ex situ* to the plasma also alleviates the energy demands placed on the ICP, thus increasing the efficiency of the excitation (OES) and ionization (MS) processes. Vaporization upstream of the plasma does result in transport efficiencies lower than the 100% theoretically attainable with DSI; nonetheless, it is still quite high, typically ranging from 20–80%.[155] Similar to DSI, the improvement seen in detection limits with ETV is typically 2–3 orders of magnitude over solution nebulization.

1.5.2.1.1 Instrumentation and sample supports

Electrothermal vaporization devices fall into two categories: tube vaporization cells and open vaporization cells. Tube vaporization cells are typically commercially available devices for ET–AAS that have been modified for ETV sample introduction.[156,157] This is usually achieved by removing the quartz windows on the ends of the furnace with tubing adapters for the carrier gas to enter and exit. Vaporization cells of this design typically have a small dead volume, usually of the order of 1 ml. By comparison, an open vaporization cell consists of a conductive sample support in a considerably larger domed enclosure made of glass or quartz with a gas inlet underneath the sample support and a transport tube outlet at the apex of the dome.[154,158,159] The volume of the chamber is usually around 10–20 ml, although designs ranging from volumes as small as 1 ml[160] and 5 ml[161] to as large as 300ml[162] and 1000 ml[158] have been used.

Metal sample supports used in ETV devices typically consist of an electrically conductive refractory metal such as Pt,[163] Ta[154] or W,[164] formed into a boat, coil, filament, foil or wire of low thermal mass that is conducive to rapid Joule heating. An example of

a suitable support that can easily be procured for an ETV device is the W filament from a halogen lamp.[165,166] Metal vaporization supports are almost exclusively used in open vaporization cell arrangements, although some cases exist where metallic supports have been used inside of graphite tube furnaces.[167,168] In general, metal supports are well suited for the vaporization of elements that would otherwise form refractory carbides with graphite supports, however, they may introduce spectral interferences due to the release of species such as metal oxides.[169]

Graphite has been used as a sample support in both tube and open vaporization cells. To protect the base material against chemical attack and to reduce sample and vapor diffusion, substrates that are coated with a highly ordered layer of pyrolytically deposited graphite are almost always used in ETV.[170,171] The application of metal carbide coatings has also been used as a means of increasing the useful lifetime of pyrolytically coated graphite supports and, in some cases, improving analyte volatilization.[159,172] In tube vaporization cells, the sample can be deposited either directly onto the walls of the graphite tube,[156,173] or onto a graphite platform inside of the tube.[157,174, 175] Since open vaporization cells do not rely on the sample support to act both as a vaporization surface and a chamber enclosure as is the case in tube furnaces, graphite supports of open designs, such as cups,[159] rods,[158] platforms[161] and boats[176] are typically used.

Unlike DSI, ETV is a technique in which the sample support has been traditionally considered a non-interchangeable fixture, however, ETV cells have recently been designed to accommodate sample support changeover. Karanassios *et al.*[177] designed an open vaporization ETV cell in which a pelletized sample pressed in graphite was placed between the electrical contacts and heated to impart analyte volatilization. Goltz *et al.*[178,179] have described an inductively heated vaporizer (IHV) in which a long,

undercut interchangeable graphite cup similar to that encountered in DSI is positioned in an open vaporization cell encircled by a load coil and is heated by contact-free induction heating in an RF-field. An in-torch vaporization (ITV) system has been described by Karanassios *et al.*,[180,181] in which samples, deposited on a wire loop attached to a ceramic insulator were inserted into a small vaporization cell incorporated into the base of the ICP torch and vaporized by Joule heating of the loop.

1.5.2.1.2 Transport efficiency

A landmark paper by Kántor[182] described ETV as a process of thermal dispersion whereby vaporized material undergoes various nucleation and coagulation processes to form a dry aerosol that can be transported to the ICP. In order to achieve efficient transport in ETV, the vaporized analyte material must form particles that are large enough to be effectively transported in a carrier gas flow yet small enough to avoid coagulation and deposition along the transport path. Furthermore, this process must be sufficiently rapid such that analyte condensation on the transport path surfaces does not take place.

The processes by which particles in ETV are formed are complex, and vary with the vapor concentration. At low vapor concentrations, particle formation is generally governed by *homogeneous nucleation*, in which clusters formed by the collision of vapor-phase species serve as condensation nuclei. The rate at which homogeneous nucleation takes place is usually dictated by the degree of turbulent mixing that occurs between the hot vapor and the colder carrier gas. When a high concentration of stable nuclei is attained, the *heterogeneous condensation* of vapor on existing particles can take place. Heterogeneous condensation can also take place on nuclei of different origin, such as analytes with higher rates of nucleation or other nuclei present in the atmosphere. As the

particle concentration increases, particles will start to collide with each other to form larger ones (*Brownian coagulation*), followed by coalescence of the finer particles and sintering of the larger ones, eventually resulting in the gravitational loss of particles.[182]

The two variables that bear the greatest consequence on transport efficiency are the matrix of the sample (which is discussed below) and the design of the ETV cell. In terms of cell designs, tube furnaces are more prone to condensation losses than open vaporization cells, as their internal volume is much smaller, resulting in cool surfaces being in close proximity to the vaporization event.[183] Approaches to solving this problem have included the use of coolant gases to introduce conditions that would promote aggregate formation[174,175,184,185] and minimizing the distance between the furnace outlet and the ICP.[186] For open vaporization cells, the dimensions of the enclosure have been optimized such that the internal volume is large enough to minimize condensation losses yet small enough to avoid substantial vapor diffusion.[161]

1.5.2.1.3 Matrix effects and chemical modification

The influence that sample matrix can bear on ETV transport efficiency was first reported by Kirkbright *et al.*[187,188] who noticed that the ICP–OES signal for nanogram levels of Cd was lower when the element was vaporized from a simple acidified sample *versus* one containing a relatively large amount of Se. It was discovered that, in the absence of the large amount of Se, Cd would undergo a low rate of nucleation, resulting in significant amounts of Cd being deposited on components of the vaporization cell and transport network. Studies have shown that the atomic vapor for Cd can persist for long distances in the ETV transport network (upwards of 3 m),[157] whereas less volatile elements such as Ag and Cu persist in their atomic form less than 2 cm from the point of vaporization.[189]

Similar transport losses have been observed with other volatile elements such as As[187] and Zn[190] as well as similar matrix-dependent sensitivity changes.[186,191,192]

These observations have led to the use of chemical modification as a means of improving the magnitude and consistency of analyte transport observed in ETV sample introduction by acting as a *physical carrier*.[182] Ediger and Beres[183] conducted a factorial study of four additives (NaCl, $Mg(NO_3)_2$, $Pd(NO_3)_2$ and $Te(NO_3)_2$ on 20 analytes and in general found that the chemical nature of the matrix made little difference in the transport enhancement seen, and that the absolute amount of analyte, rather than the relative amount with respect to the matrix, bore a greater influence on the effect observed. The latter of these observations influenced most of the research with the use of physical carriers being focused in ETV–ICP–MS, as the amount of analyte being vaporized is often on the range of picograms to femtograms. Other additives that have been used as physical carriers for ETV include selenium (Na_2SeO_3),[193] and Na in the form of diluted seawater.[194,195] Soot particles, introduced either by adding organic modifiers such as ascorbic[196] or citric acid,[183] or by incorporating an oxygen ashing step in the ETV program,[197,198] can also act as a physical carrier.

The existence or formation of refractory analytes is also an issue in ETV. Chemical modification in ETV for the purposes of enhancing the volatility of refractory elements was first explored by Kirkbright and Snook, who realized signal improvements for B, Cr, Mo, W and Zr by incorporating 0.1% CHF_3 into the carrier gas flow.[199] Since then, gaseous modification has been attempted in a similar manner by mixing halocarbons such as CCl_4,[199,200] CCl_2F_2 (Freon-12),[201,202] CHF_3 (Freon-23)[199,] $CHClF_2$ (Freon-22)[203] and Cl_2[204] in low proportion (0.1–1% (v/v)) with the argon carrier flow. The use of gaseous halogenation has also been found to improve the ETV signals for volatile

elements due to an increase in the total number of particles in the aerosol plume, earning a recommendation for its routine use in multi-element analysis.[205] Along with gaseous chemical modification, many solid additives have been used to enhance analyte volatility by imparting halogenation, some of which include NH_4Cl,[206] NH_4F,[207] and polytetrafluoroethylene (PTFE).[208]

In addition to halogenating agents, other approaches have been taken towards the problem of refractory elements and compounds. The formation of volatile metal complexes with 8-hydroxyquinoline (for Cr)[209] and 1-phenyl-3-methyl-4-benzoyl-pyrazolone [5] (PMBP) (for Eu, La, and Y)[210] has been used as a means for vaporizing analytes at temperatures around 1000°C.

1.5.2.1.4 Analytical performance and applications

The linear dynamic range of ETV sample introduction generally covers 3–4 orders of magnitude,[159,199] and in some cases can be as high as 6 depending on the type of ETV arrangement and ICP spectrometry used.[211] Precision on the order of 3–10% RSD can be expected for liquid samples with ETV, although reproducibility bettering 3% RSD has been achieved.[212] The RSD observed when solids are introduced using ETV is generally 10% or higher and, as in DSI, depends highly on the ease and reproducibility with which the analytes can be vaporized from the matrix, as well as sample homogeneity and weighing errors. Slurry sampling has been used as an approach for improving the precision with which solid samples can be analyzed using ETV,[213] resulting in RSD values as good as 1.5% in some cases.[214] Absolute limits of detection generally range from 1–100 pg for ETV–ICP–OES and 0.1–100 fg for ETV–ICP–MS,[215] depending on

the vaporization and transport characteristics of the element, and the influence of the sample matrix on the above.

Many solid and liquid samples of agricultural, biological, environmental and geological origin have been analyzed by ICP–OES and ICP–MS using ETV sample introduction, either as aqueous digests or in their native form. Recent reviews by Carey and Caruso[155] and Matusiewicz[215] provide thorough summaries of the sample types that have been analyzed using ETV sample introduction.

Outside of the straightforward analysis of solids and liquids, ETV has also been used for a series of unique applications. The ability to perform detailed temperature programming stages in ETV has led to the development of *in situ* speciation techniques, whereby the different atomic/molecular forms of a given element can be separated based on the volatility of their existing or chemically modified forms. Examples of this include methods that have been developed for discriminating between inorganic and organic Cl,[216] Hg,[217] and Cr^{III} and Cr^{VI}.[218] *In situ* and *ex situ* preconcentration schemes have also been used with ETV as a means of determining analytes whose concentration would otherwise be below the capability of the technique. Examples of substrates used and later analyzed by ETV in *ex situ* schemes include activated charcoal,[219] poly(dithiocarbamate) and poly(acrylamidoxime) resins,[220] and mercury-plated glassy carbon electrodes.[221] *In situ* preconcentration methods that have been used include the trapping of gaseous metal hydrides on Pd in the ETV furnace,[222,223] spray deposition of liquids onto a heated sample support,[224] and electrostatic particle deposition.[225]

1.6 Thesis outline

The following is a brief summary of the subsequent chapters of this thesis:

Chapter 2 recounts the development of a pyrolytically coated graphite DSI probe for the introduction of samples into the ICP. The coating process developed and the analytical performance of the coated probe with ICP–OES are described.

Chapter 3 describes an analysis method developed for direct determination of metals in wood pulps by ICP–OES using the aforementioned pyrolytically coated DSI probe. The merits of using DSI, as well as a pyrolytically coated sample probe for this type of application, are discussed.

Chapter 4 is a performance attribute study of IH–ETV sample introduction for the ICP. The temperature and heating characteristics of the IH–ETV device are described, and benchmarks such as transport efficiency and ICP–OES detection limits are established for several mixed carrier gases.

From the experiences gained in Chapter 4, **Chapter 5** describes the development of an analysis method for the determination of metals in soils by ICP–OES using IH–ETV sample introduction.

Chapter 6 is an account of a novel method for determining analyte transport efficiency in ETV sample introduction. The method, which was used for the determination of the transport efficiency figures that appear in Chapter 4, is described and validated against a reference method.

Finally, **Chapter 7** summarizes understanding gained from the DSI and IH–ETV studies described in the previous chapters. Conclusions are drawn and recommendations for future work are made based on comparisons made between the experiences

encountered in the current work with DSI and IH–ETV, as well as those reported in the literature.

1.7 References

1. Meyer, G.A., *Anal.Chem.*, 1987, **59**, 1345A.

2. Broekaert, J.A.C., *Spectrochim. Acta Part B*, 2000, **55**, 739.

3. Browner, R.F. and Boorn, A.W., *Anal. Chem.*, 1984, **56**, 786A-798A.

4. Greenfield, S., Jones, I.L., and Berry, C.T., *Analyst*, 1964, **89**, 713.

5. Wendt, R.H., and Fassel, V.A., *Anal. Chem.*, 1965, **37**, 920.

6. Tesla, N., *Elec. Eng.*, 1891, 549.

7. Hittorf, W., *Ann. Phys.*, 1891, **21**, 90.

8. Thomson, J.J., *Philos. Mag.*, 1891, **32**, 321.

9. Babat, G.I., *J. Inst. Electr. Eng.*, 1947, **94**, 27.

10. Reed, T.B., *J. Appl. Phys.*, 1961, **32**, 821.

11. Reed, T.B., *J. Appl. Phys.*, 1961, **32**, 2534.

12. Greenfield, S., Jones, I.L.W., Berry, C.T., and Spash, D.I., 1968, British Patent 1109602.

13. Greenfield, S., Jones, I.L.W., and Berry, C.T., US Patent 3467471.

14. Fassel, V.A., and Dickinson, G.W., *Anal. Chem.*, 1968, **40**, 247.

15. Dickinson, G.W., and Fassel, V.A., *Anal. Chem.*, 1969, **41**, 1021.

16. Scott, R.H., Fassel, V.A., Kniseley, R.N., and Nixon, D.E., *Anal. Chem.*, 1974, **46**, 75.

17. Montaser, A., McLean, J.A., Liu, H., and Mermet, J.-M., *An Introduction to ICP Spectrometries for Elemental Analysis*, in Montaser, A. (ed.), *Inductively Coupled Plasma Mass Spectrometry*, Wiley-VCH, New York, NY, USA, 1st edn., 1998, p.5.

18. Larson, G.F., Fassel, V.A., Scott, R.H., and Kniseley, R.N., *Anal. Chem.*, 1975, **47**, 238.

19. van der Mullen, J.A.M., *Spectrochim. Acta, Part B*, 1989, **44**, 1067.

20. van der Mullen, J.A.M., *Spectrochim. Acta, Part B*, 1990, **45**, 1.

21. Evans, E.H., and Caruso, J.A., *J. Anal. At. Spectrom.*, 1993, **8**, 427.

22. Evans, E.H., Pretorius, W., Ebdon, L., and Rowland, S.J., *Anal. Chem.*, 1994, **66**, 3400.

23. Chan, S., and Montaser, A., *Spectrochim. Acta Part B.*, 1985, **40**, 1467.

24. Montaser, A., and Koppenaal D.W., *Anal. Chem.*, 1987, **59**, 1240.

25. Koppenaal, D.W., and Qinton, L.F., *J. Anal. At. Spectrom.*, 1988, **3**, 659.

26. Pennebaker, F.M., Williams, R.H., Norris, J.A., and Denton, M.B., *Adv. At. Spectrosc.*, 1999, **5**, 145.

27. Boumans, P.W.M.J., and Vrakking, J.J.A.M., *J. Anal. At. Spectrom.*, 1987, **2**, 513.

28. Larson, G.F., Fassel, V.A., Winge, R.K., and Knisley, R.N., *Appl. Spectrosc.*, 1976, **30**, 384.

29. Davies, J., Dean, J.R., and Snook , R.D., *Analyst*, 1985, **110**, 535.

30. Nakamura, Y., Katsuyuki, T, Osami, K., Okochi, H., and McLeod, C.W., *J. Anal. At. Spectrom.*, 1994, **9**, 751.

31. Dubuisson, C., Poussel, E., and Mermet, J.-M., *J. Anal. At. Spectrom.*, 1997, **12**, 281.

32. Montaser, A., and Fassel, V.A., *Anal. Chem.*, 1976, **48**, 1490.

33. Demers, D.R., and Allemand, C.H., *Anal. Chem.*, 1981, **53**, 1915.

34. Wendt, R.H., and Fassel, V.A., *Anal. Chem.*, 1966, **38**, 337.

35. Vellion, C., and Margoshes, M., *Spectrochim. Acta, Part B*, 1968, **23**, 503.

36. Greenfield, S., Smith, P.B., Breeze, A.E., and Chilton, N.M.D., *Anal. Chim. Acta*, 1968, **41**, 385.

37. Serauskas, R. V., Brown, G. R., and Pertel, R. *Int. J. Mass Spectrom. Ion Phys.*, 1975, **16**, 69.

38. Gray, A.L., *Analyst*, 1975, **100**, 289.

39. Gray, A.L., *Anal. Chem.*, 1975, **47**, 600.

40. Houk, R.S., Fassel, V.A., Flesch, G.D., Svec, J.J., Gray, A.L., and Taylor, C.E., *Anal. Chem.*, 1980, **52B**, 2283.

41. Douglas, D.J., Quan, E.S., Smith, R.G., *Spectrochim. Acta, Part B*, 1983, **38**, 39.

42. Date, A.R., and Gray, A.L., *Analyst*, 1981, **106**, 1255.

43. Date, A.R., and Gray, A.L., *Analyst*, 1983, **108**, 159.

44. Houk, R.S., Fassel, V.A., and Svec, H.J., *Dyn. Mass Spectrom.*, 1981, **6**, 234.

45. Douglas, D.J., and French, J.B., *J. Anal. At. Spectrom.*, 1988, **3**, 743.

46. Morita, M., Ito, H., Linscheid, M., and Otsuka, K., *Anal. Chem.*, 1994, **66**, 1588.

47. Myers, D.P., Li, G., Yang, P., and Hieftje, G.M., *J. Am. Soc. Mass Spectrom.*, 1994, **5**, 1008.

48. Cromwell, E.F., and Arowsmith, P., *J. Am. Soc. Mass Spectrom.*, 1996, **7**, 458.

49. Walder, A.J., Koller, D., Reed, N.M., Hutton, R.C., and Freedman, P.A., *J. Anal. At. Spectrom.*, 1993, **8**, 1037.

50. Vaughan, M.A., and Horlick, G., *Appl. Spectrosc.*, 1986, **40**, 434.

51. Tan, S.H., and Horlick, G., *Appl., Spectrosc.*, 1986, **40**, 445.

52. Olivares, I., and Houk, R.S., *Anal. Chem.*, 1986, **58**, 20.

53. Tan, S.H., and Horlick, G., *J. Anal. At. Spectrom.*, 1987, **2**, 745.

54. Meinhard, J.E., *ICP Inf. Newsl.*, 1976, **2**, 163.

55. Kniseley, R.N., Amenson, H., Butler, C.C., and Fassel, V.A., *Appl. Spectrosc.*, 1974, **28**, 285.

56. Novak, J.W.Jr., Lillie, D.E., Boom, A.W., and Browner, R.F., *Anal. Chem.*, 1980, **52**, 576.

57. Sharp, B.L., *J. Anal. At. Spectrom.*, 1988, **3**, 939.

58. Scott, R.H., Fassel, V.A., Kniseley, R.N., and Nixon, D.E., *Anal. Chem.*, 1974, **46, 75.**

59. Vieira, P.A., Zhizhuang, H., Chan, S., and Montaser, A., *Appl. Spectrosc.*, 1986, **40**, 1141.

60. Maessen, F.J.M.J., Coevert, P., and Balke, J., *Anal. Chem.*, 1984, **56**, 899.

61. Routh, M., *Spectrochim. Acta Part B*, 1986, **41**, 39.

62. Maestra, S., Mora, J., Todolí, J.-L., and Canals, A., *J. Anal. At. Spectrom.*, 1999, **14**, 61.

63. Légère, G., and Burgener, P., *ICP Inf. Newsl.*, 1982, **13**, 521.

64. Brotherton, T., and Caruso, J., *J. Anal. At. Spectrom.*, 1987, **2**, 389.

65. Ebdon, L., and Wilkinson, J.R., *J. Anal. At. Spectrom.*, 1987, **2**, 39.

66. Ebdon, L., and Wilkinson, J.R., *J. Anal. At. Spectrom.*, 1987, **2**, 325.

67. Lawrence, K.E., Rice, g.W., and Fassel, V.A., *Anal. Chem.*, 1984, **56**, 289.

68. Liu, H. and Montaser, A., *Anal. Chem.*, 1994, **66**, 3233.

69. Doherty, M.P., and Hieftje, G.M., *Appl. Spectrosc.*, 1984, **38**, 405.

70. Layman, L.R., and Lichte, F.E., *Anal. Chem.*, 1982, **54**, 638.

71. Olson, K.W., Haas, W.J., and Fassel, V.A., *Anal. Chem.*, 1977, **49**, 632.

72. Fassel, V.A., and Bear, B.R., *Spectrochim. Acta Part B*, 1986, **41**, 1089.

73. Tarr, M.A., Zhu, G., and Browner, R.F., *Appl. Spectrosc.*, 1991, **45**, 1424.

74. Novozamsky, I., van der Lee, H.J., and Houba, V.J.G., *Mikrochim. Acta*, 1995, **119**, 183.

75. Borsier, M., and Garcia, M, *Spectrochim. Acta Part B*, 1983, **38**, 123.

76. Lamble, K.J., and Hill, S.J., *Analyst*, **123**, 103R (1998).

77. Thompson, M., Goulter, J.E., and Sieper, F., *Analyst*, 1981, **106**, 32.

78. Ishizuka, T., and Uwamin, Y., *Spectrochim. Acta Part B*, 1983, **38**, 519.

79. Gray, A.L., *Analyst*, 1985, **110**, 551.

80. Imai, N., *Anal. Chim. Acta*, 1990, **235**, 381.

81. Ducreux-Zappa, M., and Mermet, J-M., *Spectrochim. Acta Part B*, 1996, **51**, 333.

82. Thompson, M., Chenery, S., and Brett, L., *J. Anal. At. Spectrom.*, 1989, **4**, 11.

83. Günther, D., Cousin, H., Magyar, B., and Leopold, I, *J. Anal. At. Spectrom.*, 1997, **12**, 165.

84. Coleman, D.M., and Walters, J.P., *Spectrochim. Acta Part B*, 1976, **31**, 547.

85. Aziz, A., Broekaert, J.A.C., Laqua, K., and Leis, F., *Spectrochim. Acta Part B*, 1984, **39**, 1091.

86. Hirata, T., Akagi, T., and Masuda, A., *Analyst*, 1990, **115**, 1329.

87. Ivanovic, K.A., Coleman, D.M., Kunz, F.W., and Schuetzle, D., *Appl. Spectrosc.*, 1992, **46**, 894.

88. Jones, J.L., Dahlquist, R.L., and Hoyt, R.E., *Appl. Spectrosc.*, 1971, **25**, 628.

89. Jiang, S.-J., and Houk, R.S., *Spectrochim. Acta Part B*, 1987, **42**, 93.

90. Braman, R.S., Justen, L.L., and Foreback, C.C., *Anal. Chem.*, 1972, **44**, 2195.

91. Thompson, M., Pahalavanpour, B., Walton, S.J., and Kirkbright, G.F., *Analyst*, 1978, **103**, 568.

92. Thompson, M., Pahalavanpour, B., Walton, S.J., and Kirkbright, G.F., *Analyst*, 1978, **103**, 705.

93. Fry, R.D., Denton, M.B., Windsor, D.L., and Northway, S.J., *Appl. Spectrosc.*, 1979, **33**, 399.

94. Eckhoff, M.A., McCarthy, J.P., and Caruso, J.A., *Anal. Chem.*, 1982, **54**, 165.

95. Date, A.R., Gray, A.L., *Spectrochim. Acta Part B*, 1983, **38**, 29.

96. Powell, M.J., Boomer, d.W., and McVicars, M.J., *Anal. Chem.*, 1986, **58**, 2864.

97. Jin, K., Shibata, Y., Morita, M., *Anal. Chem.*, 1991, **63**, 986.

98. Anderson, K.A., Isaacs, B., Tracy, M., and Möller, G.J., *AOAC Int.*, 1994, **77**, 473.

99. Bushee, D.S., *Analyst*, 1988, **113**, 1167.

100. Hatch, W.R., and Ott, W.L., *Anal. Chem.*, 1968, **40**, 2085.

101. Lichte, F.E., Wilson, S.M., Brooks, R.R., Reeves, R.D., Holzbecher, J., and Ryan, D.E., *Nature*, 1986, **322**, 816.

102. Delves, H.T., *Analyst*, 1970, **95**, 431.

103. Kleinmann, I., and Svoboda, V., *Anal. Chem.*, 1969, **41**, 1029.

104. Salin, E.D., and Horlick, G., *Anal. Chem.*, 1979, **51**, 2284.

105. Sommer, D., and Ohls, K.D., *Fresenius' J. Anal. Chem.*, 1980, **304**, 97.

106. Sing, R., *Spectrochim. Acta Part B*, 1999, **54**, 411.

107. Salin, E.D., and Sing, R.L.A., *Anal. Chem.*, 1984, **56**, 2596.

108. Abdullah, M., and Haraguchi, H., *Anal. Chem.*, 1985, **57**, 2059.

109. Sing, R.L.A., and Salin, E.D., *Anal. Chem.*, 1989, **61**, 163.

110. Skinner, C.D. and Salin, E.D., *J. Anal. At. Spectrom.*, 1997, **12**, 725.

111. Li-Xing, Z., Kirkbright, G.F., Cope, M.J., and Watson, J.M., *Appl. Spectrosc.*, 1983, **37**, 250.

112. Karanassios, V., and Horlick, G., *Spectrochim. Acta Part B*, 1989, **44**, 1345.

113. Chan, W.T., and Horlick, G., *Appl. Spectrosc.*, 1990, **44**, 380.

114. Pettit, W.E., and Horlick, G., *Spectrochim. Acta Part B*, 1986, **41**, 699.

115. Karanassios, V., and Horlick, G., *Spectrochim. Acta Part B*, 1990, **45**, 85.

116. Blain, L., Salin, E.D., and Boomer, D.W., *J. Anal. At. Spectrom.*, 1989, **4**, 721.

117. Rattray, R., and Salin, E.D., *J. Anal. At. Sectrom.*, 1995, **10**, 829.

118. Karanassios, V., and Horlick, G., *Spectrochim. Acta Rev.*, 1990, **13**, 89.

119. Barnett, N.W., Cope, M.J., Kirkbright, G.F., and Taobi, A.A.H., *Spectrochim. Acta Part B*, 1984, **39**, 343.

120. Karanassios, V., Horlick, G., Abdullah, M., *Spectrochim. Acta Part B*, 1990, **45**, 105.

121. Skinner, C.D., and Salin, E.D., *J. Anal. At. Spectrom.*, 1997, **12**, 1131.

122. Blain, L., and Salin, E.D., *Spectrochim. Acta Part B*, 1992, **47**, 399.

123. Reisch, M., Nickel, H., and Mazurkiewicz, M., *Spectrochim. Acta Part B*, 1989, **44**, 307.

124. Zaray, G., Broekaert, J.A.C., and Leis, F., *Spectrochim. Acta Part B*, 1988, **43**, 241.

125. Liu, X.R., and Horlick, G., *J. Anal. At. Spectrom.*, 1994, **9**, 833.

126. Abdullah, M., Fuwa, K., and Haraguchi, H., *Spectrochim. Acta Part B*, 1984, **39**, 1129.

127. Umemoto, M., and Kubota, M., *J. Anal. At. Spectrom.*, 1987, **42**, 491.

128. McLeod, C.W., Clarke, P.A., and Mowthorpe, D.J., *Spectrochim. Acta Part B*, 1986, **41**, 63.

129. Umemoto, M., Hayashi, K., and Haraguchi, H., *Anal. Chem.*, 1992, **64**, 257.

130. Blain, L. and Salin, E.D., *Spectrochim. Acta Part B*, 1992, **47**, 205.

131. Styris, D.L., and Redfield, D.A., *Spectrochim. Acta Rev.*, 1993, **15**, 71.

132. Bächmann, K., *Talanta*, 1981, **29**, 1.

133. Karanassios, V., Abdullah, M., and Horlick, G., *Spectrochim. Acta Part B*, 1990, **45**, 119.

134. Purohit, P.J., Thulasidas, S.K., Goyal, N., and Page, A.G., *J. Anal. At. Spectrom.*, 1997, **12**, 1317.

135. Kirkbright, G. F., and Xing-Li, Z., *Analyst*, 1982, **107**, 617.

136. Fujimoto, K., Okano, T., and Matsumura, Y., *Anal. Sci.* 1991, **7**, 549.

137. Karanassios, V. and Wood, T.J., *Appl. Spectrosc.*, 1999, **53**, 197.

138. Boomer, D.W., Powell, M., Sing, R.L.A., and Salin, E.D., *Anal. Chem.*, 1986, **58**, 975.

139. Hall, G.E.M., Pelchat, J.C., Boomer, D.W., and Powell, M., *J. Anal. At. Spectrom.*, 1988, **3**, 791.

140. Lorber, A., and Goldbart, Z., *Analyst*, 1985, **110**, 155.

141. Shao, Y., and Horlick, G., *Appl. Spectrosc.*, 1986, **40**, 386.

142. Monasterios, C.V., Jones, A.M. and Salin, E.D., *Anal. Chem.*, 1986, **58**, 780

143. Rattray, R., Minoso, J., and Salin, E.D., *J. Anal. At. Spectrom.*, 1993, **8**, 1033.

144. Skinner, C.D., Cazagou, M., Blaise, J., and Salin, E.D. *Appl. Spectrosc.*, 1999, **53**, 191.

145. Habib, M.M., and Salin, E.D., *Anal. Chem.*, 1984, **56**, 1186.

146. Habib, M.M., and Salin, E.D., *Anal. Chem.*, 1985, **57**, 2055.

147. Zaray, G., Burba, P., Broekaert, J.A.C., and Leis, F., *Spectrochim. Acta Part B*, 1988, **43**, 255.

148. Moss, P., and Salin , E.D., *Appl. Spectrosc.*, 1991, **45**, 1581.

149. Rattray, R., and Salin, E.D., *J. Anal. At. Spectrom.*, 1995, **10**, 1053.

150. King, A.S., *Astrophys. J.*, 1905, **21**, 236.

151. King, A.S., *Astrophys. J.*, 1908, **27**, 353.

152. Walsh, A., *Spectrochim. Acta*, 1955, **7**, 108.

153. L'vov, B.V., *Spectrochim. Acta*, 1961, **17**, 761.

154. Nixon, D.E., Fassel, V.A., and Kniseley, R.N., *Anal. Chem.*, 1974, **46**, 210.

155. Carey, J.M., and Caruso, J.A., *Crit. Rev. Anal. Chem.*, 1992, **23**, 397.

156. Aziz, A., Broekaert, J.A.C., and Leis, F., *Spectrochim. Acta Part B*, 1982, **37**, 369.

157. Crabi, G., Cavalli, P., Achilli, M., Rossi, M., and Omenetto, N., *At. Spectrosc.*, 1982, **3**, 81.

158. Gunn, A.M., Millard, D.L., and Kirkbright, G.F., *Analyst*, 1978, **103**, 1066.

159. Ng, K.C., and Caruso, J.A., *Anal. Chim. Acta*, 1982, **143**, 209.

160. Mei, E., Jiang, Z., and Liao, Z., *Fresenius' J. Anal. Chem.*, 1992, **344**, 54.

161. Park, C. J., Van Loon, J. C., Arrowsmith, P., and French, J. B. *Can. J. Spectrosc.*, 1987, **32**, 29.

162. Tsukahara, R., and Kubota, M., *Spectrochim. Acta Part B*, 1990, **45**, 779.

163. Kitazume, E., *Anal. Chem.*, 1983, **55**, 802.

164. Smythe, L.E., *ICP Inf. Newslett.*, 1980, **6**, 224.

165. Dittrich, K., Berndt, H., Broekaert, J.A.C., Schaldach, G., and Toelg, G., *J. Anal. At. Spectrom.*, 1988, **3**, 1105.

166. Levine, K., Wagner, K.A., and Jones, B.T., *Appl. Spectrosc.*, 1998, **52**, 1165.

167. Nimjee, M.C., Barefoot, R.R., Balicki, M.A., and van Loon, J.C., *Spectrosc. Lett.*, 1984, **17**, 245.

168. Marawi, I., Olson, L.K., Wang, J., and Caruso, J.A., *J. Anal. At. Spectrom.* 1995, **10**, 7.

169. Park, C.J., and Hall, G.E.M., *J. Anal. At. Spectrom.*, 1988, **3**, 355.

170. Sturgeon, R.E., and Chakrabarti, C.L., *Anal. Cham.*, 1977, **49**, 90.

171. Grunke, K., Stark, H. -J., and Ortner, H. M. *Spectrochim. Acta Part B*, 1997, **52**, 1545.

172. Wildner, H. and Wuensch, G., *Fresenius' J. Anal. Chem.* 1998, **360**, 520.

173. Swaidan, J.M., and Christian, G.D., *Can. J. Spectrosc.*, 1983, **28**, 177.

174. Ren, J.M. and Salin, E.D. *J. Anal. At. Spectrom.*, 1993, **8**, 59.

175. Shen, W.L.,Caruso, J.A., Fricke, F.L., and Satzger, R.D., *J. Anal. At. Spectrom.*, 1990, **5**, 451.

176. Isoyama, H., Okuyama, S., Uchida, T., Takeuchi, M., Iida, C., and Nakagawa, G., *Anal. Aci.*, 1990, **6**, 555.

177. Karanassios, V., Ren, J.M., and Salin, E.D., *J. Anal. At. Spectrom.*, 1991, **6**,527.

178. Goltz, D.M. and Salin, E.D., *J. Anal. At. Spectrom.*, 1997, **12**, 1175.

179. Goltz, D.M., Skinner, C.D. and Salin, E.D., *Spectrochim. Acta Part B*, 1998, **53**, 1139.

180. Karanassios, V., Bateman, K.P., and Speirs, G.A., *Spectrochim. Acta Part B*, 1994, **49**, 847.

181. Karanassios, V., Drouin, P., and Reynolds, G.G., *Spectrochim. Acta Part B*, 1995, **50**, 415.

182. Kántor, T., *Spectrochim. Acta Part B*, 1988, **43**, 1299.

183. Ediger, R.D., and Beres, S.A., *Spectrochim. Acta Part B*, 1992, **47**, 907.

184. Carey, J.M., Evans, E.H., Caruso, J.A., and Shen, W.L., *Spectrochim. Acta Part B*, 1991, **46**, 1711.

185. Alary, J.-F., Hernandez, G., and Salin, E.D., *Appl. Spectrosc.*, 1995, **49**, 1796.

186. Matusiewicz, H., Fricke, F.L., and Barnes, R.M., *J. Anal. At. Spectrom.*, 1986, **1**, 203.

187. Millard, D.L., Shan, H.C., and Kirkbright, G.F., *Analyst*, 1980, **105**, 502.

188. Kirkbright, G.F., Millard, D.L., and Snook, R.D., *Anal. Proc.*, 1980, **17**, 16.

189. Dean, J.R., and Snook, R.D., *J. Anal. At. Spectrom.*, 1986, **1**, 461.

190. Kántor, T., Belzúr, L., Sztatisz, J., and Pungor, E., *Talanta*, 1979, **26**, 357.

191. Long, S.E., Snook, R.D., and Browner, R.F., *Spectrochim. Acta Part B.*, 1985, **40**, 553.

192. Schmertmann, S.M., Long, S.E., and Browner, R.F., *J. Anal. At. Spectrom.*, 1987, **2**, 687.

193. Kántor, T., and Zaray, G., *Microchem. J.* 1995, **51**, 266.

194. Sturgeon, R.E., Willie, S.N., Zheng, J., Kudo, A., Grégoire, D.C. *J. Anal. At. Spectrom.* 1993, **8**, 1053.

195. Hughes, D.M., Chakrabarti, C.L., Goltz, D.M., Grégoire, D.C., and Byrne, J.P., *Spectrochim. Acta Part B*, 1995, **50**, 425.

196. Grégoire, D.C., and Sturgeon, R.E., *Spectrochim. Acta Part B.*, 1993, **48**, 1347.

197. Fonseca, R. W.; and Miller-Ihli, N. J., *Appl. Spectrosc.* 1995, **49**, 1403.

198. Fonseca, R.W.; Miller-Ihli, N.J.; Sparks, C.; Holcombe, J.A.; and Shaver, B., *Appl. Spectrosc.* 1997, **51**, 1800.

199. Kirkbright, G.F., and Snook, R.D., *Anal. Chem.*, 1979, **51**, 1938.

200. Kántor, T., Bezúr, L., Pungor, E., and Winefordner, J.M., *Spectrochim. Acta Part B*, 1983, **38**, 581.

201. Ren, J.M., and Salin, E.D., *Spectrochim. Acta Part B*, 1994, **49**, 555.

202. Ren, J.M., and Salin, E.D., *Spectrochim. Acta Part B*, 1994, **49**, 567.

203. Barnes, R.M., and Fodor, P, *Spectrochim. Acta Part B*, 1983, **38**, 1191.

204. Matousek, J.P., Satumba, R.T., and Bootes, R.A., *Spectrochim. Acta Part B*, 1989, **44**, 1009.

205. Kirkbright, G.F., and Snook, R.D., *Appl. Spectrosc.*, 1983, **37**, 11.

206. Ng, K.C., and Caruso, J.A. *Analyst*, 1983, **108**, 476.

207. Wanner, B., Richner, P., and Magyar, B., *Spectrochim. Acta Part B*, 1996, **51**, 817.

208. Hu, B., Jiang, Z., Zeng, Y., Zhu, H., *Anal. Sci.*, 1991, **7**, 433.

209. Tao, S.Q., and Kumamaru, T., *J. Anal. At. Spectrom.*, 1996, **2**, 111.

210. Tianyou, P., and Zucheng, J., *J. Anal. At. Spectrom.*, 1998, **13**, 75.

211. Mahoney, P.P., Ray, S.J., Li, G., and Hieftje, G.M. *Anal. Chem.*, 1999, **71**, 1378.

212. Matusiewicz, H., and Barnes, R.M., *Spectrochim. Acta Part B*, 1985, **40**, 41.

213. Hu, B., Jiang, Z., and Zeng, Y., *J. Anal. At. Spectrom.*, 1991, **6**, 623.

214. Cai, B., Hu, B., and Jiang, Z. *Fresenius' J. Anal. Chem.*, 2000, **367**, 259.

215. Matusiewicz, H., *Adv. At. Spectrom.*, 1995, **2**, 63.

216. Richner, P., and Wunderli, S., *J. Anal. At. Spectrom.*, 1993, **8**, 45.

217. Willie, S.N., Grégoire, D.C., and Sturgeon, R.E., *Analyst*, 1997, **122**, 751.

218. Arpadjan, S., and Krivan, V., *Anal. Chem.*, 1986, **56**, 2611.

219. Hall, G.E.M., and Pelchat, J.C., *J. Anal. At. Spectrom.* 1993, **8**, 1059.

220. Mahanti, H.S., and Barnes, R.M. *Anal. Chem.* 1983, **55**, 403.

221. Matusiewicz, H., Fish, J., and Malinski, T., *Anal. Chem.* 1987, **59**, 2264.

222. Marawi, I., Wang, J., and Caruso, J.A., *Anal. Chim. Acta*, 1994, **291**, 127.

223. Sturgeon, R.E., and Grégoire, D.C., *Spectrochim. Acta, Part B*, 1994, **49**, 1335.

224. Alary, J.-F., and Salin, E.D., *Spectrochim. Acta Part B*, 1995, **50**, 405.

225. Bitterli, B.A., Cousin, H., and Magyar, B., *J. Anal. At. Spectrom.*, 19997, **12**, 957.

Chapter 2

Pyrolytically coated graphite direct sample insertion probe for inductively coupled plasma spectrometry

In the course of preliminary experiments undertaken with DSI–ICP–OES, attempts were made at *in situ* wet digestions of biological samples such as blood and plasma in graphite cup sample probes. This proved to be a trying process, however, as the use of strong oxidative agents, such as sulfuric acid or hydrogen peroxide, often resulted in the rapid destruction of the graphite sample support. Additionally, the digestion was difficult to constrain to the cup portion of the sample support, as the sample digest often intercalated through the cup walls onto other elements of the sample support. At this point an attempt was made to coat the interior walls of the graphite cup with a highly ordered layer of graphite as a way of imparting a heightened resistance to chemical attack and physical intercalation to the cup surface. Drawing on the ETV literature, where highly-ordered pyrolytic graphite coatings have been used on sample supports, a method was developed for pyrolytically coating a graphite DSI cup directly in the plasma using gas-phase deposition. This chapter summarizes the method developed and the analytical performance of the pyrolytically coated sample cup with DSI–ICP–OES.

2.1 Abstract

The pyrolytic coating of a graphite cup direct sample insertion (DSI) probe for inductively coupled plasma (ICP) spectrometry is described. Deposition of a pyrolytic coating on the inside walls of the DSI cup was achieved by heating the device in a 2 kW argon plasma while directing a gaseous mixture of 10% methane in argon (v/v) to the graphite cup interior. A narrow channel hollowed into the stem of the graphite cup facilitated introduction of the methane/argon mixture. A factorial study revealed that the procedure generated optimum results when the coating was applied for at least 10 minutes at a flow rate of 500 ml min^{-1}. Peak area and height reproducibility improvements for Cd, Cu, Mg, Pb, and Zn ranged from 1.7–3.4% and 2.1–6.7% RSD respectively when a pyrolytically coated DSI cup was used, versus 3–7% and 5–12% RSD when no coating was used. The abatement of multiple peaking and an increase in transient signal intensity was observed for all elements except Cu, translating into roughly a two-fold improvement in peak height limit of detection (LOD) when a pyrolytically coated DSI probe is used. Scanning electron microscopy and Raman spectroscopy of the DSI cup interior confirm the deposition of a uniform pyrolytic phase of high crystalline order on the DSI cup.

2.2 Introduction

In order to improve the performance of ICP–AES and ICP–MS alternate sample introduction methods, including electrothermal vaporization (ETV) and direct sample insertion (DSI), have been demonstrated to be viable options.[1] These approaches require less sample volume and demonstrate higher sample-transport efficiency than pneumatic nebulization and the ability to perform drying, ashing, and pyrolysis steps *ex situ* of the

plasma allows many matrix effects and spectral interferences to be minimized.[2,3] Although vaporization from metal surfaces has been investigated, graphite is widely accepted as the most suitable material for ETV cuvette and platform as well DSI probe composition.[4] Conventional graphite, however, is replete with pores and interstices, and thus highly prone to sample intercalation which results in poor signal reproducibility. The foliate surface morphology of polycrystalline graphite also makes it extremely susceptible to oxidation, which occurs by preference at lattice defects and laminae edges.[5] The use of highly crystalline ordered graphite, such as pyrolytically coated and totally pyrolytic graphite, as a means by which intercalation and surface oxidation can be diminished, has long been advocated in electrothermal atomic absorption spectrometry (ETAAS),[6,7] and has been applied to ETV–ICP since its inception.[8] While total pyrolytic carbon components for ETV require special manufacturing processes, pyrolytic coating of polycrystalline graphite can be conveniently performed *in situ via* high temperature gaseous deposition.[9,10] There has been speculation as to the potential benefits of a pyrolytically coated DSI cup probe,[11] but no successful means of accomplishing this have been reported. The recent description of a graphite DSI cup with a hollow stem to facilitate the introduction of gases directly into the cup[12] presents a means by which *in situ* gaseous deposition of pyrolytic graphite on the vaporization surface of a DSI cup can be accomplished.

The characterization of thin graphite films by SEM[13] and Raman spectroscopy[14,15] has been performed previously with the SEM technique fulfulling a primarily qualitative role and Raman a more quantitative one. Typically, two features in graphite Raman spectra predominate: an omnipresent peak at 1580 cm^{-1}, which corresponds to an E_{2g}

mode, predicted as the only Raman active transition based on group theory arguments for an infinite graphite lattice; and a less intense, broad peak at 1350 cm^{-1}, commonly referred to as a disorder transition (*D*), which arises as a result of the finite size of graphite crystallites. Furthermore, it has been demonstrated that the ratio of the intensities of the *D* and E_{2g} transitions is inversely proportional to the crystallite size,[14] *i.e.*:

$$\frac{I_D}{I_{E_{2g}}} \propto L_a^{-1} \qquad \text{(Eqn. 2.1)}$$

where I_D is the intensity of the disorder transition, $I_{E_{2g}}$ the intensity of the E_{2g} transition, and L_a the crystallite size. As pyrolytic graphite will have crystallites of larger size than those found in polycrystalline graphite, the above may be used as an indicator of the crystalline order, and hence the quality of the pyrolytic coating.

The aim of this study was to apply the method of deposition of a coating of pyrolytic graphite on the interior walls of a graphite cup DSI probe, to characterize the pyrolytic deposition, and to evaluate the effectiveness of the deposition process and the performance of the coated DSI cup for ICP spectrometry.

2.3 Experimental

Graphite DSI probes were machined in house from graphite electrodes (#S-8 HD, Bay Carbon, Bay City, MI, USA) using high speed steel tools on a benchtop lathe (Emco Compact 5, Emco Maier, Columbus, OH, USA). Details of the machining procedure have been previously described,[12] with the dimensions of the probe and its components given in Fig. 2-1. The two principal design constraints for the probe were (*i*) that it

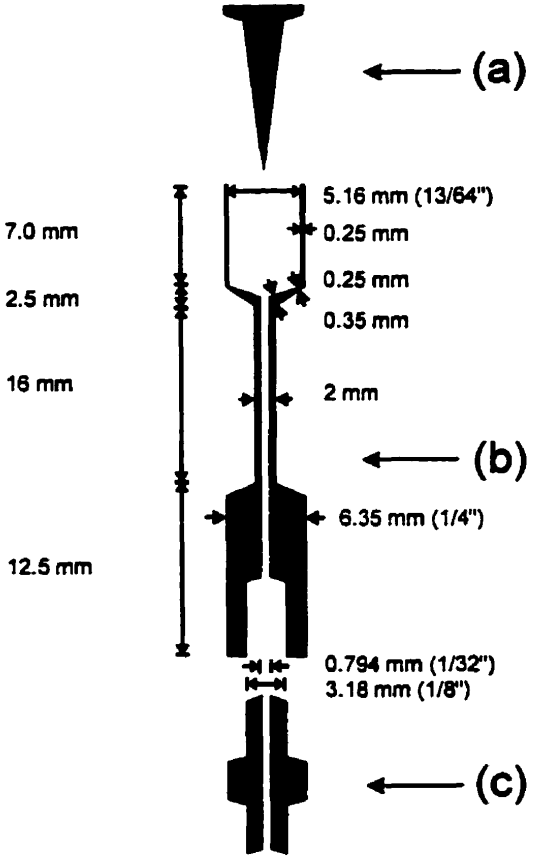

Figure 2-1 Dimensions of DSI probe and components: (a) 'tack'; (b) sample probe; (c) connector. Measurements in Imperial units (except for diameter of probe base) indicate dimensions of tools used for machining component indicated.

should have a hollow stem, and (*ii*) that it should be of a thin-walled, undercut design. The first consideration allowed the introduction of the pyrolytic coating gas mixture to the inside of the DSI cup, and the latter ensured that the probe was heated efficiently and attained sufficiently high temperatures for both pyrolytic deposition and for analyte volatilization.[16,17] A graphite union with a hollow center [Fig. 2-1] facilitated the connection of the DSI probe to the hollow glass shaft of the DSI assembly.

The direct sample insertion device (DSID) and plasma source used in this study have been described previously.[12] The DSID was mounted on a 27.12 MHz inductively

coupled plasma unit (HFP-2500, Plasma Therm, Inc., Kresson, NJ, USA) with an automatching network (AMN-2500E, Plasma Therm, Inc.). Spectra were obtained by imaging the plasma onto the entrance slit of a direct reader (Model 750, Thermo Jarrell Ash, Franklin, MA, USA) that has been modified to meet the demands of transient signal processing.[18] These modifications include a galvanically driven quartz refractor plate for background correction, and high-speed electronics (Trulogic Systems, Mississauga, ON, Canada). Signal processing was handled by software authored in-house by G. Légère (SF20). Grams/32 (Galactic Industries Corp., Salem, NH, USA) was used for interpretation of transient signals.

A summary of the instrumental parameters used for pyrolytically coating DSI probes and for sample introduction and analysis is given in Table 2-1. The top of the load coil is used as a reference point by which insertion depth is measured for both the coating process and sample introduction. The insertion of a DSI cup to a position such that the top of the DSI probe is even with the top of the load coil is designated as 0 mm above the top of the load coil (0 mm ATOLC). The convention follows that positions above 0 mm ATOLC be designated by positive values, and positions below by negative values.

Throughout this study the *in situ* coating process was conducted using a 2.0 kW argon plasma and a 10% (v/v) mixture of methane in argon. A minimum in the density of the deposited graphite surface is experienced around 1600 °C at atmospheric pressure, with the density approaching the theoretical value for graphite below 1200 °C and above 2000°C.[19] The crystalline order of the surface also improves with increasing temperature. A 2.0 kW plasma was used to heat the probe to a temperature in excess of 2000 °C,[20,21]

Table 2-1 Instrumental Settings

Pyrolytic Coating Process—	
Plasma forward power	2.0 kW
Reflected power	0 - 8 W
Plasma gas flow rate	16 l min^{-1}
Auxiliary flow rate	2 l min^{-1}
Coating gas flow rate	100, 250, 500, 750 ml min^{-1}
Coating time	1, 5, 10, 15 min
Insertion depth	0 mm ATOLC
Direct Sample Insertion Analysis—	
Plasma forward power	1.25 kW
Reflected power	0 - 5 W
Plasma gas flow rate	14 l min^{-1}
Auxiliary flow rate	1.6 l min^{-1}
Sample volume	25 µl
Sample concentration	400 ppb in each element
Insertion depth	0 mm ATOLC[a]
Viewing height	20 mm ATOLC[a]
Insertion time	15 s
Exposure time	20 ms / position
Number of exposures / trace[b]	300
Galvanometer settle time	3 ms
Probe Cleaning—	
Plasma forward power	1.75 kW
Reflected power	0 - 8 W
Plasma gas flow rate	16 l min^{-1}
Auxiliary flow rate	2 l min^{-1}
Insertion depth	0 mm ATOLC
Insertion time	45 s
Cooling time	2 min

[a] ATOLC: above top of load coil.
[b] Includes both on-line and off-line exposures.

sufficiently high that advantage could be taken of this phenomenon, as the density minimum would be avoided. The percentage of methane in the argon carrier was fixed at 10% as the literature[9,10,19] suggests that 15% (v/v) for most hydrocarbon–carrier gas mixtures appears to be an approximate upper limit before excessive soot formation occurs.

The coating process was initiated by the ignition of a 2.0 kW plasma, and insertion

of the DSI probe to a position of 0 mm ATOLC in the plasma. The gases for the coating process were then introduced in sequence: first the argon carrier gas; followed by the methane component. The starting time of the coating process was marked by the opening of the methane inlet, which was typically followed by the appearance of a bright green C_2 Swan band emission in the plasma. The coating process was then terminated by the removal of the gas mixture in the opposite sequence from the initiation. Although closing the methane flow was used to mark the stop time for the coating process, it should be noted that the green emission from methane in the plasma disappeared gradually after about 1 min.

After the probe has been left in the plasma for one additional minute to anneal the newly formed pyrolytic coating, the plasma was extinguished, and the probe was allowed to cool for 3–5 min. The DSI probe was then removed from the sample introduction assembly and physically examined. If soot had accumulated in the well of the DSI cup or adhered to the surface of the probe, it was removed, first by gently shaking out the probe contents, and then, if need be, gently breaking off any hard amorphous carbon residue. Hard soot formation was typically only observed at the top edge of the probe, and could be removed by tweezers. Soot accumulation on the outside walls, stem or base of the probe was not viewed as a problem and was left untouched.

The hollow stem of the graphite probe presented a problem if liquid samples were to be introduced into the cup for DSI analysis, as fluid samples would seep down this orifice upon deposition. This problem was corrected by tightly plugging the opening of the hollow stem in the well of the cup with a piece of graphite after completion of the coating process. A graphite electrode machined into the shape of an elongated

'thumbtack' was used to accomplish this [Fig 2.1]. The point of the graphite 'tack' was inserted into the cup until the tip was tightly mated to the hollow stem orifice. The tip was then snapped off flush with the cup base, and the rest of the tack was removed.

In the determination of the optimum conditions for pyrolytically coating the DSI probe, a full factorial study of four flow rates for the methane/argon mixture (100, 250, 500 and 750 ml min^{-1}) and four coating periods (1, 5, 10, and 15 min) was performed. Several criteria, both objective and subjective, were employed in evaluating the effectiveness of each set of conditions. These included: (*i*) physical examination of the coating by eye and under a microscope; (*ii*) the presence or absence of visible liquid sample seepage from the interior to the exterior of the probe; (*iii*) the intensity, reproducibility, and appearance of transient signals for various analytes by DSI; and later in the study (*iv*) analysis by scanning electron microscopy and Raman spectroscopy.

Multi-element (Cd, Cu, Mg, Pb and Zn) standard solutions were used for the majority of the DSI study. The focus of this study was on the analysis of relatively volatile, non-refractory elements since the preferential volatilization of analytes in DSI due to sample intercalation is most pronounced with these elements. Standard solutions were prepared by successive dilution of multi-element standards (SCP Science, St-Laurent, QC, Canada) with 5% trace metal grade nitric acid (Instra-Analyzed, J.T. Baker, Phillipsburg, NJ, USA) in distilled deionized water (Milli-Q water system, Millipore Corp., Bedford, MA, USA). In the deposition of a sample, the DSI probe was first elevated to a position of about 50 mm ATOLC. A 25 µl sample of the multielement standard was transferred into the bottom of the cup. The probe was then positioned at 0

mm ATOLC and dried *via* induction heating in the load coil for 1.5 minutes at 50–100 W forward power. The probe was subsequently retracted to the lowest point of the device travel, and the plasma was ignited and set to 1.25 kW forward power. A stepper motor was then used to elevate the probe to a height of –20 mm ATOLC, where the DSI device was halted for two seconds (2 s), to allow for stabilization of the plasma,[12] followed finally by the introduction of the cup to 0 mm ATOLC in the plasma. The data acquisition was started at the stabilization position, to avoid the possibility of missing part of an analyte emission event.

Scanning electron micrographs of the inside wall of the DSI cups were obtained by breaking away a portion of the probe wall to expose the cup interior. Micrographs were acquired with a Jeol 840A scanning electron microscope (Jeol USA, Peabody MA, USA), with an accelerating voltage of 1 kV being used throughout. The following information is displayed from left to right on the bottom of the micrographs: SEM micrograph number; acceleration voltage, in kV; the scale of the micrograph, in μm; and the working distance, *i.e.*, the distance from the final electromagnetic lens of the SEM to the surface of interest, in mm.

Raman spectra of the inner walls of both pyrolytically coated and uncoated DSI probes were obtained using a system based on a 0.74 m single focal length monochromator equipped with a liquid N_2 cooled 1024×256 element charge coupled device (CCD) detector (JY Spex 740 M, Jobin Yvon-Spex Instruments, S.A. Inc., Edison, NJ, USA). Excitation was provided by the 514.5 nm line of an argon ion laser (Coherent Innova, Coherent Inc., Santa Clara, CA, USA). A power setting of 2W was used for all

spectra. The walls of the DSI cups were broken away in a radial pattern until only a narrow portion of the wall, of the order of a few millimeters across, remained attached to the probe. Spectra were obtained for the inside wall of an uncoated probe (single measurement) and for a pyrolytically coated probe, in 1 mm and 0.5 mm increments along the height of the probe wall, starting at a height of approximately 0.5 mm from where the wall meets the base of the DSI cup.

2.4 Results and discussion

2.4.1 Optimization

The best results for the pyrolytic coating process were attained when a flow rate of 500 ml min^{-1} for the 10% methane in argon mixture was used, and the coating process in the 2 kW plasma was carried out for a minimum of 10 min. Of the two variables investigated, the flow rate of the coating gas mixture proved to be the most important in the factorial design. Flow rates of 100 and 250 ml min^{-1} proved to be insufficient, even after a 15 min coating period, as only the lower part of the DSI cup showed signs of pyrolytic graphite deposition. This incomplete coating was accompanied by an appreciable amount of amorphous carbon (soot) accumulation in the cup, suggesting that complete pyrolysis in the gaseous phase was occurring before the hydrocarbon mixture could coat the higher portions of the probe. Flow rates of 500 and 750 ml min^{-1} resulted in the deposition of a coating over the entire cup interior, with little to no soot accumulation. When liquid samples were deposited into the probe coated at 750 ml min^{-1}, "wetting" of the outside wall and stem of the DSI probe was observed after only a few sample insertions, indicating that the coating had failed to prevent sample intercalation. This behavior was

not observed for the deposition carried out at 500 ml min $^{-1}$. It is suspected that the relatively high flow rate of 750 ml min^{-1} subjected the DSI cup walls to an excessive cooling effect, resulting in a pyrolytic coating of relatively low density and poor crystalline order being deposited.

Fig. 2-2 shows the mass of carbon added to the probe plotted against the time for the pyrolytic coating process. The deposition process appears to be a linear function of time for all of the flow rates studied, with lower flow rates resulting in greater deposition rates. It is important to note, however, that the mass added reflects the sum of carbon deposited, irrespective of its being in the form of pyrolytic graphite or amorphous carbon. Thus at flow rates of 250 ml min^{-1} and less, where soot comprised a great percentage of the carbon deposited, the total mass added to the probe was a poor reflection of the amount of pyrolytic graphite deposited. When the amorphous carbon residue was extracted from the probe, the mass remaining was more representative of the amount of pyrolytic graphite deposited. This adjusted rate of mass deposition was considerably lower by comparison with those observed at higher coating flow rates where soot accumulation was minimal and the bulk of the deposit was pyrolytic graphite [Fig. 2-2]. With the practice of soot removal in place, the highest rate of pyrolytic graphite deposition appeared to occur at a flow rate of 500 ml min^{-1}.

2.4.2 Characterization

The image of an uncoated DSI probe made of polycrystalline graphite is provided in Fig. 2-3(a). The surface was extremely foliate and laden with cavities, with individual polycrystalline grains of graphite easily discernible on the surface. Repeated use of the

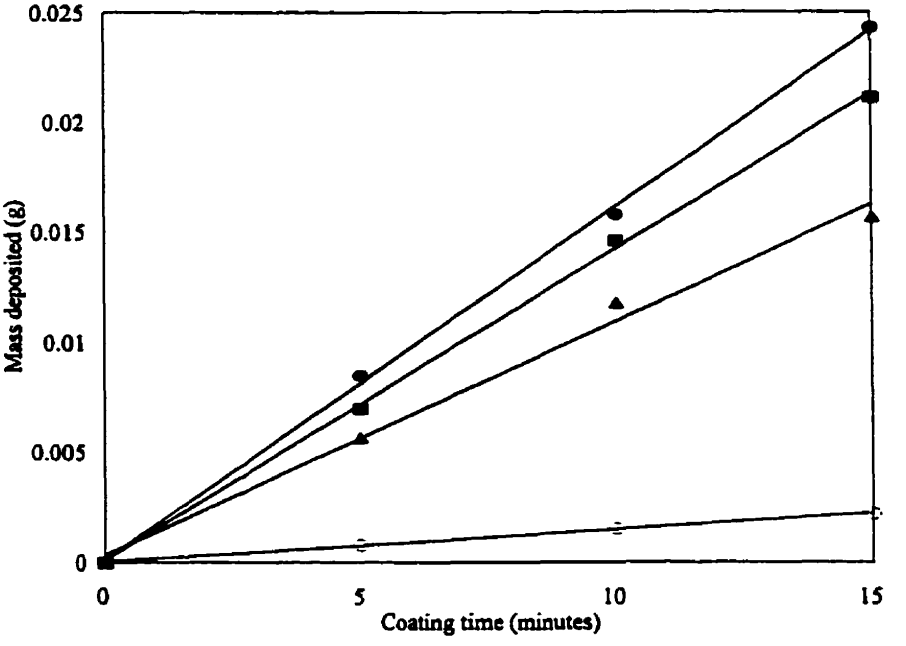

Figure 2-2. Mass of carbon deposited as a function of time for various flow rates of the DSI probe pyrolytic coating process. (●, 250 ml min^{-1}; ■ , 500 ml min^{-1}; ▲,750 ml min^{-1}; O, 250 ml min^{-1} after the removal of amorphous carbon deposit). All coatings were done at 2 kW plasma forward power, 10% methane in Ar, at 0 mm ATOLC.

uncoated surface [Fig. 2-3(b)] resulted in a roughening of the surface morphology and the growth of amorphous carbon nodules consistent with that observed in ETV.[13] The increase in roughness results in part from the expansion–contraction stresses undergone by the graphite when heated in the harsh plasma environment, but more so from the volatilization of small graphite crystallites and graphite binder material upon intense probe heating. The nodular soot formations observed in Fig. 2-3(b) are a result of the vaporized graphite material recondensing on relatively cooler parts of the probe surface, namely protruding surface elements which are more susceptible to cooling by gas flows in the plasma atmosphere. In comparison, the appearance of the pyrolytically coated DSI probe, shown in Figs. 2-3(c) and 2-3(d), presents a compelling visual argument

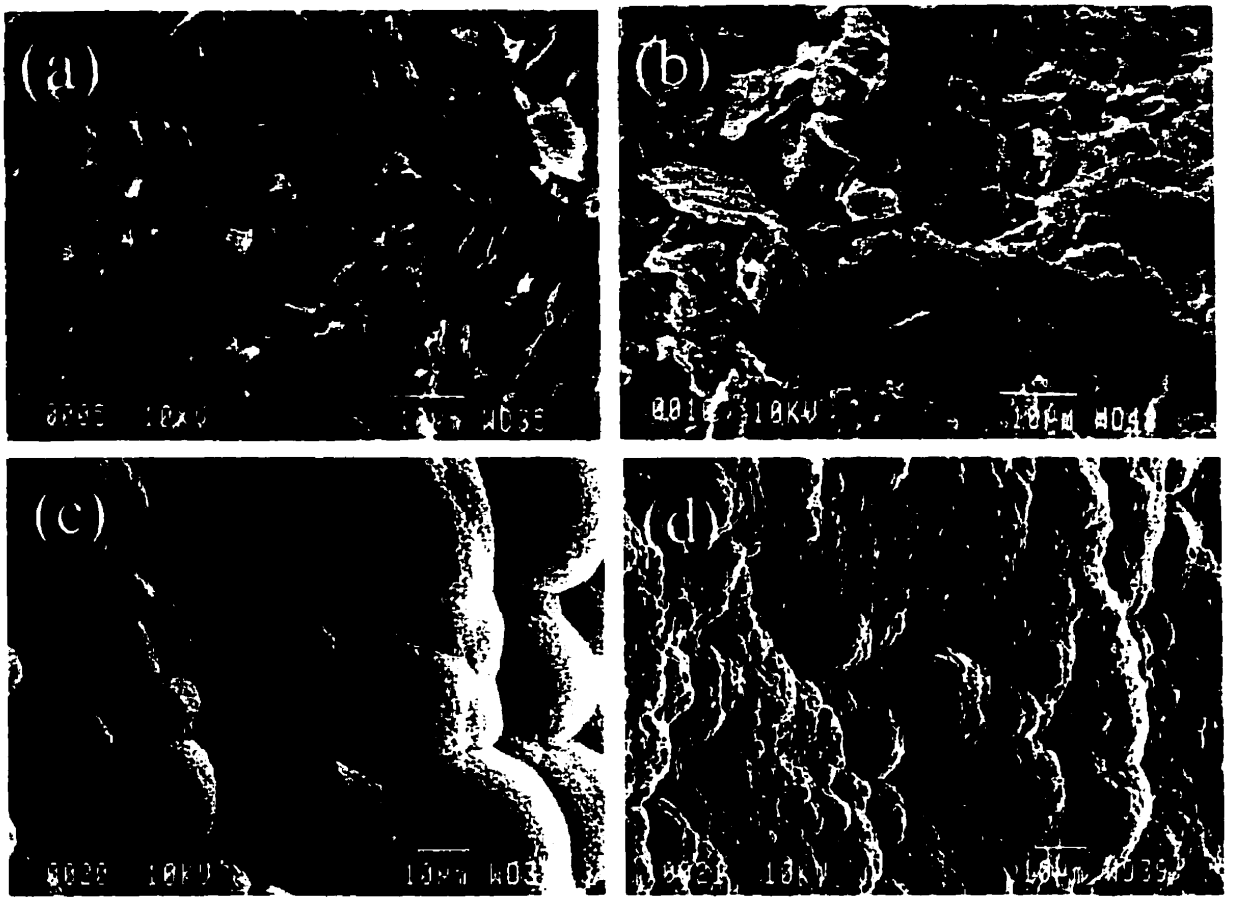

Figure 2-3 Scanning electron micrographs of the inside wall of (a) an unused, uncoated probe; (b) an uncoated probe used for 25+ sample insertions; (c) a pyrolytically coated, unused probe; (d) a pyrolytically coated probe used for 25+ sample insertions. DSI probes in (c) and (d) were coated at 2.0 kW plasma forward power, 10% methane in Ar at 500 ml min^{-1}, for 10 minutes, at 0 mm ATOLC. All figures are at 1000× magnification.

advocating the coating process. The pyrolytic coating, although highly nodular in appearance, was much smoother than the uncoated surface and virtually free of pores. When a DSI probe was made from polycrystalline graphite, the machining process smoothed the material surface to a certain extent, but in spite of this action, the surface of the graphite remained quite jagged and uneven [Fig. 2-3(a)]. It is on this imperfect substrate that the coating process must be initiated, and the presence of these asperities,

depressions and foreign particles causes nodules to form. Incipient carbon nuclei in the gas phase, resulting from a sufficiently high concentration gradient of gaseous hydrocarbon, results in a coating mechanism called continuous nucleation which also causes nodule formation.[22] With repeated use, the pyrolytically coated probe still appears smooth [Fig. 2-3(d)], but small imperfections and soot nodules start to appear. These features are the result of processes identical to those described for Fig. 2-3(b).

The Raman spectra of the interior wall of a pyrolytically coated and an uncoated polycrystalline are compared in Fig. 2-4. The spectra have been background corrected to reduce fluorescence and scattering contributions to the spectra, and normalized to the height of the E_{2g} peak (~ 1580 cm^{-1}). The omnipresent 1580 cm^{-1} peak was slightly sharper for the coated probe, and as expected the 1335 cm^{-1} transition was stronger in the uncoated probe spectrum. The ratio of intensities for these two peaks (Equation 2.1) was 0.324 and 0.115, obtained for the uncoated and pyrolytically coated probes, respectively. This indicates that the graphite crystallites were around three times larger in the pyrolytic coating and implies a higher crystalline order. In comparison, a commercially manufactured pyrolytically coated graphite surface such as those used in ETV typically has an E_D / E_{2g} intensity ratio an order of magnitude less and crystallites upwards of five times larger than that observed for commercial graphite.[14,15] The disparity in these values can be attributed to the fact that the commercial pyrolytic coatings are generated under more controlled conditions in comparison with the in-plasma coating technique described here. A pyrolytic coating for an ETV tube is also deposited on a graphite substrate two orders of magnitude thicker and much smoother than the walls of a DSI probe: the thicker surface ensures uniform heating of the substrate, and the smoother surface permits a more

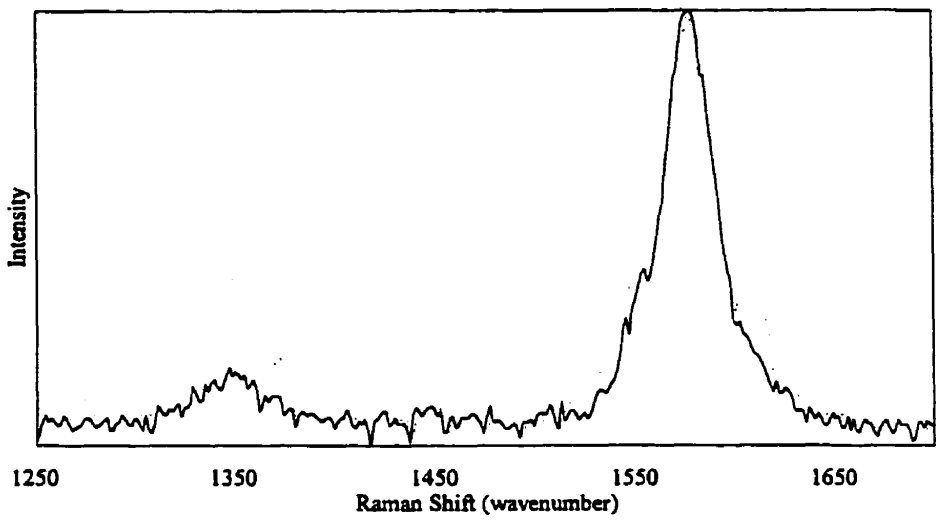

Figure 2-4 Raman spectra of the interior wall of pyrolytically coated and uncoated DSI probes. The pyrolytically coated DSI probe was coated at 2.0 kW plasma forward power, 10% methane in Ar at 500 ml min^{-1}, for 10 minutes, at 0 mm ATOLC. (———, pyrolytically coated probe; ·····, uncoated probe).

ordered growth process to initiate.

Characterization of the graphite coating along the height of the probe wall by Raman spectroscopy is illustrated in Fig. 2-5, with the intensity ratios for the peaks summarized in Table 2-2. Inspection of this data verifies that the entire wall of the probe was coated in the deposition process, and the coating was relatively uniform although a slight decrease in crystallite size is apparent with increasing wall height.

2.4.3 Analytical performance

Once the DSI probes had been coated, cleaned and plugged, upwards of five sample insertions are needed before stable signals are achieved. For this study, probes were fired 10 times before analytical signals were recorded. This type of 'breaking in' period is common to other sample introduction methods where pyrolytic coatings are used.[23,24]

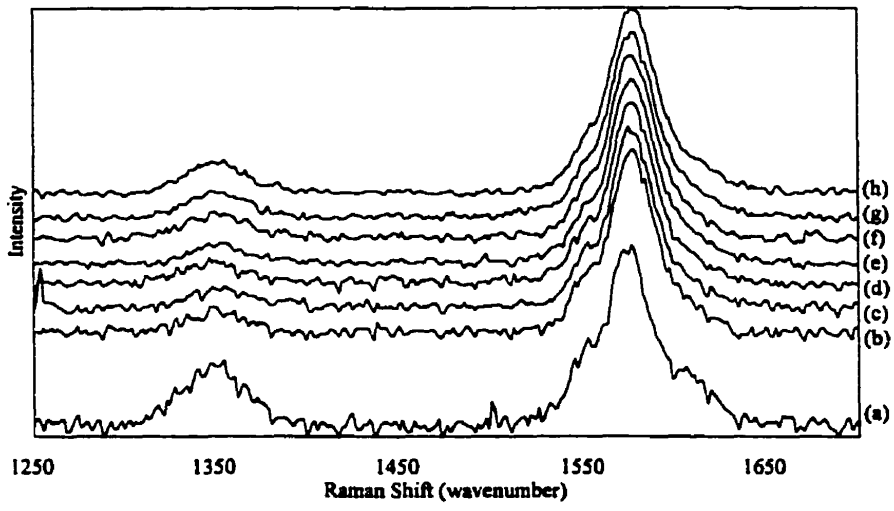

Figure 2-5 Raman spectra of the interior wall of: (a) an uncoated probe; and a pyrolytically coated probe, at a height of (b) 0.5 mm; (c) 1.5 mm; (d) 2.5 mm; (e) 3.0 mm; (f) 3.5 mm;, (g) 4.0 mm; and (h) 4.5 mm from the bottom of the interior wall. The pyrolytically coated DSI probe was coated at 2.0 kW forward power, 10% methane in Ar at 500 ml min^{-1}, for 10 minutes, at 0 mm ATOLC.

Table 2-2 Intensity ratios of peaks in Raman spectra

Raman spectrum[a]	Height on cup wall relative to base (mm)	$\frac{I_D}{I_{E_{2g}}}$
a	-	0.324
b	0.5	0.115
c	1.5	0.113
d	2.5	0.132
e	3.0	0.135
f	3.5	0.139
g	4.0	0.138
h	4.5	0.148

[a] Corresponds to label in Fig. 2.5

Fig. 2-6 demonstrates the effect of the deposition time (at 500 ml min^{-1}) on the DSI volatilization of a 25 µl sample of a 400 ppb multi-element standard. Notwithstanding copper, multiple peaking was observed for analytes volatilized from

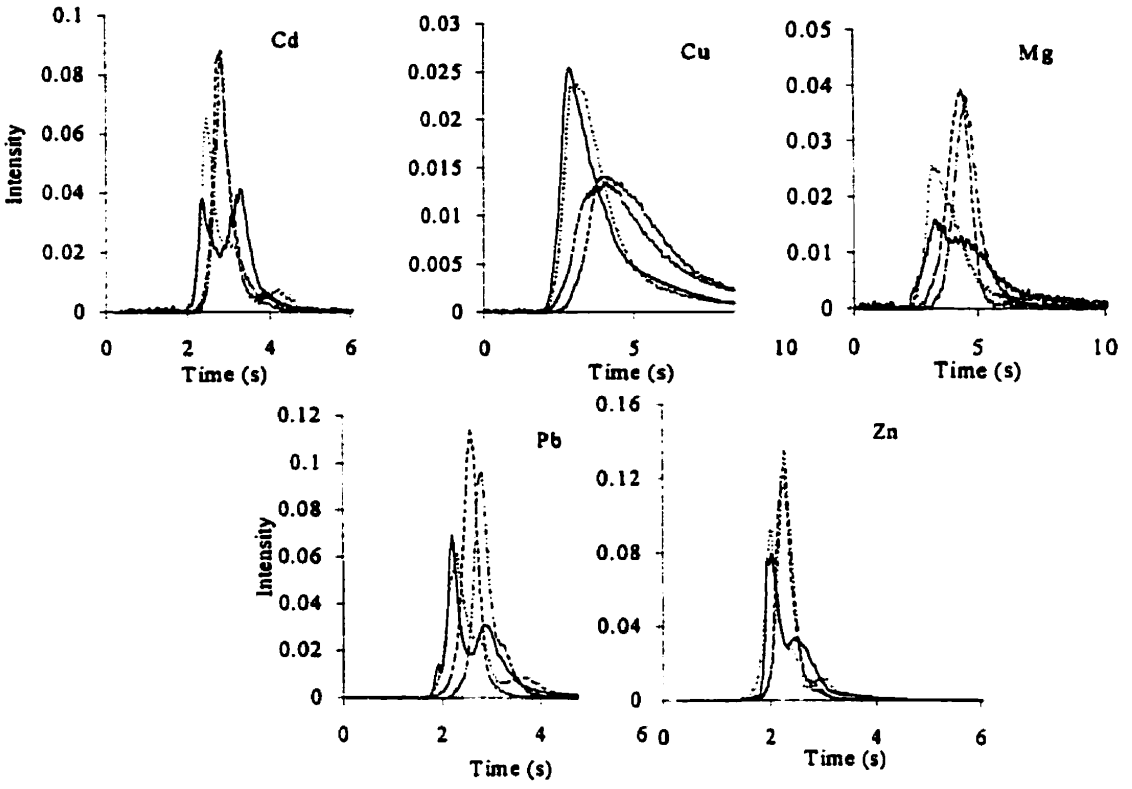

Figure 2-6 Emission signals for Cd (228.8 nm); Cu (324.8 nm); Mg (279.6 nm); Pb (220.4 nm); Zn (213.9 nm) for DSI probes pyrolytically coated for different time durations. (——, 0 min; — — —, 1 min; ------, 5 min, — - — -, 10 min). DSI probes in all cases were coated at 2 kW plasma forward power, 10% methane in Ar at 500 ml min^{-1}, at 0 mm ATOLC.

probes coated for relatively short times (1 and 5 min) and from an uncoated probe. Seepage of liquid from the cup interior to the outside walls and stem of the cup was also observed upon sample deposition in these cases. When the coating process was carried out for 10 min or longer, sharp, single peaks were observed for these elements. The visually detectable sample intercalation witnessed earlier was also absent in these instances. These observations suggest that the multiple peaks in the transient signals represent the volatilization of analyte deposited over a spatial distribution. When a DSI probe is inserted into an inductively coupled plasma, it undergoes extremely rapid heating

until the maximum temperature of the probe is attained. This means that the vaporization of elements with relatively low volatilization temperatures occurs at a time when the probe is undergoing a rapid temperature change and significant temperature disparities between spatial regions of the probe exist; the result is an enhanced severity in preferential volatilization due to sample intercalation. The earliest peak in the transient signal, usually quite sharp and intense in appearance, most likely represented volatilization of analyte that had been deposited on the outermost surface elements of the probe. This type of analyte accumulation would undergo relatively rapid heating and would be the most freely volatilized. The second peak of the transient signal was representative of the volatilization of analyte which had intercalated deeper into the graphite. The later appearance time and broader appearance of this signal results as this analyte deposit experiences less intense heating and undergoes repeated volatilization and condensation as progress from the inner laminae of the graphite to the outer surface is made. The ability of a pyrolytically coated DSI probe to confine analyte more so to the surface of the probe and abate deep sample intercalation will reduce the spatial distribution of analyte in the probe material and thus mitigate this type of preferential volatilization.

The transient signals for copper, in comparison with the previous elements, exhibit strikingly different behavior as a function of pyrolytic coating time. The multiple peaking observed with other elements was absent when an uncoated polycrystalline graphite probe was used, and the presence of a pyrolytic deposition decreased the intensity of the signal, shifted the emission maximum to a later appearance time, and caused the transient signal to broaden and tail [Fig. 2-6]. The absence of multiple peaking in the uncoated probe Cu

signal can be accounted for by the fact that the vaporization temperature of Cu is relatively high when compared with the other elements tested, and much closer to the maximum temperature that the DSI probe reached upon insertion into the plasma. Consequently, the volatilization of Cu occurs at a point in time where the probe is not undergoing a rapid change in temperature and the temperature throughout the probe is more uniform. As for the broad, tailing appearance of the pyrolytically coated probe Cu signal, one must consider the fact that the coating process resulted in the deposition of graphite, which as previously mentioned, increased the mass of the probe. The increased mass of the inserted portion of the probe lowers the maximum temperature attainable by the probe and decreases the rate of probe heating slightly. With the maximum probe temperature now closer to the volatilization temperature for the Cu, and a decreased rate of temperature change occurring, the broadening of the Cu signal results. Additionally, if it is assumed that conduction is the principle mechanism of heat transfer through the probe, then the poor conduction of heat in pyrolytic graphite in directions perpendicular to the basal planes should also be considered as a contributing factor in the wide appearance of the Cu signal.

The presence of two types of graphite in contact with the sample (the pyrolytic graphite coated on the walls of the probe and the high density electrographite plug inserted into the center channel) presented a dilemma, as the latter is highly susceptible to sample intercalation. When a liquid sample was deposited in the probe, the intercalation of liquid into the graphite plug was visually discernible. The amount of sample that intercalated, however, was a small fraction of sample of the order of the physical volume of the plug itself (< 5 μl), and the extent of intercalation appeared to be confined strictly

to the graphite plug. The latter occurs since about 5 mm of the probe center channel below the base of the cup is also coated with pyrolytic graphite. When the practice of blocking the center channel with electrographite is employed, the observed improvement in signal appearance and reproducibility [Fig. 2-6, Table 2-3] appears to support the following arguments: that appreciable preferential volatilization does not occur despite this small amount of sample intercalation; and that the intercalation that occurs is reproducible. Notwithstanding this signal behavior, attempts were made to pyrolytically 'seal' this plug by repeatedly depositing 25 μl of a 5% (m/v) solution of citric acid and inserting the sample into a 2 kW plasma, since the pyrolysis of any suitable hydrocarbon will cause a pyrolytic phase to form.[25] No improvement in signal appearance or reproducibility was observed even after more than 20 sample firings, and in some cases the existing pyrolytic coating was damaged in the process.

For each of the elements studied, the percent relative standard deviation (%RSD) of the peak height and integral signals from both a pyrolytically coated and an uncoated probe were determined [Table 2-3]. In all cases, 10 replicate measurements of a 25 μl, 400 ppb multi-element sample were used. The precision values reported show an improvement for all elements studied with the pyrolytically coated probe, with the most significant improvement generally being the peak height measurement. Included in this observed improvement in signal reproducibility was copper, even though the transient signal showed no drastic visual improvement [Fig. 2.6]. An increase in peak height sensitivity was also observed for all elements except for copper, with little to no change in the amount of noise in blank signal. This resulted in roughly a two-fold improvement in peak height LOD [Table 2-3]. In terms of the useful lifetime of the pyrolytic coating,

Table 2-3 Performance comparison of uncoated and pyrolytically coated DSI probes.

		Signal reproducibility (% RSD)				
		Pyrolytically coated probe		Uncoated probe		
Analyte	Wavelength /nm	Peak area	Peak height	Peak area	Peak height	Relative LOD improvement[b]
Cd	228.8	1.9	3.1	3.1	8.4	1.5
Cu	324.8	1.7	2.6	4.1	4.9	0.5
Mg	279.6	2.3	6.7	7.1	7.0	2.4
Pb	220.4	3.4	2.1	4.6	6.7	2.1
Zn	213.9	2.3	4.4	5.7	12.1	1.8

[a] Pyrolytically coated probe was coated at 2.0 kW plasma forward power, 10% methane in Ar at 500 ml min^{-1}, for 10 min, at 0 mm ATOLC.
[b] Relative LOD improvement determined as the LOD obtained using a coated probe divided by the LOD obtained with an uncoated probe. LOD is defined as 3× the standard deviation of the integrated blank signals divided by the sensitivity, *i.e.*, the slope of the calibration curve.

about 80–100 insertions of the probe into a 1.25 kW plasma could be performed with the peak area sensitivity dropping by only 10–20% for Cd, Mg Pb and Zn. Beyond 100 insertions, serious drops in sensitivity and higher %RSD values were observed. The lifetime of the pyrolytic coating will naturally vary depending upon the conditions of the plasma into which insertion is performed, as well as the nature of the sample and analytes being tested. Endurance tests of pyrolytic graphite media in ETAAS show similar sensitivity drops and precision compromises with time.[23,24] The pyrolytic coating can be renewed by removing the graphite plug and recoating the probe; however, this can only be done a few times before the increase in probe mass appreciably compromises the maximum temperature that the probe can attain upon insertion. When complete failure of the pyrolytic coating occurred, the event was simple to detect, as an unexpected drop in peak height and integral sensitivity was observed. In addition, the appearance of the

transient signal reverted to what would be expected from an uncoated probe and 'wetting' of the probe upon deposition of a new sample was observed.

2.5 Conclusion

The pyrolytic coating process by vapor phase deposition was successfully applied to graphite DSI cup probes. The pyrolytic coating process is facile, renewable and can be performed *in situ* using existing DSI instrumentation with minimal modification. An improvement in reproducibility was observed for both peak height and area parameters when a pyrolytically coated probe was used, and an increase in peak height sensitivity was experienced for most elements in this study, translating into an improvement in LOD by a factor of 1.5–2.5 (element dependent). Although industry is capable of generating superior pyrolytic coatings under more controlled conditions, the cost–benefit ratio of this in-plasma technique is excellent by comparison. The pyrolytically coated DSI probe now presents an environment resistant to liquid intercalation and less prone to the effects of oxidative reagents in which extensive *in situ* sample pretreatment can be performed.

2.6 Acknowledgments

Sincere thanks are extended to Helen Campbell of the Department of Mining and Metallurgical Engineering, for providing the scanning electron micrographs, and to Andrew Vreugdenhil of the Department of Chemistry, for acquiring the Raman spectra. The financial support of the Province of Québec through a Fonds pour la Formation des Chercheurs et l'Aide à la Recherche (FCAR) grant is also gratefully acknowledged.

2.7 References

1. Hall, G.E.M., Pelchat, J.-C., Boomer, D.W., and Powell, M., *J. Anal. At. Spectrom.* 1988, **3**, 791.

2. Karanassios, V., and Horlick, G., *Spectrochim. Acta*, 1981, **44B**, 1361.

3. Karanassios, V., and Horlick, G., *Spectrochim. Acta*, 1989, **44B**, 1387.

4. Karanassios, V., and Horlick, G., *Spectrochim. Acta Rev.* 1990, **13**, 89.

5. Huettner, W., and Busche, C., *Fresenius Z. anal. Chem.*, 1986, **323**, 674.

6. L'vov, B.V., Pelieva, L.A., and Sharnopolsky, A.I., *Zh. Prikl. Spektrosk.*, 1977, **27**, 395.

7 L'vov, B.V., *Spectrochim. Acta*, 1978, **33B**, 153.

8. Matusiewicz, H., *Chem. Inz. Chem.*, 1986, **16**, 75.

9. Clyburn, S. A., Kantor, T., and Veillon, C., *Anal. Chem.*, 1974, **46**, 2213.

10. Manning, D.C., and Ediger, R.D., *At. Absorption Newslett.*, 1976, **15**, 42.

11. Karanassios, V., Abdullah, M. and Horlick, G., *Spectrochim. Acta*, 1990, **45B**, 119.

12. Skinner, C.D., and Salin, E.D., *J. Anal. At. Spectrom.*, 1997, **12**, 725.

13. Welz, B., Schlemmer, G., Ortner, H.M., and Wegscheider, W., *Prog. Analyt. Spectrosc.*, 1989, **12**, 111.

14. Tuinstra, F. And Koenig, *J.L., J. Chem. Phys.*, 1970, **53**, 1126.

15. Yoshikawa, M., Katagiri, G., Ishida, H., Ishtiani, A., and Akamatsu, T., *J. Appl. Phys.*, 1988, **64**, 6464.

16. Barnett, N.W., Cope, M.J., Kirkbright, G.F., and Taobi, A.A.H., *Spectrochim. Acta*, 1984, **39B**, 343.

17. Karanassios, V., Horlick, G., and Abdullah, M., *Spectrochim. Acta*, 1990, **45B**, 105.

18. Légère, G., and Burgener, P., *ICP Inf. Newslett.*, 1987, **13**, 521.

19. Ishikawa, T., and Nagaoki, T. (eds.), *Recent Carbon Technology*, JEC press, 1983, pp. 70-78.

20. Page, A.G., Godbole, S.V., Madraswala, K.H., Kulkarni, M.J., Mallapurkar, V.S., and

Joshi, B.D., *Spectrochim. Acta*, 1984, **38B**, 551.

21. Abdullah, M., and Haraguchi, H., *Anal. Chem.*, 1985, **57**, 2059

22. Coffin, L.F.,Jr., *J. Am. Ceram. Soc.*, 1964, 47, 473.

23. Dymott, T.C., Wassall, M.P., and Whiteside, P.J., *Analyst*, 1985, **110**, 467.

24. Littlejohn, D., Duncan, I.S., Hendry, J.B., Marshall, J., and Ottaway, J.M., *Spectrochim. Acta*, 1985, **40B**, 1677.

25. Mai, S., Nishiyama, Y., Tanaka, T. And Hayashi, Y., *J. Anal. At. Spectrom.*, 1995, **10**, 439.

Chapter 3

Rapid determination of Cu, Fe, Mg, Mn and Zn in wood pulp by direct sample insertion inductively coupled plasma–optical emission spectrometry using a pyrolytically coated graphite sample probe

---

After successfully developing and testing a pyrolytically coated graphite DSI probe, the next logical step was to develop an application in which it would be useful. At this point, the *in situ* wet digestion of blood and plasma samples was revisited. The pyrolytic coating served well at preventing sample intercalation and resisting chemical attack, however, the analysis of these digests was not possible by DSI–ICP–OES, as the concentration levels of the elements of interest (Cd and Pb) in representative samples were below the detection limit of the technique. Although this shortfall could have been overcome by sample preconcentration, it was difficult to devise a safe and effective way of doing this. Consequently, the analysis of biological samples was abandoned.

It was at this time that Kevin Thurbide, then a researcher at the Pulp and Paper Research Centre at McGill University, expressed an interest in developing methods for the determination of metals in wood pulp samples. It was decided that DSI would be a convenient approach to the determination, as the wood pulp samples could be analyzed rapidly with minimal pretreatment. The opportunity was also taken to evaluate the performance of the pyrolytically coated DSI probe for this type of analysis. This chapter

summarizes the method developed and its capabilities, as well as the performance of the pyrolytically coated probe.

3.1 Abstract

A rapid method for screening wood pulp samples by direct sample insertion–inductively coupled plasma–optical emission spectrometry (DSI–ICP–OES) is described. Solid wood pulp samples were introduced directly into an ICP using a pyrolytically coated graphite DSI sample probe, after *in situ* chemical treatment with HCl and NaF. Drying and ashing steps were performed by inductively heating the sample probe in the ICP coil prior to plasma ignition. The analysis time of the method from sample acquisition to analysis was of the order of several minutes per sample, as compared to several hours when conventional dissolution methods are used. Agreement with reference values for wood pulp samples ranged from 3.4–16% (absolute) for high-concentration analytes (Mg, Mn) and 1.7–50 % (absolute) for low-concentration ones (Cu, Fe, Zn) using external standards. Precision ranged from 6–50% RSD and was highly dependent on the element and pulp sample studied. Absolute detection limits for the method were of the range of 50–1000 pg, translating into relative detection limits of 20–400 ppb based on a 2.5 mg pulp sample. The merits of using DSI–ICP–OES for the direct analysis of wood pulps, and of using a pyrolytically coated graphite probe for this type of application are discussed.

3.2 Introduction

The detrimental environmental ramifications from bleaching wood pulps with chlorinated reagents have recently led to increased regulatory pressure to use a totally chlorine free (TCF) bleaching process in the pulp and paper industry.[1] In TCF bleaching, hydrogen

peroxide (H_2O_2) by means of its alkaline reacting species (HOO^-) and decomposition intermediates ($HO\cdot$ and $O_2\cdot^-$) is used to delignify and brighten the pulp. The decomposition of H_2O_2 is integral to the delignification and bleaching processes, but it must be carefully controlled in order to accomplish TCF bleaching efficiently. While the hydroperoxy anion (HOO^-) is primarily responsible for the brightening of the pulp, the hydroxide ($HO\cdot$) and superoxide ($O_2^{-}\cdot$) radicals account for much of its delignification. These radicals, however, only show marginal selectivity towards lignin over cellulose, and destruction of the cellulose results in a lower yield and a weaker pulp. To further complicate matters, certain transition metal species (e.g., MnO_2, Mn^{2+}, Cu^{2+}, and Fe^{2+}) are known to accelerate H_2O_2 decomposition, whereas other species (e.g., Mg^{2+}, SiO_3^{2-}) will inhibit this acceleration.[2] The aforementioned metal species are commonly present in wood, and because of their influence on hydrogen peroxide degradation, there exists an ideal metal content profile for effective TCF bleaching.[3] The metal profile of the pulp sample may be adjusted either by chelation of the metals with ethylenediaminetetraacetate (EDTA) or diethylenetriaminepentaacetate (DTPA), or by washing the pulp at a low pH (1.5–3.0) followed by replenishment of the magnesium ion.[4]

With the metal content profile of the pulp having such a great influence on the TCF bleaching process, and the adjustment of this profile a common practice in the paper industry, there exists a need for a means by which the levels of metals present in the pulp can be determined with reasonable speed and accuracy. Magnesium and manganese, the two most important elements in terms of their influence on the TCF bleaching process, are found in relatively high concentration in pulps. Typical concentration ranges are 200–400 ppm for Mg and 50–250 ppm for Mn in Canadian kraft (chemically treated) pulps.

Other elements that occur in lower concentrations include Cu and Zn (0–10 ppm) and Fe (20–100 ppm). The desired metal profile for a pulp destined for TCF bleaching is such that the Mg level is maintained at least within the natural range expected, and that the concentration of the transition metals is reduced to its lowest level possible (of the order of 1 ppm or less). Considering the range of metal concentrations expected to occur naturally, and the thresholds for these metals deemed acceptable for TCF bleaching, the desired technique for determining these analytes in wood pulp should have at least semi-quantitative capabilities, with quantitative results for the most influential elements being desireable.

The current method used by the paper industry for the determination of these metals in pulp samples involves dry or wet ashing of the sample followed by hot-plate digestion in HCl, and subsequent analysis by flame atomic absorption spectrometry (FAAS).[5,6] The use of inductively coupled plasma optical emission spectrometry (ICP–OES) in the above methods in place of FAAS is now a common practice in the pulp and paper industry, primarily because of the multi-element capabilities of ICP–OES. Although they are commonplace for preparing solid samples for analysis, hot-plate digestions have several inherent disadvantages: volatile element losses; contamination of the sample from air, contact with the sample vessel, or reagents required for sample digestion; and unacceptably long sample dissolution times. An expeditious alternative to dissolution of the solid pulp sample would be the direct analysis of the solid itself. Many solid samples have been successfully determined by ICP–OES by taking advantage of thermal sample introduction techniques such as electrothermal vaporization (ETV)[7,8] or direct sample insertion (DSI).[9,10,11,12] In many of these cases solids were introduced into

the ICP by ETV or DSI with minimal *a priori* sample treatment and any necessary sample treatment was performed *in situ*. Of these two techniques, the open design of the DSI lends itself most conveniently to rapid replacement of the sample holder, and the addition of both solid samples and liquid reagents. Consequently, it was decided that the direct analysis of pulp samples would be approached using this technique.

In its most conventional configuration, DSI entails the axial elevation of a sample directly into the center channel of the annular plasma discharge by means of a sample carrying probe. The intrinsic benefits of DSI are obvious: 100% of the sample is introduced into the excitation source, and cup-shaped sample probes facilitate the introduction of various solids and liquids, as well as the addition of reagents for *in situ* chemical sample treatment. Physical sample treatment steps, such as drying and pyrolysis, can also be performed either by proximate positioning of the sample underneath the plasma, or by induction heating in the ICP load coil prior to ignition of the plasma.[13] Graphite cup DSI, like ETV, is hampered by the formation of refractory carbides that prove difficult to volatilize, by sample intercalation into the pores and interstices, of the graphite, which results in poor reproducibility in the volatilization event, and by the susceptibility of graphite to chemical attack. Intercalation can be minimized and a resistivity to chemical attack can be imparted to a graphite surface by depositing a highly ordered layer of pyrolytic graphite.[14] Recently, a means of depositing a pyrolytic graphite coating on the interior of a graphite DSI cup in the ICP was developed.[15] Promising improvements in signal reproducibility and sensitivity were observed, but the performance of the new coated probe had yet to be evaluated in terms of its resistance to chemical attack and usefulness for routine analysis.

The scope of this study was two-fold: to evaluate the utility of DSI as an expeditious means of screening wood pulps for metals that influence the efficiency of the TCF bleaching process; and to evaluate the performance of pyrolytically coated graphite DSI probes for performing routine analyses with extensive *in situ* chemical treatment.

3.3 Experimental

3.3.1 Pyrolytically coated graphite probes and DSI apparatus

Hollow-stemmed, long undercut graphite cup sample probes were machined in-house from ¼" high density graphite electrodes (S-8 HD, Bay Carbon, Bay City, MI, USA) on a benchtop lathe (Emco Compact 5, Emco Maier, Columbus, OH, USA) according to the dimensions indicated in Fig. 3-1(a). The interior of the cup portion of the DSI probe was then pyrolytically coated with graphite directly in the plasma[15] by means of a vapor phase deposition procedure depicted schematically in Fig. 3-1(b). In brief, a 10% (v/v) mixture of methane in argon was directed through the hollow stem of the probe toward the walls of the cup interior as the cup portion of the probe was positioned in a 2 kW argon plasma. The methane undergoes gas-phase pyrolysis, large aromatic molecules are generated by dehydrogenation, and collision of these macromolecules with the substrate result in a pyrolytic graphite deposit. Details of the experimental conditions used in the coating process appear in Table 3-1, and fine points pertaining to the pyrolytic coating procedure have been previously described.[13]

A stepper motor controlled direct sample insertion device (DSID)[13] was used to elevate the DSI sample probes axially into a 27.12 MHz inductively coupled plasma source with an automatching network (HFP-2500 and AMN-2500E respectively, Plasma

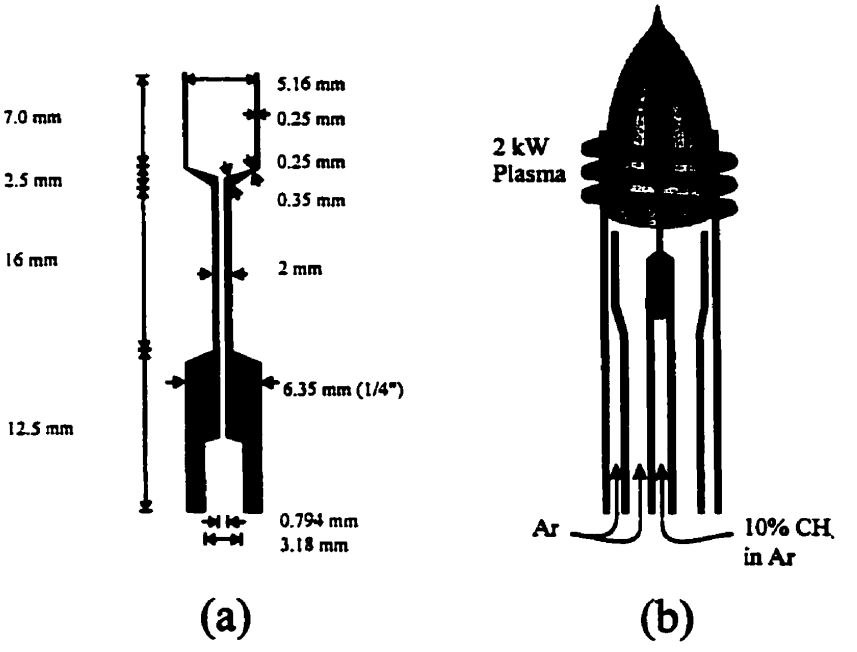

Figure 3-1 Pyrolytically coated direct sample insertion (DSI) probe: (a) dimensions of probe used; (b) depiction of the pyrolytic coating process.

Therm, Inc., St. Petersburg, FL, USA). Optical emission signals collected from the ICP were imaged to the entrance slit of a Rowland circle-type polychromator with a Pachen-Runge mount (Model 750, Thermo Jarrell Ash, Franklin, MA, USA) equipped with a galvanically driven quartz refractor plate in the incident light path for off-peak background correction and capable of high-speed signal processing suitable for transient signals[16] (Trulogic Systems, Mississauga, ON, Canada). Signals were interpreted using Grams/32 (Galactic Industries, Salem, NH, USA).

Table 3-1 Experimental Summary

Pyrolytic coating process—	
Plasma forward power	2 kW
Reflected power	0–8 W
Plasma gas flow rate	16 l min^{-1}
Auxiliary flow rate	2 l min^{-1}
Coating gas flow rate	500 ml min^{-1}
Coating time	20 min
Insertion depth	0 mm ATOLC[a]
Sampling and sample pretreatment—	
Sample size	1–4 mg of dried pulp
Chemical treatment	20 µl of conc. HCl
	10 µl of 10% (m/v) NaF
Inductive drying forward power	50 W (~ 150°C)
Inductive drying reflected power	8 – 10 W
Drying time	90 seconds
Inductive pyrolysis forward power	150 W (~ 550°C)
Inductive pyrolysis reflected power	50 – 55 W
Pyrolysis time	90 seconds
Drying/pyrolysis probe position	0 mm ATOLC
Direct sample insertion analysis—	
Plasma forward power	2 kW
Reflected power	0–5 W
Plasma gas flow rate	16 l min^{-1}
Auxiliary flow rate	1.8 l min^{-1}
Insertion depth	0 mm ATOLC[a]
Viewing height	20 mm ATOLC[a]
Insertion time	25 seconds
Exposure time	40 ms / position
Number of exposures / trace[b]	300
Galvanometer settle time	3 ms
Wavelengths monitored	324.8 nm (Cu I)[c]
	259.9 nm (Fe II
	279.6 nm (Mg II)
	293.3 nm (Mn II)
	213.9 nm (Zn I)

[a] ATOLC: above top of load coil
[b] Includes both on-line and off-line traces.
[c] Origin of emission lines are designated as I (ground state) or II (singly ionized).

3.3.2 *Samples, standards and reagents*

Wood pulp samples used throughout this study were obtained from the Pulp and Paper Research Institute of Canada (Paprican, Pointe-Claire, QC, Canada). The unavailability of a certified reference material for wood pulp necessitated the use of pulp samples that had been analyzed using a standardized method (Canadian Pulp and Paper Association Standard Method G.34P with ICP–OES, analyses performed by Paprican) for this study. Two pulp samples representative of the most common types encountered in routine wood pulp analysis were selected: a kraft pulp (brownstock) [Fig. 3-2(a)], in which alkaline attack is used to chemically fragment the lignin molecules of the wood chips (by cooking the chips in a solution of NaOH and Na_2S at approximately 175 °C.), and a thermomechanical pulp (TMP) [Fig. 3-2(b)], which is generated by pressurized steam pretreatment of wood chips followed by mechanical shredding and defibering of the chips by means of a rotary-disk refiner.[17] These same samples are currently being developed and characterized by Paprican for use as industry standard reference materials.

Mixed-element standard solutions were prepared by serial dilution of both multi-element and single-element standards (High-Purity Standards, Charleston, SC, USA, and Fisher Scientific, Nepean, ON, Canada, respectively) with 0.5% trace metal grade HNO_3 (Instra-Analyzed, J.T. Baker, Phillipsburgh, NJ, USA) in distilled, deionized water (Milli-Q water system, Millipore Corp., Bedford, MA, USA). Trace metal grade HCl (Instra-Analyzed) and ACS grade NaF (Baker-Analyzed, J.T. Baker) were used for *in situ* treatment of the pulp samples.

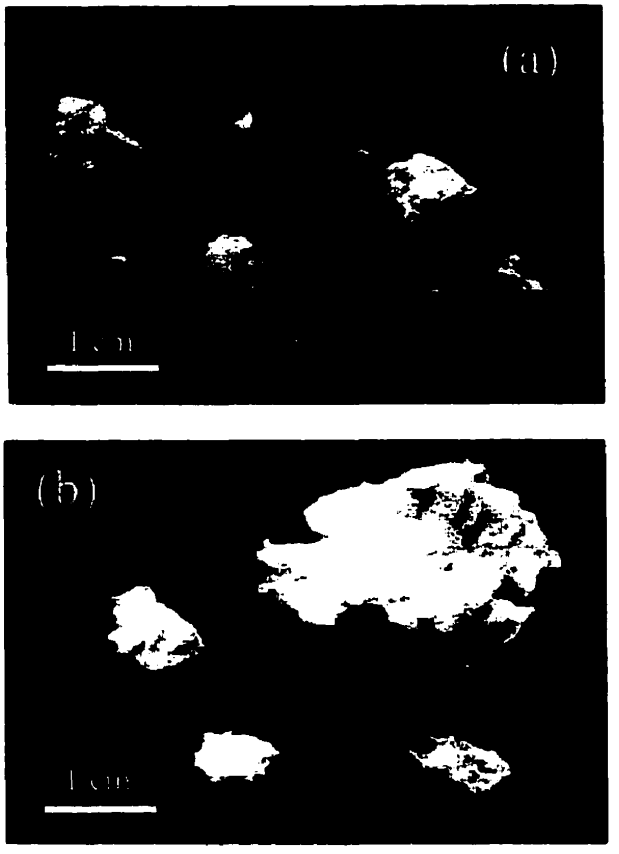

Figure 3-2 Pulp samples used in this study: (a) kraft pulp (brownstock); (b) thermomechanical pulp (TMP).

3.3.3 Procedure

An accurately determined mass of dried wood pulp on the range of 1–4 mg was deposited directly into a graphite DSI cup on a 0.01 mg readable balance. The probe was then mounted on the DSID, and 20 µl of concentrated HCl and 10 µl of a 10% (m/v) solution of NaF were added to the cup [Fig. 3-3(a)]. The DSI cup was then positioned such that the top of the cup was even with the top of the highest turn of the ICP load coil, *i.e.*, 0 mm above the top of the load coil (ATOLC). Forward power was then applied to the ICP load coil at settings of 50 W for 120 s to dry the sample and 150 W for 120 s to ash the sample by inductively heating the graphite DSI probe [Fig. 3-3(b)]. These power settings have

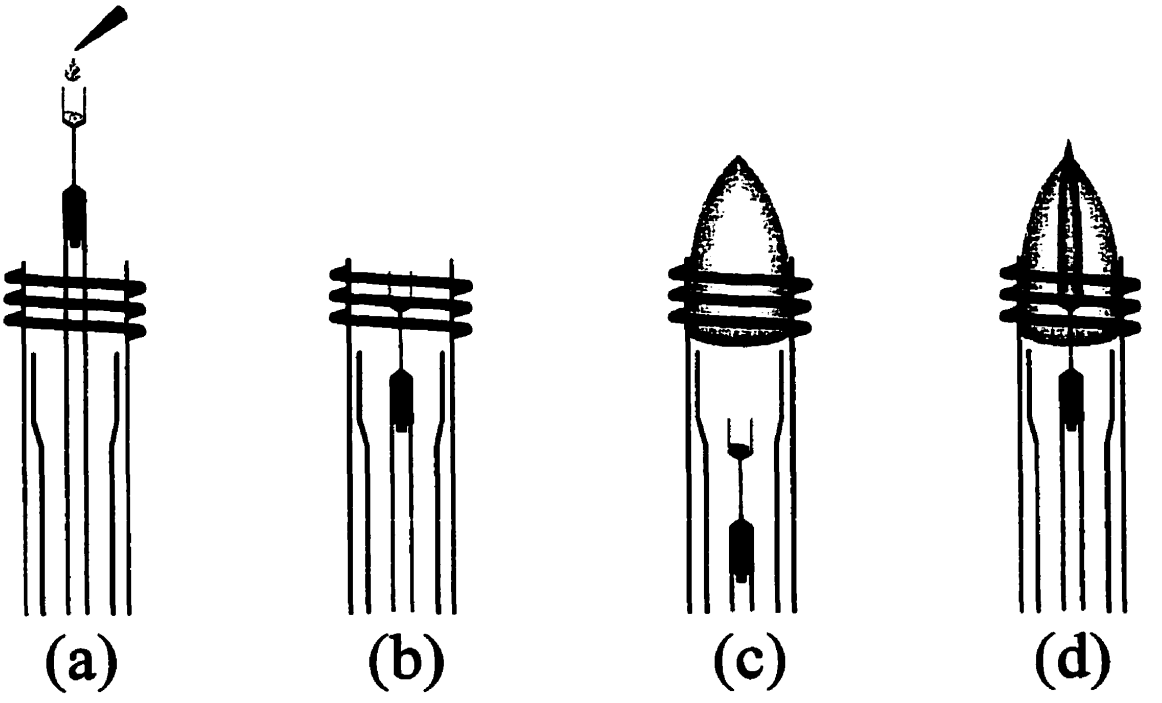

Figure 3-3.. Schematic depiction of the DSI procedure: (a) 10 μl of 10% (m/v) NaF and 20 μl of conc.HCl are added to a pulp sample of known mass; (b) inductive drying (50 W forward power) and pyrolysis (150 W) of the treated sample; (c) retraction of the sample probe and ignition of the 2.0 kW ICP; (d) insertion of the sample.

been determined to correspond to probe temperatures of approximately 150 °C and 550 °C respectively. Although more conservative drying and pyrolysis times on the order of 30–60 seconds would have been sufficient for each respective task, longer times were employed as a conservative approach. The sample probe was then retracted below the ICP coil and the plasma was ignited and set to a forward power of 2.0 kW [Fig. 3-3(c)]. The probe was then elevated by the stepper motor until it was just below the plasma discharge (–20 mm ATOLC) and stopped there for 2 s prior to insertion so that the plasma could recover from disruption in the Ar flow caused by the initial probe elevation. Finally the probe was inserted into the plasma [Fig. 3-3(d)] for 30 s at a position of 0 mm

ATOLC, retracted and cooled. Signal acquisition was started upon the arrival of the probe at the stabilization position. Details regarding other instrumental settings appear in Table 3-1. Unless explicitly stated otherwise, it can be assumed that the procedure described above was used throughout the study.

External standardization was used to determine the concentration of the metals present in the pulp samples. Calibration curves were constructed from signals acquired using aqueous multielement standards. The standard solutions were analyzed in a manner identical to that described above for the pulp samples, including drying and pyrolysis steps, except that 20 μl of standard were deposited in the sample probe in place of the pulp sample.

3.4 Results and discussion

3.4.1 Method development

In developing the procedure used for the direct analysis of wood pulps by DSI, the wood pulp was at first analyzed using no chemical pretreatment, and drying and pyrolysis steps were performed only out of necessity so as to prevent plasma overloading. Although a transient signal could be obtained by this simple procedure it was found to be highly irreproducible (when corrected for sample mass) and the signals would evolve over a relatively long period of time, often on the order of 5–15 s for most elements. Since HCl is used in the pulp and paper industry standard solution dissolution methods[5,6] to treat the pulp sample after ashing, the addition of an aliquot of concentrated HCl was incorporated into the DSI procedure. No appreciable improvement in signal was observed when HCl was added to the DSI cup with the deposited pulp sample after the drying and ashing

steps. When HCl addition *preceded* the desolvation and pyrolysis events, however, the time over which the signals would evolve was diminished, although the signals were still irregular in appearance and poor in terms of reproducibility. Sodium fluoride, as well as other halide-containing solids and gases are known to act as halogenating agents, forming relatively volatile metal–halide compounds. Agents such as these have been used to improve the volatilization of analytes in DSI from graphite probes, especially for refractory carbide and oxide forming elements.[18] In experiments in the present study in which NaF was added, improved analyte volatilization was observed when addition was incorporated prior to drying and ashing of the pulp sample. The best results in terms of signal appearance and reproducibility, however, were achieved when HCl and NaF were added together before sample drying and pyrolysis.

Fig. 3-4 shows the signals obtained from a brownstock sample inserted using a pyrolytically coated DSI probe when 20 µl of concentrated HCl and 10 µl of 10% (m/v) NaF are added prior to drying and ashing. Most analytes were completely vaporized in less than 5 s, with extremely volatile elements such as Zn being completely volatized in 2 s. Iron, however, was very difficult to volatilize, with analyte still being vaporized from the probe 25 s after insertion into the plasma [Fig. 3-4]. This is not a fault of the analysis procedure, but rather a shortcoming of DSI as an analytical technique. The longer time needed to vaporize Fe results simply because the temperature at which Fe is volatilized is relatively high in comparison to the other elements studied, and that the maximum temperature that the sample probe can attain upon insertion, close to 2000 °C, was insufficient for rapid volatilization. The maximum temperature that a DSI probe can reach upon insertion can be increased by using a mixed-gas plasma, such as an oxygen–

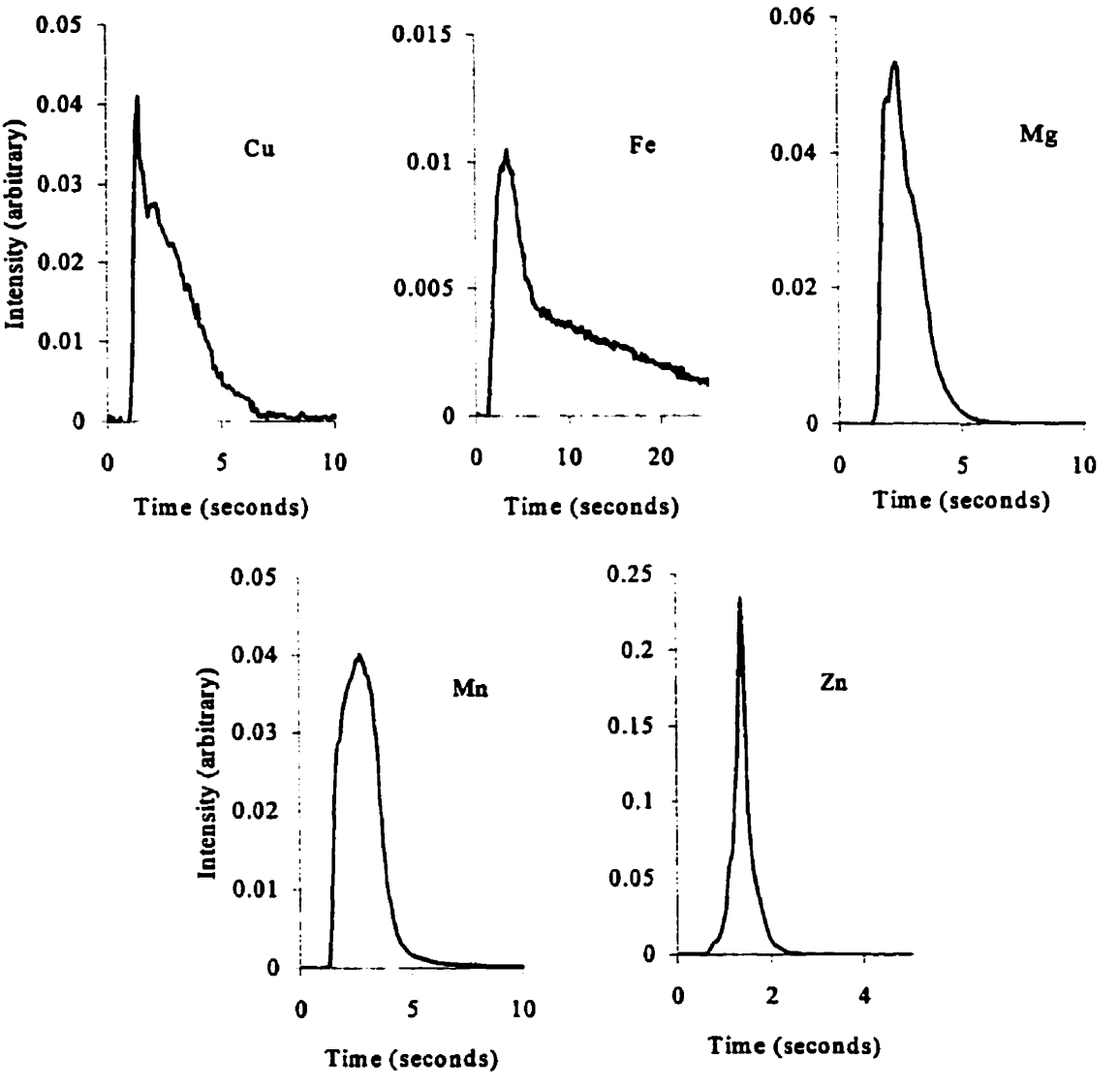

Figure 3-4 Typical signals for a kraft pulp (brownstock) sample treated with 10 µl of 10% (m/v) NaF and 20µl of concentrated HCl using a pyrolytically coated DSI probe. Sample mass is approximately 1.5 mg.

argon plasma,[19] but the use of such conditions will result in consumption of the sample probe.

When solid samples are analyzed by DSI, the reproducible deposition of a given mass of solid sample for each assay is often not a practicality, thus necessitating the incorporation of an acceptable sample mass range for insertion analysis. In this study, a

range of 1–4 mg was established as suitable for the mass of pulp that could be used in DSI. The rationale behind this directive takes the following points into consideration. Since sample mass was being determined on a balance readable to 0.01 mg, the use of samples less than 1 mg would greatly compromise the precision to which the pulp mass could be determined and thus degrade the overall precision of the technique. The metals of interest present in wood pulp occur often at concentrations of 1 ppm or higher, meaning that the detection limit of the technique used would have to be at least 1 ng absolute if a 1 mg pulp sample was used. This is well above the detection limits that have been previously demonstrated with the instrumentation used in this study.[13] With at least 1 mg of pulp sample, transient signals were visually discernable from the background emission for all analytes of interest in both the brownstock [Fig. 3-4] and TMP samples. For the mass range of 1–4 mg, a linear response of signal area as a function of sample mass was observed for the analytes of interest. Fig. 3-5 shows this behavior for Mg and Mn, the highest-concentration analytes in both pulp samples. Although larger sample masses could be determined with greater precision, non-linearity in the analyte transient signal area as a function of pulp mass was observed at higher sample masses (>8 mg).

3.4.2 Probe comparison

Fig. 3-6 shows the signals obtained with both pyrolytically coated and uncoated DSI probes for a fluffed softwood TMP sample. As expected, the pyrolytically coated probe yielded sharp transient signals with little to no multiple peaking as compared to the uncoated probe. Since the uncoated probe surface is thinner, highly irregular and more porous in comparison to the pyrolytically coated surface, it was more susceptible to

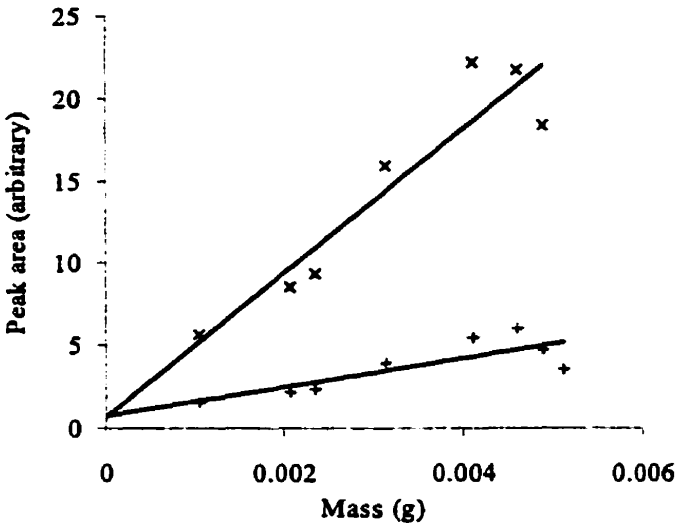

Figure 3-5 Analyte transient signal area as a function of pulp sample mass (brownstock). (+, Mn; ×, Mg).

factors such as intercalation and preferential volatilization due to spatial temperature disparities, both of which lead to multiple peaking. Table 3-2 compares the signal reproducibility between a pyrolytically coated probe and an uncoated probe for the analysis of the same fluffed softwood TMP. Surprisingly, when both probes were relatively new (less than 25 sample insertions) there was a marginal difference between the % RSD values of the integrated signals for most of the elements studied. This is in stark contrast to what had been observed with pyrolytically coated DSI probes previously.[15] In explaining this, the origin of the primary analyte volatilization event upon sample insertion must be considered. Wood pulp is a highly polymerized, fibrous material, and when a pulp sample was dried and pyrolyzed, the sample was reduced to a carbonaceous residue with a high surface area. After pyrolysis, the metals initially present in the pulp sample were most likely still in contact with this carbon residue and were

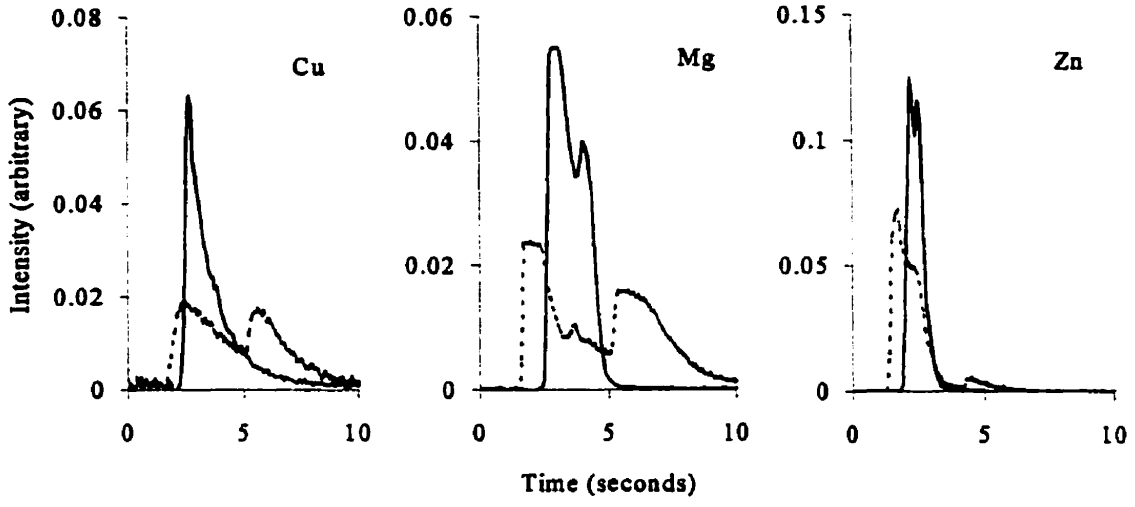

Figure 3-6 Influence of the pyrolytic coating on analyte volatilization for a fluffed softwood thermomechanical pulp. (-----, uncoated probe; —— pyrolytically coated probe).

Table 3-2 Signal reproducibility comparison (fluffed softwood TMP)

	RSD (peak area, n=10) (%)	
Element	Uncoated probe (<25 insertions)	Pyrolytically coated probe
Cu	23	23
Fe	11.5	13
Mg	6.3	6.0
Mn	14	4.1
Zn	10.3	10.8

vaporized from the surface upon insertion into the plasma. The result was an initial vaporization event that was influenced greatly by the sample residue, which was identical in both cases. While this may explain the similarities in signal reproducibility, vaporization from the carbon residue alone does not account for the marked difference in signal appearance in Fig. 3-6. The difference in signal appearance probably arises from secondary recondensation and revaporization events on the probe surface subsequent to

vaporization from the carbonaceous pulp residue. Although recondensation–revaporization after the initial vaporization event will influence the appearance of the peak shape, the initial vaporization event will be the predominant influence in signal reproducibility.

While the observed signal reproducibility was virtually identical for both pyrolytically coated and uncoated probes that were relatively new, the precision achieved with the latter degraded rapidly after 25–50 insertions to the point where the signal RSD was on the order of 100–200%. Visual inspection of the probe revealed that the cup portion of the probe was being oxidized and was disintegrating with repeated use. It is obvious that damage to and disintegration of the sample probe will degrade signal reproducibility due to sample losses, intercalation and the like, and that the highly crystalline ordered non-porous surface of the pyrolytically coated probe will demonstrate ameliorated resistivity to oxidative attack. Less obvious was the source of the oxidative attack. Several potential sources of oxidation exist. Firstly, it has been documented that Na, as well as other alkali and alkaline earth elements have a catalytic effect on the rate of oxidation from graphite.[14] As an example, 20–40 ppm of Na, K, V or Cu has been shown to increase the rate of dry oxidation of graphite by upwards of 6-fold. Since O_2 and CO_2 both support the oxidation of graphite, and both were expelled from the pulp sample during the pyrolysis step, a catalytic oxidative effect from the Na deposited as NaF was probably occurring. Additionally, the reaction of fluorine with graphite could be taking place, resulting in the loss of graphite from the probe due to the formation of various fluorocarbon species such as CF_4 and C_2F_6, which are known to occur at temperatures less than 700 °C.[20]

3.4.3 Limit of detection (LOD)

Determining the limit of detection (LOD) for the method was not trivial due to the unavailability of a true field blank, *i.e.*, a blank consisting of a matrix representative of the sample being analyzed (a wood pulp sample in this case).[21] Although a blank was used in the external standardization curve, it was an aqueous sample, and the use of its standard deviation for the purposes of estimating the LOD would be inappropriate. A better approach would be the duplicate analysis of samples with analyte concentrations 10–30 times the expected detection limit, and then using the observed standard deviation in the LOD estimation. Owing to the limitations of the samples available, this approach was also not possible. As a compromise, the off-peak transient signals used for background correction were taken from the pulp samples analyzed, corrected for their respective offset from zero along the ordinate axis, and integrated. The standard deviation from these integrated signals was then incorporated into the LOD definition as recommended by IUPAC:

$$c_L = 3\sigma_B / m \qquad \text{(Eqn. 3.1)}$$

where c_L is the concentration LOD, σ_B is the standard deviation in the blank signal, and m is the slope of the calibration curve. The calculated LODs using this practice appear in Table 3-3. For the values reported in Table 3-3, it is important to mention that the off-peak signals were not corrected for sample mass, and that the standard deviations were pooled from the two different samples analyzed (n=10 for each sample of brownstock and TMP). This was done because the external calibration curve was assumed to be valid for all pulp samples irrespective of sample type or mass. By comparison these values are, with the exception of Mg, approximately one order of magnitude higher than those

Table 3-3 Limit of detection (LOD) for pulp analysis

	LOD	
Element	Absolute (ng)	Relative (ppb)[a]
Cu	0.052	21
Fe	0.94	375
Mg	6.7	2700
Mn	0.56	225
Zn	0.20	80

[a] Based on a 2.5 mg pulp sample (median of mass range used in this study),

obtained when the standard deviation of the integrated aqueous blank signal was used in Eqn. 3.1 (Mg was approximately 10^2 higher). Care should be taken in extracting a practical quantitation limit (PQL) from these LOD values (normally 3–10 times the method detection limit), as they are not based on the standard deviation of low-concentration samples. The PQL will as a result most likely be somewhat higher than expected.

3.4.4 Precision and accuracy

Table 3-4 presents a comparison of the precision and accuracy for the analysis of the two pulp samples studied using DSI (with external standards) and the industry standard method (CPPA Method G.34P). In terms of precision, the wet oxidation method almost always faired better than DSI. With aqueous solutions, DSI has been shown capable of achieving precision that rivals that of solution nebulization. Percentage RSD values typically of less than 5%, and in extraordinary cases less than 1% have been realized.[22] Irreproducibility in sample deposition, insertion and volatilization are the primary influences in the observed precision. However, when analyzing a solid directly by DSI

Table 3-4 Determination of Cu, Fe, Mg, Mn and Zn in pulp samples

		Direct sample insertion (n=7)		CPPA Method G.34P (Paprican) (n=3)		
Pulp sample	Element	Concentration (ppm)	RSD (%)	Concentration (ppm)	RSD (%)	Error (%)
Brownstock	Cu	1.27	11	0.84	7.39	51
	Fe	10.7	20	19.4	12.5	-45
	Mg	593	13	515	1.9	15
	Mn	93.2	6.7	80.3	0.99	16
	Zn	11.8	20	11.6	1.9	1.7
TMP	Cu	1.64	18	1.10	40	49
	Fe	40	44	56.7	1.6	-29
	Mg	201	39	212	15	-5.2
	Mn	91	41	88	15	3.4
	Zn	11.8	16	14.0	7.7	-16
Average error						4.1

the precision is often much worse, as the previously mentioned factors are now more influential, and new factors such as inter-sample heterogeneity and sample size variability further compound the imprecision of the technique. Evidence of the influence of sample homogeneity on precision can be seen when the % RSD values obtained for the TMP sample in Table 3-4 are compared with those obtained for a similar TMP sample that had been mechanically fluffed [Table 3-2]. Although low concentration elements (Cu and Zn) show no appreciable improvement in precision, for high concentration elements (Mg and Mn) the % RSD is reduced by approximately an order of magnitude when the sample is fluffed. It is also important to note that the physical constraints of DSI in terms of sample size dictated the use of an extremely small sample (of the order of 1–4 mg). Although this mass of pulp was more than sufficient to generate detectable signals for the analytes

of interest, slight errors in accurately determining such a minute sample mass can greatly influence the observed precision.

When the DSI precision was compared between the two pulp types studied, the reproducibility of the brownstock was generally better than the TMP sample, with RSD values ranging from 7–20 % versus 16–44 % respectively [Table 3-4]. A similar trend in reproducibility was also observed with the wet oxidation values, suggesting that an inherent difference that exists between the two pulps plays a role. The difference is that in the kraft pulping process (brownstock), the lignin is dissolved away chemically, leaving cellulose and hemicellulose in the form of intact fibers, whereas thermomechanical pulping (TMP) yields a distribution of shortened fibers resultant from a mechanical shredding and defibering process.[17] It should be noted, however, that the kraft process, in practice, also chemically degrades a certain amount of the cellulose and hemicellulose fibers, while thermomechanical pulping leaves most of the cellulose and hemicellulose intact. Metals in wood such as Ca, K, and Mg are often partially bound to the carboxyl groups present in the cellulose and hemicellulose, and heavy metals such as Fe and Mn are often chelated by wood constituents.[23] The chemical damage from the conditions experienced in the kraft process make the analytes easier to liberate from the ashed pulp in both the wet oxidation and DSI analyses, thus yielding the improved precision in the brownstock values.

When the accuracy (using the CPPA Method G.34P values as a reference) was compared for the pulps, a trend opposite to that observed with the precision values was evident. For Mg and Mn, the two elements present in the highest concentrations, agreement with the TMP values was 5.0% and 4.4% respectively, as compared to 15 and

16 % for the brownstock sample [Table 3-4]. The discrepancy in accuracy can be attributed in part to sampling of the pulp for analysis. The TMP sample upon air drying took the form of rather large, fibrous pieces [Fig. 3-2(b)] that had to be physically separated into smaller pieces with plastic tweezers in order to fit into the DSI sample probe, and this action probably assisted in homogenizing the TMP sample. By comparison, the brownstock sample [Fig. 3-2(a)] was not as fibrous, but occurred in a variety of sizes, the smaller of which were suitable for deposition into the DSI cup. Sampling was consequently favored towards these smaller pieces, as the larger pieces of the brownstock pulp proved difficult to manually separate into smaller ones.

The same trend was true of Fe although the agreement between the values was somewhat poorer (29% versus 44% for TMP and brownstock, respectively). In both pulp samples, the value for Fe concentration as determined by DSI was always lower than that determined by the wet oxidation method, due most likely to the incomplete volatilization of Fe from the sample probe as described earlier [Fig. 3-4]. The concentrations reported for Cu and Zn were quite low in comparison to the previous three elements, with Cu being close to the detection limit of the wet oxidation technique. Consequently, the % RSD was relatively high by comparison and no definite correlation between sample and % RSD could be obtained. Notwithstanding Fe, the error in the determination of the elements does not appear to be biased low or high of the reference value. This is reinforced by the fact that the average error for all of the determinations is only 4% [Table 3-4].

Standard additions were performed on both the brownstock and TMP samples, but no apparent benefit was seen in adopting this calibration approach for the pulp analysis.

In addition to being more laborious in terms of the number of samples that had to be run, the obtained precision and accuracy were most often poorer than obtained with external standards. This is attributable to the way that the reproducibility of the pulp signals influences the determined analyte concentration differently in external standards and standard additions. With standard additions, the uncertainty in the slope and intercept of the calibration curve was considerably higher than that in the external standards curve, a consequence of the fact that the standard additions curve was generated from pulp samples, as opposed to liquid standards in the external calibration case. Furthermore, the curve itself is used in standard additions to determine the analyte concentration (by determining the point of intercept with the abscissa), whereas analyte concentration is determined by interpolation of signals from a more precise curve in external standards.

3.5 Conclusion

The respective merits of rapidly analyzing wood pulps for various metals by DSI–ICP–OES and using a pyrolytically coated graphite cup DSI probe for this type of routine analysis have been demonstrated. The pulp and paper industry has a persistent need for on-line and extremely rapid off-line methods of monitoring various process parameters so as to prevent unnecessary delays in production and the production of off-grade products.[24] The use of DSI for rapidly determining the trace metals profile of wood pulps prior to TCF bleaching proves excellent in fulfilling this mandate. Considering the short times needed to dry, ash, and insert the sample into the plasma, a raw pulp sample analysis by DSI can be completed in 5 min from pulp sample procurement. The expeditious nature of

the DSI analysis compares extremely well relative to the several hours needed to digest pulp using industry standard wet oxidation methods.[5,6]

Although precision and accuracy do suffer somewhat when a solid sample is analyzed directly by DSI, quantitative results were obtained for process-influential metals in wood pulp samples (Mg and Mn), and semiquantitative results were realized for low concentration, but still process-influential metals (Cu, Fe, and Zn). With the exception of the values obtained for Fe, there appears to be little bias in the error of the determination (average error of 4%). It is common for industry pulp samples to have typical metal concentrations that vary (or will be varied by means of chemical treatment) in concentration over several orders of magnitude. With this reality considered, the demonstrated accuracy and precision of DSI–ICP–OES appears more than adequate for the purposes of a rapid screening technique. It is important, however, to consider that these results are indeed preliminary, as they are based on the replicate analysis of only two, albeit well characterized, samples (one of each wood pulp type). The replicate analysis of more samples of each pulp type covering the expected concentration range for the analytes of interest would give a more comprehensive picture statistically in terms of the expected precision and accuracy of the technique.

Precision can be improved by homogenizing the pulp sample prior to analysis, *e.g.*, by mechanical fluffing (compare % RSD for fluffed TMP in Table 3-2 with TMP in Table 3-4), and by using a larger sample. Although DSI and ETV have physical constraints that limit the size of sample that can be deposited, higher capacity thermal sample introduction techniques, such as induction heating vaporization (IHV)[25] are quite

capable of handling larger samples. The direct analysis of wood pulps using a technique such as IHV should be explored in the future.

The pyrolytically coated graphite DSI probe demonstrated a greatly enhanced resistivity to oxidative and chemical attack, resulting in a longer useful lifetime than an uncoated graphite probe. Although an improvement in precision was not observed for the pulp samples, greater signal sensitivity and shorter signal evolution times were observed when a pyrolytically coated probe was used.

3.6 Acknowledgements

The Analytical Services Division of the Pulp and Paper Research Institute of Canada is gratefullly acknowledged for the generous provision of wood pulp samples and analyses for this study. For scholarship funding, the financial support of the Province of Québec through Fonds pour la Formation des Chercheurs et l'Aide à la Recherche (FCAR) (Michael Rybak), as well as the Natural Sciences and Engineering Research Council of Canada (NSERC) (Panos Hatsis) is sincerely appreciated. Funding from NSERC through an NSERC Operating Grant is also gratefully acknowledged.

3.7 References

1. Van Lierop, B., Liebergott, N., and Faubert, M., *J. Pulp Pap. Sci.*, 1994, **20**, J193.

2. Sinkey, J.D., and Thompson, N.S., *Pap. Puu*, 1974, **5**, 473.

3. Prasakis, J., Sain, M., and Daneault, C., *TAPPI J.*, 1996, **79**, 161.

4. Bouchard, J., Nugent, H.M., and Berry, R.M., *Preprints CPPA International Pulp Bleaching Conference*, 1994, 33.

5. Standard Method G.34P, Canadian Pulp and Paper Association.

6. Standard Method T 266 om-88, Technical Association of the Pulp and Paper Industry (TAPPI).

7. Hull, D.R., and Horlick, G., Spectrochim. Acta, 1984, 38B, 843.

8. Atsuya, I., Itoh, T., Kurotaki, T., Spectrochim. Acta, 1991, 46B, 103.

9. Lorber, A., Goldbart., Z., *Analyst*, 1985, **110**, 155.

10. Salin, E.D., Monasterios, C.V., and Jones, A.M., *Anal. Chem.*, 1986, **58**, 780.

11. Pettit, W.E., and Horlick, G., *Spectrochim. Acta*, 1986, **41B**, 699.

12. Zaray, G., Broekaert, J.A.C., and Leis, F., *Spectrochim. Acta*, 1988, **43B**, 241.

13. Skinner, C.D., and Salin, E.D., *J. Anal. At. Spectrom.*, 1997, **12**, 725.

14. Huettner, W., and Busche, C., *Fresenius Z. Anal. Chem.*, 1986, **323**, 674.

15. Rybak, M.E., and Salin, E.D., J. Anal. At. Spectrom., 1998, **8**, 707.

16. Légère, G., and Burgener, P., *ICP Inf. Newsl.*, 1987, **13**, 521.

17. Smook, G.A., *Handbook for Pulp and Paper Technologists*, Angus Wilde, Vancouver, 2nd edn., pp. 36-45.

18. Karanassios, V., Abdullah, M.,and Horlick, G., *Spectrochim. Acta*, 1990, **45B**, 119.

19. Liu, X.R., and Horlick, G., J. Anal. At. Spectrom., 1994, 9, 833.

20. Rüdorff, W., and Rüdorff, G., *Z. anorg. u. allgem. Chem.*, 1947, **253**, 281.

21. Analytical Methods Committee, *Analyst*, 1987, **112**, 199.

22. Sing, R.L.A., and Salin, E.D., *Anal. Chem.*, 1989, 61, 163.

23. Sjöström, E., *Wood Chemistry: Fundamentals and Applications*, Academic Press, San Diego, 2nd edn., p. 107.

24. Sitholé, B.B., *Anal. Chem.*, 1995, **67**, 87R.

25. Goltz, D.M., Skinner, C.D., and Salin, E.D., *Spectrochim. Acta*, 1998, **53B**, 1139.

Chapter 4

Development and characterization of induction heating–electrothermal vaporization (IH–ETV) sample introduction for inductively coupled plasma spectrometry

Prior to completing the experiments involving the analysis of wood pulps by DSI–ICP–OES, a decision was made to shift the focus towards IH–ETV sample introduction and to compare the capabilities of this technique with DSI. Doug Goltz, then a postdoctoral fellow in the laboratory, had spearheaded the development of this sample introduction arrangement in which samples could be vaporized from a graphite cup in an induction field. Although the ability of this "inductively heated vaporizer (IHV)" to introduce aqueous samples into both ICP–OES and ICP–MS had been demonstrated (references 8 and 7 of this chapter, respectively), little was known about its capabilities in terms of its heating rates and temperature control and many benchmarks regarding its analytical performance had yet to be objectively evaluated. Knowledge of these characteristics would be valuable in terms of allowing objective performance comparisons to be made between IH–ETV and DSI sample introduction, as well as enabling the optimization of future IH–ETV applications. Consequently, a thorough study of the performance attributes of the IH–ETV system was conducted, the results of which are presented in this chapter.

4.1 Abstract

A general study of performance attributes was conducted for a prototypical electrothermal vaporization (ETV) sample introduction system in which induction heating (IH) was used to facilitate the drying, pyrolysis, and vaporization of samples from long, undercut graphite cup susceptors in a radio-frequency (RF) induction field. In the first part of this study, experiments were carried out to determine the heating characteristics and temperature control aspects of an IH–ETV arrangement. Using a remote-sensing infrared thermocouple, it was determined that a 3/8" (9.53 mm) outer diameter graphite cup sample probe could be heated to a maximum temperature of 1860 °C in the induction field of the IH–ETV under full forward power (1.5 kW). The IH–ETV device was found to have a rapid heating response (1/*e* time-constant of (2.0 ± 0.2) s) that was independent of the initial/final temperatures chosen. Linear temperature control was possible by regulating either the DC voltage applied to the plate or the current flowing to the grid of the RF generator oscillator tube. The second part of this work consisted of studies to establish benchmarks such as limits of detection (LOD) with inductively coupled plasma–optical emission spectrometry (ICP–OES) and transport efficiency for analyte vaporization under several *x*–Ar mixed gas atmospheres (where *x*=15% N_2, 10% O_2, HCl (sparged), or 15% SF_6 (v/v)). In general, reproducible transient signals with evolution times of 5–15 s were seen for the vaporization of most elements studied, with peak area intensity and reproducibility generally being the best with SF_6–Ar. A 10× increase in transport efficiency was seen for refractory-carbide forming analytes (Cr, V) when vaporization was conducted in a halogenous (*x* = HCl, SF_6) *versus* ahalogenous (*x* = N_2, O_2) environment, with a 2× improvement being observed for most other non-refractory

elements (Cd, Cu, Fe, Mn, Ni, Pb, Zn). The transport of arsenic proved to be a special case unto itself, with its transport efficiency increasing to 90% when vaporized in the presence of SF_6 (a 3× improvement over all other carrier mixtures) due to the formation of volatile AsF_5. Using the concept of transport-independent analyte sensitivity, the introduction of the aforementioned *x*–Ar mixtures into the center channel of the plasma appeared to not have any appreciable effect on plasma excitation conditions with N_2 being the only exception (a 70% reduction in transport-independent sensitivity was observed). Detection limits ranged from 0.08–70 ng absolute and were highly dependent on the analyte studied and the vaporization atmosphere used. Based on the above information, the feasibility of an induction heating arrangement for thermal sample introduction was evaluated, with recommendations being made for the future design of the IH–ETV instrumentation.

4.2 Introduction

Sample introduction has always been a contentious issue in plasma source spectrometry.[1] Although conventional solution nebulization is a convenient, and clearly the most common means of introducing samples into inductively coupled plasma–optical emission spectrometry (ICP–OES) and ICP–mass spectrometry (ICP–MS) systems, it is far from ideal. Highly inefficient sample transport (of the order of 1–5%) is an inherent characteristic of the nebulizer/spray chamber apparatuses used in pneumatic nebulization and inevitably results in the wasteful consumption of large amounts of sample. Solution nebulization also does nothing to reduce the level of concomitant species present in a sample. High levels of such concomitants often prove to be the principal contributing

factor behind the two most commonly observed sources of error in ICP spectrometry: interfering peak overlaps along the spectral abscissa (wavelength for OES, and charge to mass (*m/z*) ratio for MS); and matrix effects resulting in spurious signal enhancements or suppressions. Finally, the preparation of solid and liquid samples for solution nebulization often requires laborious and time-consuming digestion procedures that introduce the risk of sample contamination and inevitably result in sample dilution.

In order to circumvent the inherent drawbacks of solution nebulization, fundamentally different means of introducing samples have been pursued. Of these, thermal sample introduction methods such as electrothermal vaporization (ETV)[2,3] and direct sample insertion (DSI)[4,5] have proven quite practical, especially in their capacity to introduce both solid and liquid samples that have had minimal *a priori* sample treatment. With ETV and DSI, a thermal vaporization event facilitates the introduction of a finite amount of sample into a plasma source as either a dry aerosol or a gaseous plume. Considerably improved transport efficiency is observed over solution nebulization (20–80% for ETV and 100% for DSI, notwithstanding refractory volatilization events) and a miniscule amount of sample is needed by comparison. Parsing of volatilization events is also possible by temperature programming (ETV) or chemical modification,[6] thus allowing potentially interfering analyte and concomitant signals and effects to be separated over a temporal dimension.

Thermal sample introduction methods are, however, not without their own limitations. One of the inherent advantages of DSI is the use of an interchangeable sample probe, and while much freedom is permitted in terms of sample probe design, the probe geometry and composition must be compliant both physically and chemically with the

plasma environment. The loading capabilities of the plasma further limit DSI to the introduction of relatively small samples that must be dry and pyrolyzed of any organic material in order to avoid the possibility of quenching the plasma. It is possible to dry and pyrolyze DSI samples directly in the sample probe being used, but the means often proves to be inconvenient or imprecise. For instance, the probe can be heated inductively in the ICP load coil prior to plasma ignition and sample insertion for the purposes of sample pretreatment, but this process requires that the plasma be extinguished and re-ignited between insertions. Probe heating can also be performed by proximal positioning underneath the plasma discharge, but this is a blind process with no temperature feedback.

Where DSI seems to be somewhat deficient in terms of a sample introduction technique, ETV unquestionably excels. The ability to generate detailed, reproducible heating programs makes the drying and pyrolysis of samples a much simpler and more reliable process in ETV, and the location of the analyte vaporization event *ex situ* to the plasma alleviates the energy demands placed on the ICP. The physical environment of graphite tube ETV furnaces, however, greatly restricts the amount and type of sample that can be deposited on the vaporization surface. While cup-based ETV units have the capacity to accommodate much larger samples than tube furnaces, including solids, they still require dimensions that conform to the electrical contact requirements of the power supply being used.

It is clear from the above that DSI and ETV have their respective, and in some cases exclusive merits, and an obvious step in designing a novel thermal sample introduction technique would be to synergistically combine the best attributes of both techniques. Ideally, one would want to meld the rapidly interchangeable sample probe

and contact-free heating of DSI with the temperature programming capabilities and *ex situ* vaporization event of ETV, while at the same time increasing sample size capacity in order to minimize sample inhomogeneity concerns and possibly improve detection limits. This is the role that induction heating–electrothermal vaporization (IH–ETV) has been designed to serve. In IH–ETV, long undercut graphite probes akin to those used in DSI are used to support samples in a cylindrical quartz chamber axially encircled by an induction coil. Application of a radio-frequency (RF) current to the coil causes the probe to be heated inductively without the need of electrical contact. Heating of the probe consequently dries, pyrolyzes, and vaporizes the sample, and the sample plume is swept out of the chamber by a gaseous flow into a plasma excitation source located downstream. Temperature control similar to that possible with ETV can be accomplished by simply adjusting the RF current or by adjusting the position of the probe in the RF field. Sample probes can be used interchangeably in IH–ETV with the relatively large vaporization chamber being able to accommodate larger and more elaborate probe designs than with DSI.

To date, the inductively heated vaporizer (IHV) described by Goltz *et al.*[7,8] is the only existing experimental setup that uses induction heating as a means of thermal sample introduction for inductively coupled plasma source spectrometry. Prior to this IH–ETV instrument, the only other thermal sample introduction application described that utilized induction heating was an instrument used to introduce volatile metal salts (maximum B.P. of 1000 °C) into a microwave induced plasma by means of a quartz crucible packed in carbon black.[9] Other applications of induction heating in plasma source spectrometry have been strictly auxiliary, consisting of the heating of direct sample insertion devices

for spray deposition preconcentration[10] and for sample drying and ashing prior to sample insertion.[11]

While the instrument described by Goltz *et al.* has demonstrated an ability to thermally introduce a variety of analytes into both ICP–OES[8] and ICP–MS,[7] there are some points in terms of its utility for sample introduction that should be addressed. One such issue is temperature control and heating characteristics. Towards this juncture, IH–ETV has only been used for the full-power, high-temperature vaporization of pre-dried samples, and while temperature control has been described as one of its attributes, it has yet to be thoroughly examined. Additionally, other heating characteristics, such as heating rates and set-point stability also require elucidation so as to enable a complete and objective comparison of the heating capabilities of IH–ETV arrangement *versus* a conventional ETV system. Another issue is the use of mixed-gas atmospheres for the vaporization of samples in IH–ETV. The practice of introducing a second gas into the otherwise exclusively argon carrier gas used in ETV has been exploited in the past as a means of enhancing analyte volatility/transport,[12,13,14] and although this idea has been implemented in IH–ETV, the merits of using various *x*–Ar mixtures as vaporization atmospheres has yet to be objectively compared across pertinent variables such as transport efficiency and limits of detection. The use of mixed vaporization atmospheres in IH–ETV has also served a concerted role in suppressing occasional electrical discharging in the induction field during vaporization events, however, the origins of this phenomena have yet to be thoroughly discussed, along with the mechanism of suppression imparted by the gaseous mixture.

The long-term goal of this research is to develop IH–ETV as a more flexible, adaptive, and efficient alternative to conventional ETV with improved detection limits and greater sample throughput. The purpose of this study was to examine aspects of IH–ETV that are relevant to its development as a sample introduction technique for plasma source spectrometry. The general heating characteristics and temperature control capabilities of a prototypical IH–ETV system are explored and their application to analyte volatilization is discussed. Considerations for the selection of the mixed gas carrier in terms of analyte volatilization, transport effects, effects on plasma excitation conditions, analyte sensitivity, electrical-discharging suppression, and potential interferences are presented.

4.3 Experimental

4.3.1 IH–ETV–ICP–OES system

The IH–ETV system used in this work was a modified version of the original device described by Goltz and Salin[7] depicted schematically in Fig. 4-1(a). At the heart of the IH–ETV is a free-running 13.1 MHz, 1.5 kW nominal forward power induction furnace (Leco Model 521 Induction Furnace, Leco Corporation, St. Joseph, MI, USA) with its original combustion chamber, sample pedestal and screen enclosure removed. These components have been replaced by a screen enclosure that supports a 31 mm i.d. / 35 mm o.d. cylindrical quartz vaporization chamber. At the top of the chamber is a female ball joint adapter which is connected to male counterpart that links the IHV to the injector tube of the ICP torch via a short length of Tygon tubing. A quartz rod held by a Teflon base assembly [Fig. 4-1(b)] is used to support the IH–ETV probe which is to be

positioned in the induction field. This base assembly slides directly into the vaporization chamber from underneath and is held in place by a series of tension fitting O-rings. It is also from this base assembly that the vaporization chamber gas flow originates. The long design of the base assembly ensures that the sample probe is positioned reproducibly in the induction field while at the same time greatly reducing the dead volume of the vaporization chamber over previous designs, and the small gas inlets in the base assembly ensure a uniform, positive flow that reduces vapor recirculation.

Samples vaporized with the IH–ETV device were introduced into a Thermo Jarrell Ash IRIS ICP–OES (Thermo Jarrell Ash Corp., Franklin, MA, USA). The IH–ETV device was interfaced to the ICP–OES by simply disconnecting the existing spray chamber from the base of the ICP torch injector tube and connecting the outlet tubing of the IH–ETV device in its place. Details concerning the instrumental settings and signal acquisition parameters for the ICP–OES can be found in Table 4-1. Transient signals were interpreted with the standard IRIS operating software (ThermoSPEC/CID, Thermo Jarrell Ash Corp.) and a software routine authored in-house (Appendix A).

All samples were vaporized from graphite sample probes machined in house from 3/8" diameter graphite rod stock (HLM grade, SGL Carbon Group, Speer Canada Inc., St.–Laurent, QC, Canada) using high speed steel tools on a benchtop lathe (Emco Compact 5, Emco Maier, Columbus, OH, USA). The graphite probes used in this study were machined to the dimensions given in Fig. 4-1(c), and a detailed description of the machining process appears elsewhere.[11]

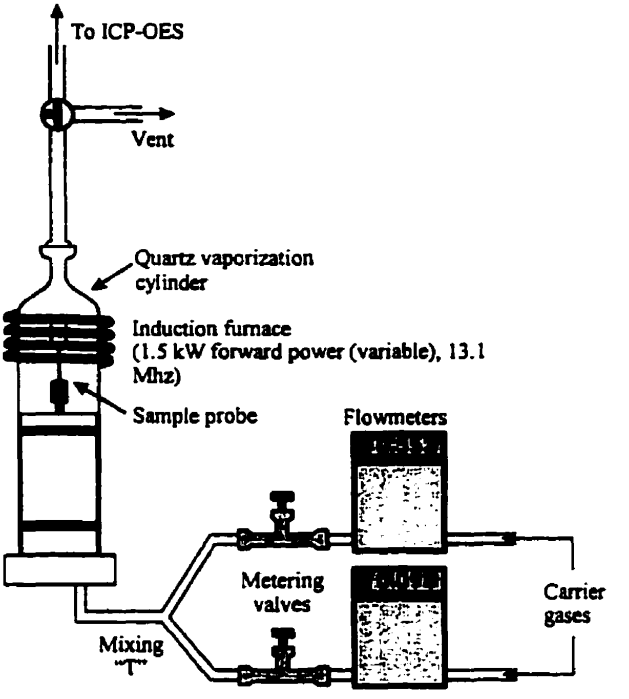

(a)

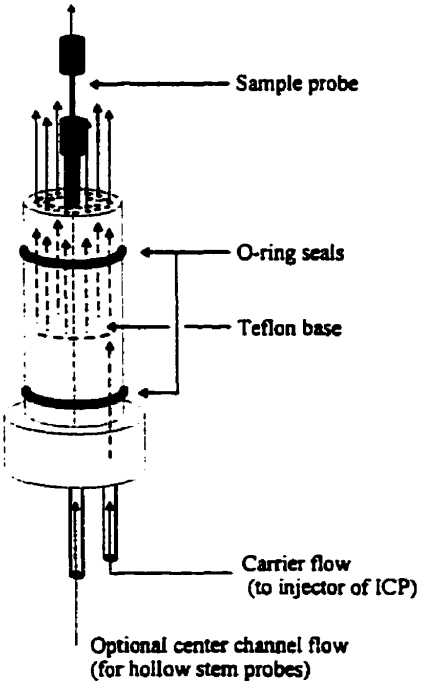

(b)

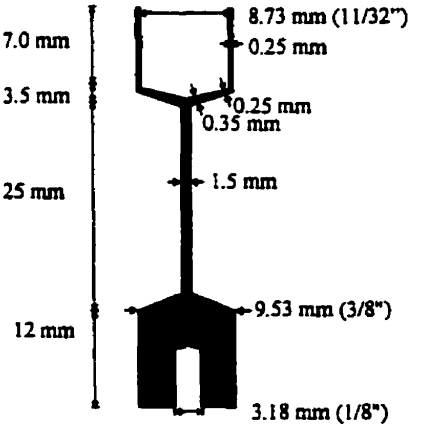

(c)

Figure 4-1 Schematic diagrams of the IH-ETV system and its components (not to scale): (a) overall scheme of the IH-ETV system; (b) detail of the probe base assembly; and (c) dimensions of the graphite sample probe used (c). Measurements in (c) designated in Imperial units indicate the dimensions of the tools used to machine the element indicated, with the exception of the diameter of the probe base (3/8").

Table 4-1 Instrumental settings

Sample vaporization step (IH–ETV)—	
Carrier gas	15 % N_2–Ar, 10 % O_2–Ar, 15 % SF_6–Ar, HCl–Ar (sparged)
Carrier gas flow rate	0.50–0.65 l min^{-1} [a]
Standards	0.1, 0.3, 1, 3, 10, 30, 100 ppm (nominal) in each of As, Cd, Cr, Cu, Fe, Mn, Ni, Pb and Zn; 5% (v/v) HNO_3 matrix
Sample volume	100 µl
Drying step	*Ex situ*
Pre-vaporization flush time	30 s
Vaporization temperature	ca. 1900°C
Vaporization time	60 s
Post-vaporization flush time	30 s
ICP–OES (Thermo Jarrell Ash IRIS – radial view, Echelle spectrometer, CID detection)—	
Plasma forward power	1150 W
Ar plasma gas flow rate	15.0 l min^{-1}
Ar auxiliary flow rate	0.5–1.0 l min^{-1}
Ar injector flow rate	0.50–0.65 l min^{-1} [a]
Wavelengths monitored (nm)	As: 189.042, Cd: 214.438, Cr: 283.563, Cu: 324.754, Fe: 238.204, Mn: 257.610, Ni: 221.647, Pb: 220.353, V: 309.311, Zn: 213.856
Signal increment (% full well capacity)	75%
Number of time slices	300
Time per slice	0.2 s

[a] Total flow for gaseous mixture.

For the transport efficiency studies conducted, a closed-system trapping method was used.[15] In brief, a commercially available 3 liter capacity gas-sampling bag filled with 100 ml of 10% HNO_3 was connected to the exhaust of the IH–ETV transport tube, and used to collect and seal the product of a vaporization event. The contents of the bag were then analyzed using standard additions by solution nebulization ICP–MS to determine the analyte transport efficiency, *i.e.*, the percent of the analyte initially deposited in the IH–ETV that was recovered in the sampling vessel. These experiments

were procedurally identical to those performed in the cited study, [15] with the exception that the septa found in the shut-off valves of the sampling bags were replaced with Teflon™/polyimide coated septa (Puresep–T (7/16" dia.), Chromatography Research Supplies Inc., Louisville, KY, USA).

4.3.2 Temperature measurements

Temperature measurements were made using an R-type infrared (IR) thermocouple (Omega IRt/c series model OS37-60CF, Omega Engineering, Laval, QC, Canada) which had a focal length of 305 mm and a minimum spot size of 5 mm diameter at its focus. Prior to its use, the IR–thermocouple was calibrated by measuring the temperature of a high emissivity surface set to two different accurately known temperatures. For temperature measurements in the IH–ETV device, the infrared thermocouple was positioned above the sample probe at an angle of 30° off its axis at a distance of approximately one focal length from the center of the cup portion of the probe. This position allowed a clear downward view of the interior side and bottom walls of the IHV sample probe. Discreet temperature measurements were made by using the infrared thermocouple with a digital temperature display and integrated circuit cold junction compensator (Omega DP45 Single Input Temperature Meter, Omega Engineering). Time vs. temperature curves were recorded by using the thermocouple with a cold junction compensator/matched amplifier circuit assembled in-house (LTK001AMJ, Linear Technology, Milpitas, CA, USA) (Appendix 2) and interfacing this circuit to an A/D converter and/or a strip chart recorder.

4.3.3 Samples, standards, and reagents

Multi-element standard solutions containing a mixture of relatively volatile (As, Cd, Mn, Pb, Zn), involatile (Cu, Fe, Ni), and refractory carbide forming (Cr, V) analytes were used throughout the IH–ETV study. Standard solutions were prepared by consecutive dilution of multi-element stock solutions (High-Purity Standards, Charleston, SC, USA) with 0.5% trace metal grade HNO_3 (Instra-Analyzed, J.T. Baker, Phillipsburgh, NJ, USA) in 18 MΩ distilled deionized water (DDW) (Milli-Q water system, Millipore Corp., Bedford, MA, USA). All standards were stored in polypropylene containers (Nalgene) that had been preconditioned with a mixture of 1:1 HNO_3 (ACS grade), in DDW for a period of 24 hours and rinsed with DDW.

4.4 Results and discussion

4.4.1 Temperature/Heating characteristics

4.4.1.1 General observations

In the first IH–ETV study by Goltz *et al.*[7], temperature measurements were taken on graphite cups with outer diameters (o.d.) of 1/4" (6.35 mm) and 3/8" (9.53 mm) using an optical pyrometer. The study found that under a full power firing in an N_2–Ar atmosphere, the cup portion of the 6.35 mm o.d. probe attained a maximum temperature of (1660 ± 20) °C for the inside walls and (1370 ± 20) °C for the platform of the cup. Similarly, the 9.53 mm o.d. probe attained wall and platform temperatures of (1890 ± 20) °C and (1470 ± 20) °C respectively. Whereas an optical pyrometer, such as the one used above, is capable of resolving the temperature of a surface spatially due to its ocular operational principle, the infrared thermocouple used in this study has no such

capabilities, and could only be aligned until a maximum temperature reading was reached. Measurements taken with the infrared thermocouple on a 3/8" (9.53 mm) graphite cup used in this study [Fig. 4-1(c)] yielded on average a value of 1860 °C, correlating well with the inside wall temperature reported by Goltz *et al.*.[7] This value appeared to be independent of the atmosphere (*i.e.*, $N_2/O_2/HCl/SF_6$–Ar) in which the firing was conducted, with reproducibility being as good as ±3 °C when multiple measurements (n=8) were made on the same sample probe, and increasing to ±13 °C when single measurements were made on multiple probes (n=5) machined to identical dimensions. It should be noted that the targeting of the infrared thermocouple needed to be re-optimized whenever the sample probe was changed due to slight differences in probe positioning. This could be a contributing factor in the inter-probe precision value observed in addition to slight differences in the dimensions of the sample probes machined by hand.

Varying the flow rate of the carrier gas through the IH–ETV unquestionably affects the energy conditions experienced by vaporized analytes as they pass through the ICP. Fig. 4-2(a) illustrates how this phenomenon manifests itself in the observed signal intensity of a variety of analytes vaporized in an SF_6–Ar carrier. For most of the analytes presented in Fig. 4-2(a), maximum signal intensity was observed at a flow rate of 500 ml min^{-1}, with the decrease towards lower flow rates due primarily to difficulties in effectively forming a center channel for analyte transport through the annular ICP discharge, and the decrease towards higher flow rates resulting from cooling of the center channel and a decreased analyte residence time in the plasma. There also exists the possibility that moving to high carrier gas flow imparts a cooling effect on the sample probe significant enough that it may act as a contributing factor towards the lower signal

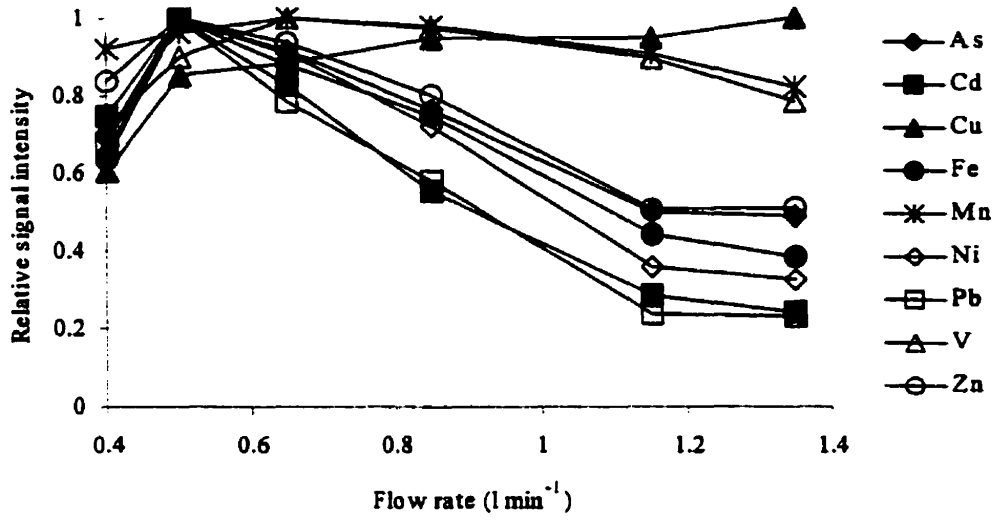

(a)

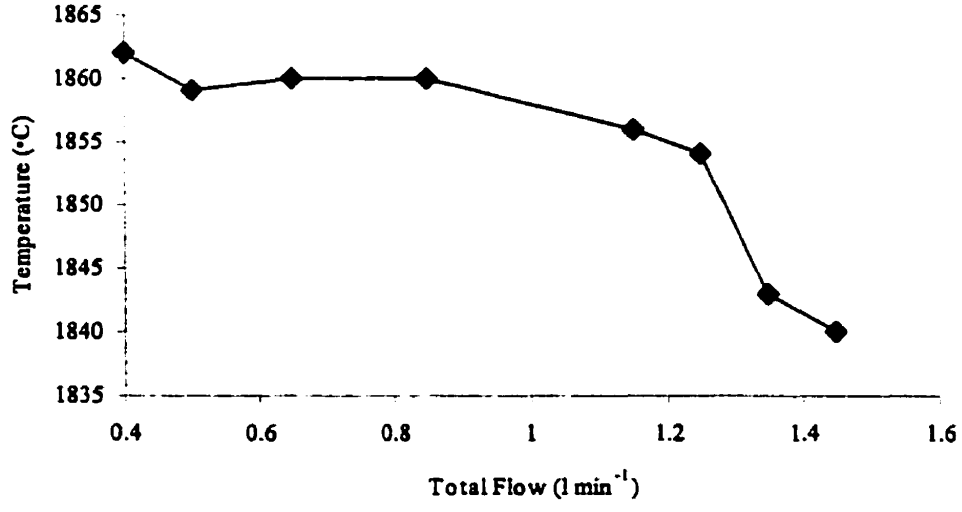

(b)

Figure 4-2 Behavior of (a) analyte emission signal intensity (peak area) and (b) vaporization surface temperature as a function of carrier gas flow rate. In (a) 300 ng of each analyte was vaporized in a 15 % (v/v) SF_6-Ar carrier. Signals in (a) are normalized to their highest value.

intensities observed. This appears not to be the case when the effect of the carrier gas flow rate on the temperature of the vaporization surface is actually monitored [Fig. 4-2(b)]. For an SF_6-Ar carrier, increasing the flow rate though the vaporization chamber from 500 ml min^{-1} to 1.25 l min^{-1} results in a negligible drop in probe temperature (inside wall of cup) when the furnace is operated at full power. This temperature drop is also insignificant in light of the sensitivity drops (upwards of 80% in some cases) experienced by certain analytes when the carrier gas flow is increased and suggests that plasma effects such as those described above are the most influential. A benefit arising from the fact that the temperature of the vaporization surface in the IH–ETV unit does not change considerably with carrier gas flow rate points to the likelihood of robust heating performance when interfacing it to ICP systems that have wide and varied sample introduction flow rate demands.

4.4.1.2 Temperature control, heating rates and set-point stability

The induction furnace at the heart of the IH–ETV apparatus used in this study was equipped with two existing means of temperature control: a variable transformer (autoformer) through which the plate voltage of the oscillator tube could be varied; and a 10 kΩ resistor with nominal tap settings of 5 kΩ, 7.5 kΩ, and 10 kΩ for adjusting the electrical current to the grid of the oscillator tube. Based on the operational principles of induction heating, both of these measures are expected to have a proportional effect on the forward power applied, and thus should have a linear effect on the temperature of the susceptor (in this case, the sample probe). Fig. 4-3 shows the vaporization surface temperature behavior, as well as the behavior of the grid and plate currents, as a function of each method of temperature control. From Fig. 4-3(a) it can be seen that the

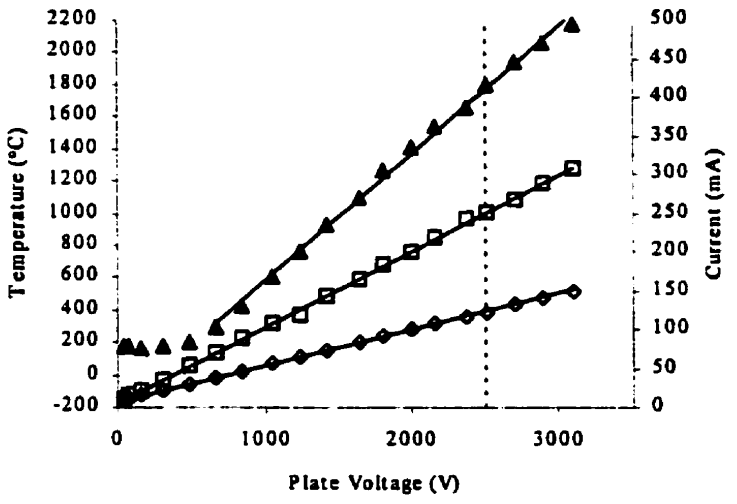

(a)

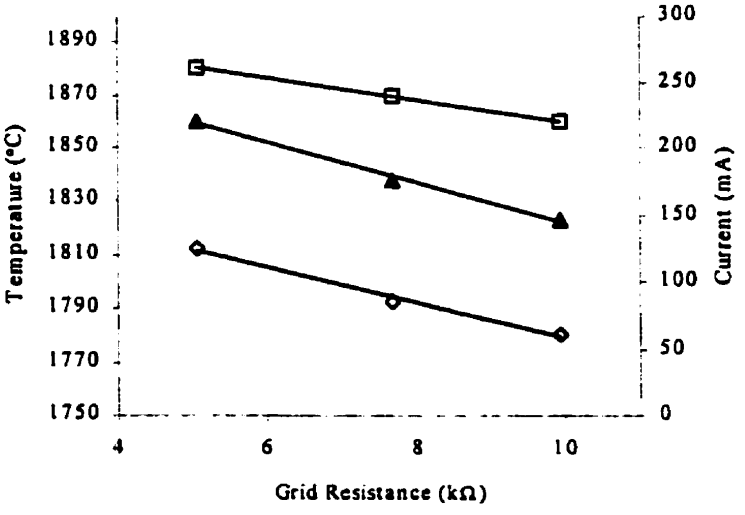

(b)

Figure 4-3 Methods of IH-ETV temperature control: (a) regulation of plate voltage; and (b) regulation of grid resistance. (▲, temperature; □, plate current; ◇, grid current).

vaporization surface temperature was linear with applied plate voltage from temperatures as low as 300 °C through to the upper limits of the IH–ETV operating range. At temperatures below 300 °C, this behavior appeared to deviate from linearity but was a result of attempting to measure temperatures well outside of the accepted linear range of the infrared thermocouple (540–2700 °C). This being said, a non-linearity at low temperatures is expected considering the ordinate-axis intercept (ca. –200 °C) encountered when the linear trend in Fig. 4-3(a) is extrapolated downward. This deviation from linearity is probably a result of either the generator being unable to effectively generate an RF current at low oscillator settings, or for this current to couple inductively to the graphite cup. From Fig. 4-3(a) it is apparent that the grid and plate currents are also linear with plate voltage, and as one would expect, if temperature is plotted as a function of these values linear relationships result. This is promising in that it presents the possibility of using the grid and/or plate current as a means of temperature feedback instead of an optical transducer that would require frequent realignment.

As for the possibility of temperature control by adjusting the grid resistance, Fig. 4-3(b) demonstrates that a linear trend was also seen for vaporization surface temperature, as well as the grid and plate currents when the grid resistance was varied,. The use of the grid tap resistor, however, restricts the user to three predetermined settings and results in a narrow range of vaporization temperatures making this approach limited in comparison to varying the plate voltage.

Along with the obvious importance of being able to control the vaporization temperature in the IH–ETV furnace, it is imperative that the device possess heating characteristics, such as response time and set-point stability, that are prerequisite of a

technique intended for thermal sample introduction. In Fig. 4-4, heating rate curves are shown for various temperature settings in the IH–ETV furnace when a "step" firing was performed (*i.e.*, a given forward power setting was applied instantaneously). The heating of the vaporization surface appears to undergo an initial lag period of 2–3 s, after which the heating rate is quite rapid with most of the curves depicted in Fig. 4-4 reaching their respective maxima in a matter of seconds with no apparent bias due to the final temperature reached. When the set-point temperature of the vaporization surface was eventually achieved, the temperature reading was usually stable to within ±2 °C over a period of 15 s. If the convention of a time constant (time needed to reach (1–1/*e*) of the final steady temperature) is applied to these curves after the initial lag period the value of the time constant is (2.1±0.2) s. Acknowledging the fact that the thermocouple itself had a significant time constant of 80 ms associated with its response (manufacturer specification), when this is factored into the observed time constant, the value of the true time constant of the IH–ETV system drops to (2.0±0.2) s. There are also two additional observations related to the time constant value that are worth noting: firstly, when a "hot" sample firing was performed (*i.e.*, a higher forward power level was applied to the sample probe when a lower power level was already being applied,), the value of the time constant remained virtually unchanged, with the most influential factor in its value being the speed with which the plate voltage could be adjusted on the autoformer; and secondly, the lag period of 2–3 s that was observed during the "cold" firings was notably absent during these "hot" firings.

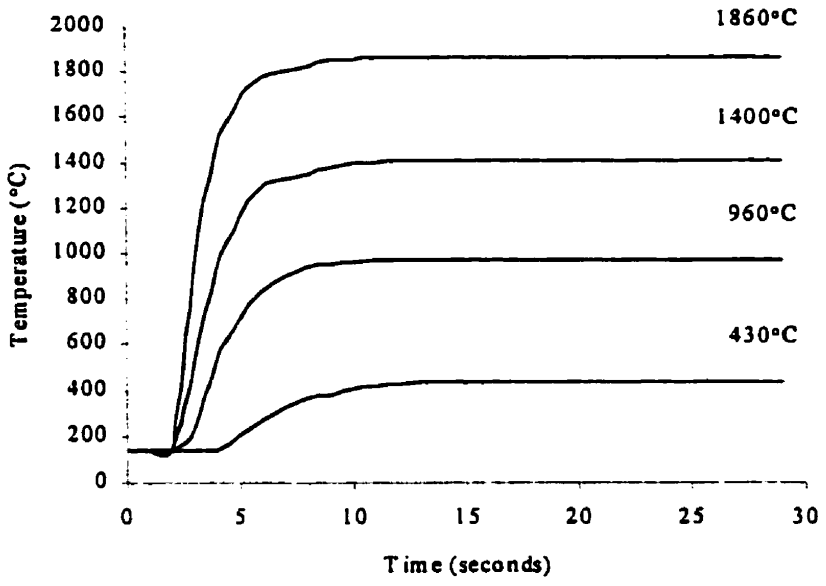

Figure 4-4 Temperature *vs.* time response curves for various final temperature settings. Forward power was applied instantaneously at $t = 0$ s (*i.e.*, "cold" firing). Measurements were taken under a 15% (v/v) SF_6-Ar atmosphere

4.4.2 Use of mixed-gas vaporization atmospheres

4.4.2.1 General discussion

Argon is the most common atmosphere used for sustaining ICP discharges for the purposes of OES and MS. It logically follows, then, that for a sample introduction technique to be ideally interfaced to an Ar–ICP source, it too should utilize an argon atmosphere. When a vaporization event is attempted in an exclusively argon atmosphere with the present IH–ETV unit, electrical discharging in the furnace frequently occurs. This electrical discharging sometimes appears in the form of a localized plasma discharge around the probe itself, but most often appears as a wildly wandering arc between the sample probe and induction coil. The IH–ETV device described here is capable of consistent arc-free operation in a strictly Ar atmosphere at relatively low temperatures

(150 °C) for the purposes of sample drying, but any substantial increase in temperature beyond this range often initiates electrical discharging, with the severity of the discharging increasing as forward power in the furnace and probe temperature is increased.

The temperature dependence of both the appearance and the severity of the electrical discharge observed in the IH–ETV device when a graphite probe is heated strongly suggests that the thermionic emission of electrons from the graphite probe surface is a contributing factor. When a material such as graphite is heated, if the average energy of the higher-energy electrons (i.e., the Fermi energy) exceeds the work function of that material, thermionic emission of electrons results. The number density, n_e, of generated electrons near the surface of interest is represented by the expression:[16]

$$n_e = \left[2(2\pi m_e kT)^{3/2} / h^3\right] e^{-\phi/kT} \qquad \text{(Eqn. 4.1)}$$

where m_e is the mass of an electron, k is Boltzmann's constant, T is absolute temperature, h is Planck's constant, and ϕ is the thermionic work function of graphite. From Eqn. 4.1 it is apparent that the range of the electron number density due to thermionic emission is drastic, from 10^{-64} cm^{-3} at room temperature to 10^{12} cm^{-3} at 2500 K. The occurrence of this phenomenon has also been confirmed experimentally in electrothermal atomization–atomic absorption spectrometry (ET–AAS) with graphite furnaces by means of microwave attenuation measurements.[16] The introduction of such a high concentration of electrons into the RF field of the induction furnace can easily result in electrons coalescing in an eddy current and creating a plasma discharge, and if an average potential difference exists between the RF coil and the sample probe, an arc may form.

There is no obvious way that thermionic electron emission from a graphite IH–ETV probe can be outright eliminated, and with the presence of the RF field, the possibility of electrical discharges forming in the vaporization chamber of the IH–ETV will persist. A possible solution would be the addition of a gas that would act as an "electron scavenger" and effectively pick up thermionically emitted electrons before any electrical discharge could form. This is where electron affinity, *i.e.*, the energy difference between the lowest (ground) state of an atom or molecule and the lowest state of its corresponding negative ion, comes into play. All noble gases, including argon, have positive electron affinities, meaning that the formation of a negative ionic form is unfavorable relative to the atomic form, explaining why electrical discharging occurs when the IH–ETV was operated not only in an argon atmosphere, but when helium was tried as well. When one looks at some of the gases that have been mixed with the argon atmosphere to prevent electrical discharging in IH–ETV (HCl, for example), there exist species with suitable electron affinities such that effective electron scavenging would take place. It is important to remember, however, that the mechanism of "electron scavenging" is not exactly known, and although electron affinity is probably the most influential factor, other chemical reactions may be playing a role. This is probably the case with arc suppression using an N_2–Ar atmosphere, which has no obvious electron-affinitive species present.

Although a binary mixture of argon with a gas of suitable electron affinity may prove successful at preventing electrical discharging in an induction field, other factors need to be taken into consideration if the mixture is to be suitable for routine IH–ETV sample introduction. For instance, although 3–5% (v/v) N_2–Ar has proven to be sufficient

to suppress electrical discharging during an IH–ETV event and did not introduce any significant spectral interferences in ICP–MS, the small amount of N_2 resulted in considerable cooling and widening of the plasma center channel, and a consequential reduction in analyte sensitivity.[7] Aspirating the argon carrier flow through a flask of concentrated HCl also provided arc suppression, and furthermore has the additional effects of enhancing analyte volatility by means of halogenation, and improved transport efficiency through physical carrier effects. This approach was used successfully in ICP–OES, but if used for ICP–MS would result in additional interferences, some of which would be problematic (e.g., $^{40}Ar^{35}Cl^+$ on the monoisotopic $^{75}As^+$ signal). Situations such as those mentioned above point to the need to carefully consider the potential effects a certain vaporization atmosphere may have on experimental processes that are native to the spectrochemical system as a whole (*e.g.*, spectral interferences, matrix effects, plasma perturbation, detection limits) as well as those confined to the sample introduction component (vaporization effects, transport efficiency).

4.4.2.2 Study of N_2–Ar, O_2–Ar, HCl–Ar and SF_6–Ar IH–ETV atmospheres

A comparative study of the utility of several *x*–Ar binary gas mixtures as atmospheres for IH–ETV provided general figures of merit such as limit of detection (LOD), transport efficiency and the effect of each gas mixture on excitation conditions. In addition to the study of established IH–ETV vaporization atmospheres such as N_2–Ar and HCl–Ar, two new mixtures, namely SF_6–Ar and O_2–Ar were also studied. The use of SF_6–Ar and O_2–Ar as IH–ETV vaporization atmospheres was proposed because of their anticipated respective abilities to suppress electrical discharging (based on the electron affinities of either their native molecular species and/or their predicted IH–ETV products)

and enhance analyte volatilization and/or transport. Sulfur hexafluoride (SF_6) is a non-toxic, colorless, odorless gas that has found considerable use in the electrical industry as an insulator in high-voltage lines and switchgear due to its chemical inertness and relatively high dielectric constant.[17] At a temperature of approximately 500 °C, SF_6 will thermally decompose to form sulfur tetrafluoride (SF_4) and fluorine radicals (F·), with the latter providing a means of enhancing analyte volatilization by forming volatile metal halides with otherwise involatile and refractory carbide-forming elements. Although it has not been used previously in ETV sample introduction, SF_6 has found use in enhancing analyte volatility in DSI studies,[18] suggesting that similar effects could be realized with an SF_6–Ar atmosphere in IH–ETV. As for oxygen (O_2), it is well known that O_2 in an appreciably elevated temperature environment will commonly support the oxidation of many carbon-containing compounds to products of CO, CO_2, and amorphous carbon (*i.e.*, soot). Of these species, amorphous carbon is of particular interest in ETV. Soot particles often have the ability to travel efficiently through ETV transport systems and can serve as a condensation site for vaporized analyte, thereby acting as a physical carrier increasing the amount of analyte reaching the plasma. This phenomenon has been observed in studies in which an O_2-ashing step was incorporated into the analysis of organic samples by ETV–ICP–MS.[19,20] Based on this observation, it was postulated that an O_2–Ar atmosphere would result in the eventual consumption of the graphite sample probe being used, with soot particles resulting from this process facilitating analyte transport in a similar manner.

Mixtures (v/v) of 15% N_2–Ar 10% O_2–Ar and 15% SF_6–Ar were found to be the minimum concentrations needed in each respective case to eliminate electrical

discharging in the IH–ETV device when vaporization events were conducted at full power. Sparging of the Ar carrier through a flask of conc. HCl entrained a sufficient amount of HCl vapor into the Ar flow to accomplish the same in the case of HCl–Ar studies. Under these four atmospheres, reproducible transient signals with evolution times of 5–15 s could be obtained for most analytes studied under a full-power IH–ETV sample firing, with linear dynamic ranges of 3–4 orders of magnitude typically being observed. It was also generally observed that, irrespective of the vaporization atmosphere used, elements with relatively high volatilities (Cd, Pb, Zn) tended to have the shortest peak evolution times, followed by analytes with medium- to low-volatility (Cu, Fe, Mn, Ni) and refractory-carbide behavior (Cr, V), and finally by As.

Outside of the general trends cited above, the mixture in which the vaporization was conducted was found to be the underlying factor bearing the greatest influence on signal behavior. To illustrate this point, Fig. 4-5 provides signals for As, Cu and V vaporized under full power in each of the atmospheres described above. From the strikingly disparate transient signals presented in Fig. 4-5, it is immediately apparent that the atmosphere under which analyte vaporization occurs can bear a specific and sometimes unique consequence on the vaporization and transport mechanisms experienced by each analyte. Vanadium, an analyte well known for its propensity to form refractory-carbides, experienced an expected enhancement in signal intensity in cases where a halogen-containing atmosphere (HCl–Ar, SF_6–Ar) was used. In the case of Cu, a rather involatile and unreactive analyte, generally robust transient signal behavior was observed, with somewhat enhanced signals being observed in the halogenous cases. Finally, for As, an instance was seen where optimal transient signals were obtained under

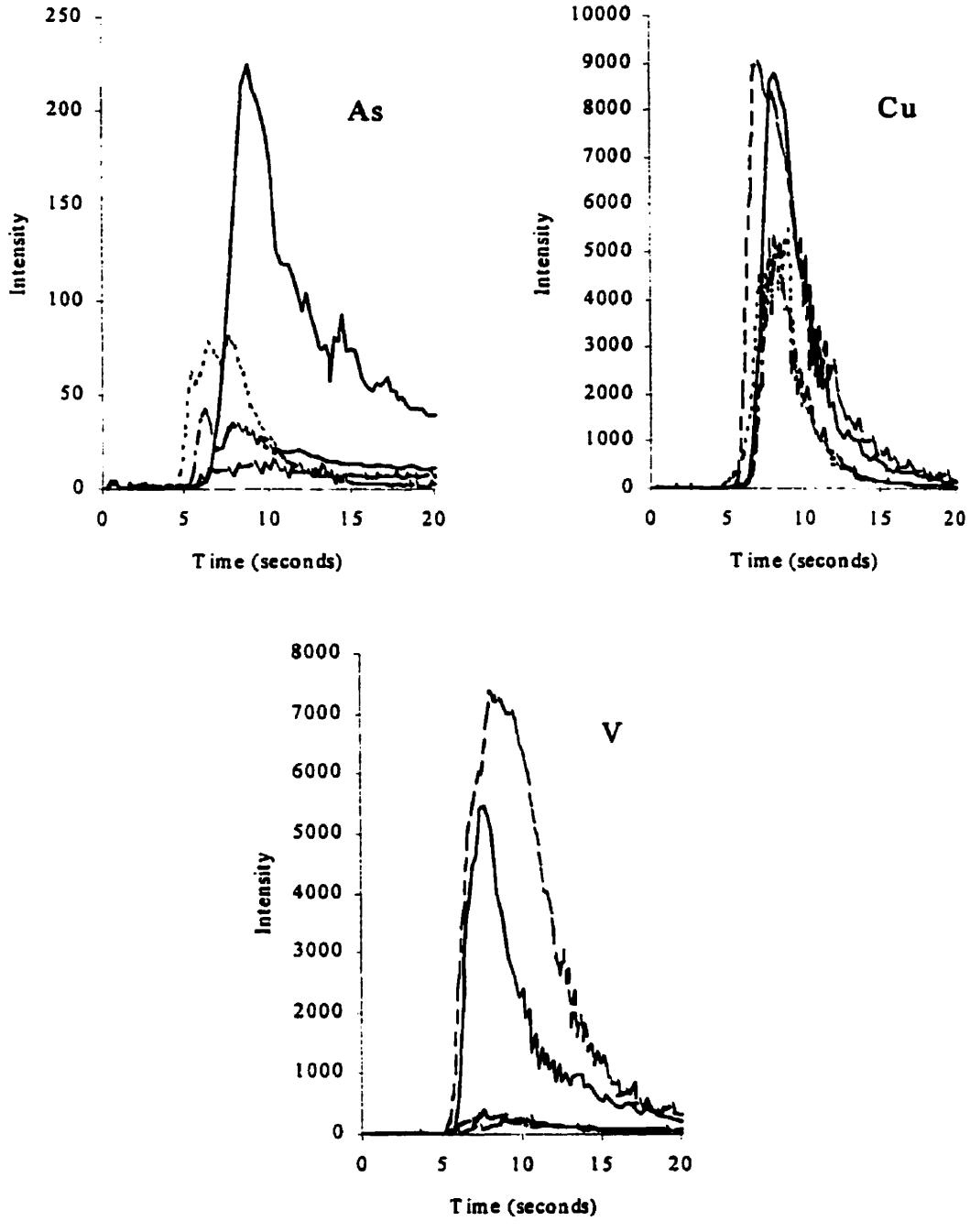

Figure 4-5 Influence of vaporization atmosphere on temporal analyte emission signal behavior. (— - - —, 15 % N_2–Ar; - - - - - -, 10 % O_2–Ar; — — —, HCl–Ar (sparged); ——, 15 % SF_6-Ar). In each case, 3 μg of analyte was vaporized.

one set of conditions (SF_6–Ar). In addition to signal intensity, signal reproducibility behavior was also highly dependent on the atmosphere used. Notwithstanding the vaporization of As and refractory carbide analytes (Cr, V), for the repeated vaporization of 300 ng of analyte, the best signal precision (in terms of % RSD of the integrated peak area), was observed with vaporization atmospheres of N_2–Ar (1.3–5.5% RSD) and SF_6–Ar (1.6–7.1% RSD). The precision observed with HCl was slightly poorer (4.5–16% RSD), probably a result of the relatively crude sparging arrangement. The highest degree of imprecision, observed for the case with O_2–Ar (6.1–24% RSD) was due primarily to destruction of the probe with the vaporization event.

4.4.2.3 Transport efficiency

Although evidence as presented above regarding the appearance and reproducibility of analyte transient signals does offer insight in terms of how a certain vaporization atmosphere affects the transport and sensitivity of an analyte, it is somewhat perilous to draw strong conclusions based on such evidence without looking at more specific, objective figures of merit. Whereas most figures of merit found in atomic spectroscopy, such as limits of detection, evaluate the overall capabilities of a complete spectrochemical system, transport efficiency serves as a benchmark specific to the performance of the sample introduction component. Defined essentially as the amount of analyte that successfully reaches the atomization–excitation–ionization source of a spectrochemical system, transport efficiency is often expressed as a percent of the gross amount of analyte initially presented to the sample introduction system.

The transport efficiency of the IH–ETV system was evaluated across the different vaporization atmospheres used in this study by means of a closed-system trapping

Table 4-2 Comparison of analyte transport efficiency for various *x*–Ar binary gas mixtures (expressed as %*x* (v/v)).

	% analyte transport efficiency (± 95 % c.l.)			
Element	15% N_2–Ar	10% O_2–Ar	HCl–Ar (sparged)	15% SF_6–Ar
As	36.0 ± 0.6	30.2 ± 5.1	27.8 ± 7.2	89.6 ± 3.1
Cd	40.6 ± 1.6	48.8 ± 3.2	69.9 ± 4.8	65.8 ± 2.5
Cr	5.4 ± 0.8	8.4 ± 7.1	72 ± 18	71.9 ± 6.4
Cu	47.2 ± 2.5	39.2 ± 2.5	77.9 ± 4.6	60.1 ± 1.9
Mn	45.1 ± 2.7	42.0 ± 3.9	73.5 ± 5.7	76.1 ± 8.2
Ni	27.0 ± 1.3	19 ± 11	75 ± 12	66.3 ± 3.3
Pb	47.3 ± 2.0	60.6 ± 4.6	75.1 ± 4.7	81.4 ± 2.8
V	0.4 ± 0.3	0.1 ± 0.5	46 ± 15	24.6 ± 1.9

method[15] as described in the Experimental section, with Table 4-2 summarizing the observed values. Immediately evident upon examination of these values is the profound improvement halogenation has on transport efficiency. The average analyte transport efficiency across all of the analytes studied in Table 4-2 increases from ca. 30% for non-halogenating conditions (N_2–Ar and O_2–Ar) to ca. 65% for halogenating conditions (HCl–Ar and SF_6–Ar). The greatest enhancement in analyte transport was expected in the case of refractory carbide-forming (Cr, V) elements, as halogenation provides a means for the formation of a easily vaporized metal–halide species in the IH–ETV over what would otherwise be a highly-involatile carbide species. This proved to be the case, as the transport of Cr, the "weaker" of the refractory carbides studied, was improved by a factor of approximately 10 when a halogenating vaporization atmosphere was used, and the transport of the highly-refractory carbide of V was improved by a factor of around 100.

Notwithstanding the above case with Cr and V, and the special case observed in the transport of As (which is discussed later), the observed transport efficiencies for the remaining volatile (Cd, Mn, Pb) and less volatile (Cu, Fe, Ni) analytes bore strikingly

similar values within each volatilization atmosphere studied, irrespective of the volatility of the analyte. The average transport efficiency observed for these analytes was (42 ± 10)% with N_2–Ar, (42 ± 17)% with O_2–Ar, (74 ± 4)% with HCl–Ar, and (70 ± 10)% with SF_6–Ar. This was somewhat surprising, as the ability of an analyte to be transported is most often dependent on its ability to form a solid aerosol subsequent to vaporization, and less volatile elements typically have higher rates of nucleation and form more stable nuclei than more volatile elements. What must be taken into consideration, however, is the fact that these samples were vaporized under full-power in the IH–ETV, and consequently underwent extremely rapid heating. Under such conditions, one can expect the vapor of the volatile elements to be partially mixed with the stable nuclei incipient from the less volatile elements such that heterogeneous nucleation process takes place.[21] If conditions are sufficiently turbulent and adequate mixing occurs, it is feasible that the above process could improve the transport of the high-volatility analytes to a level equivalent to that expected of the low-volatility analytes, even if both groups exist in equally minute quantities.

As for the bimodal distribution of analyte transport efficiencies that appears to be correlative with the two types (halogenous/non-halogenous) of vaporization atmospheres used, improved condensation/aggregate formation is probably playing a role paired with the increased analyte volatility synonymous with halogenation, leading to better overall transport in the halogenous case. Analyte condensation could occur on particles whose origin is extrinsic to the sample being vaporized, with these particles acting as physical carriers for sample transport. An example of this would be analyte condensation on amorphous carbon particles either thermally ablated from the graphite probe or displaced

by chemical attack of fluorine or chlorine radicals. Furthermore, in the case of an SF_6–Ar atmosphere, the thermal decomposition of SF_6 will eventually lead to the formation of sulfur particles, which may also act as a physical carrier. In addition to heterogeneous nucleation on foreign particles, one must also acknowledge the possibility of chemical condensation taking place. In the case with the HCl–Ar atmosphere, for instance, introduction of HCl into the Ar carrier is achieved by sparging the stream through concentrated HCl, and this process will undoubtedly introduce water vapor into the Ar stream as well. If it is assumed that the presence of HCl results in volatilization of most of the analytes as chlorides, the likelihood that these species would hydrolyze upon contact with the water vapor to form less-volatile oxides exists. These oxides would have higher rates of nucleation and in turn would more readily form transportable aggregates. Similarly, an argument could be made for the formation of involatile sulfides in the case with SF_6–Ar. Nonetheless, it is apparent that for all atmospheres tested, heterogeneous nucleation takes place due to the rapid co-volatilization of the analytes deposited, resulting for the better part in similar transport efficiencies for all the analytes vaporized in a given atmosphere. In the cases with halogenous atmospheres, however, this rapid co-volatilization occurs under more volatile conditions in an environment conducive to foreign particle nucleation and/or chemical condensation resulting in better overall transport efficiency.

The transport of As, as seen in Table 4-2, appears to be a special case unto itself. With vaporization atmospheres of N_2–Ar, O_2–Ar and HCl–Ar, the average transport efficiency observed for As was approximately 30%, however, upon vaporization in an atmosphere of SF_6/Ar, the transport efficiency improved significantly to almost 90%. To

explain this observation, the thermochemical nature of SF_6 must be considered, specifically the fact that SF_6 will begin to lose fluorine radicals upon thermal decomposition. The fluorine lost from SF_6 can react directly with As^0 to form AsF_5,[22] which is volatile at room temperature (b.p. –53.2 °C). Since transport losses arise when analyte vapors condense on the components of an ETV system as opposed to transportable nuclei, it logically follows that an analyte that never condenses should undergo highly efficient transport. This rationale is the impetus behind established sample introduction techniques such as the "cold vapor" technique for the introduction of Hg[23], and hydride generation for As, Se, Sb, Bi, Ge, Sn, Te and Pb[24], both being cases where ambient volatile forms of the analyte are generated to facilitate their transport to an atomization–excitation–ionization source.

4.4.2.4 Analyte sensitivity and detection limits

Analyte transport bears a direct consequence on benchmarks such as analyte sensitivity and limits of detection (LOD) for an ETV–ICP–OES system. For trends in sensitivity and LOD to be concerted, however, in both magnitude and direction with those observed for analyte transport across varying experimental conditions, the implication is made that these conditional changes have no influence on process such as atomization, excitation and ionization conditions in the plasma source. This is certainly not the case with the use of different gaseous mixtures in the central channel flow. Goltz *et al.* reported that the use of N_2 in IH–ETV widened the center channel of the annular ICP discharge and cooled plasma conditions[7,8], and fundamental studies of mixed-gas ICP discharges support this observation. For instance, the addition of 2.5–16.7% N_2 to the injector flow has been reported to cause a depression in electron number density (n_e), a drop greater than 5000 K

in electron temperature (T_e), a smaller drop in the gas-kinetic temperature (T_g), and a 20× reduction in the Ca emission intensity (398.6 nm line, radial view) with solution nebulization.[25] Explanation of this phenomena rests in the fact that N_2 has a much higher heat capacity than Ar at temperatures typically observed in an ICP discharge (3000–7000 K), and that rotational and vibrational modes are available for heat transfer in N_2 due to its diatomic nature, in addition to the translational (and to a lesser extent, electronic) modes common to both Ar and N_2. Oxygen also has a higher heat capacity than Ar and rotational and vibrational modes available for heat transfer, but its heat capacity reaches a local maximum at a temperature much lower (~3800 K) than that observed for N_2 (~7200 K),[26] suggesting that its effects on n_e, T_e and T_g when introduced into the injector flow would not be as pronounced.

From Fig. 4-5 it is difficult to elucidate the effect of the various gases relying strictly on the appearance of the transient signals, knowing that the transport efficiency does vary with the vaporization atmosphere. Proposed herein as an indirect means of assessing the effects of each gas mixture introduced into the plasma is the transport-independent analyte sensitivity, m_0, defined as:

$$m_0 = m/\phi \qquad \text{(Eqn 4.2)}$$

where m is the slope of the calibration curve for a given analyte, and ϕ is the normalized transport efficiency (dimensionless). What Eqn. 4.2 yields is the hypothetical sensitivity for a given analyte if 100% of the raw sample introduced into the IH–ETV system was capable of reaching the plasma. Table 4-3 lists these values relative to those obtained with 15% SF_6–Ar. Values are reported for elements whose transport efficiency was reported in Table 4-2 except for Cr and V, as their respective transport efficiencies were

Table 4-3 Comparison of transport-independent analyte sensitivity for various *x*–Ar binary gas mixtures (expressed as %*x* (v/v)).

Element	Transport-independent analyte sensitivity (normalized, relative to SF_6-Ar values)			
	15% N_2-Ar	10% O_2-Ar	HCl-Ar (sparged)	15% SF_6-Ar
As	0.21	0.88	0.78	1
Cd	0.25	1.15	0.71	1
Cu	0.40	0.65	0.82	1
Mn	0.52	0.50	1.41	1
Ni	0.39	1.18	1.10	1
Pb	0.22	1.39	0.78	1
Average[a]	0.33 ± 0.13	0.94 ± 0.29	0.96 ± 0.36	–

[a] Values represent the average for the elements specified ± 95 % confidence interval.

exceptionally low with a high degree of associated uncertainty, leading to unreliable values for m_0 when incorporated into the denominator of Eqn. 4.2. Inspection of these values reveals that that HCl–Ar and O_2–Ar have analyte sensitivities that on average are quite similar to that attainable with SF_6–Ar, although an inter-element variability does exist. In stark contrast, the transport-independent analyte sensitivity observed with N_2–Ar is on average 70% lower than that realized with SF_6–Ar, suggesting that energy conditions in the plasma were highly suppressed. This apparent perturbation of plasma conditions when N_2–Ar was introduced was confirmed visually as the ICP appeared compressed axially from the bottom of the annulus and had a considerably wider center channel than the plasma discharges observed under the other *x*–Ar mixtures studied.

Table 4-4 reports the absolute LODs evaluated under all of the vaporization atmospheres studied as well relative solution nebulization LODs for each of the analytes studied. Detection limits were determined by dividing 3× the standard deviation of the average integrated blank signal (n=6) by the slope of the calibration curve. Examination

Table 4-4 Comparison of ICP–OES limits of detection (LODs) for IH–ETV sample introduction with various *x*–Ar binary gas mixtures (expressed as %*x* (v/v)) and solution nebulization.

		Limit of detection (LOD)[a]				
		IH-ETV /ng				Solution nebulization /ng ml^{-1}
Element	Wavelength /nm	15 % N_2–Ar	10 % O_2–Ar	HCl-Ar (sparged)	15 % SF_6–Ar	
As	189.042	20	6	30	0.9	10
Cd	214.438	2	0.4	0.3	0.08	0.8
Cr	283.563	8	6	2	1	-
Cu	324.754	2	2	1	0.2	2
Fe	238.204	5	5	12	1	0.1
Mn	257.610	1	1	8	0.5	0.1
Ni	221.647	20	7	3	3	1
Pb	220.353	20	2	2	0.5	8
V	309.311	70	60	10	3	2
Zn	213.856	1	0.4	2	0.1	7

[a] Limit of detection (LOD) determined $3\sigma_b/m$ where σ_b is the sample standard deviation of the blank and m is the slope of the calibration curve.

of these values reveals that generally the lowest LODs were realized under an SF_6–Ar atmosphere, with absolute detection limits ranging from 0.08–3 ng in this study. These values were, on average, a factor of 5 better than those obtained with HCl–Ar, a factor of 8 better than those observed with O_2–Ar, and a factor of 13 improved over those realized with N_2–Ar. The difference between the LODs for the two halogenating cases (SF_6, HCl) was generally the result of a higher level of uncertainty in the blank measurements with HCl–Ar atmosphere. This higher uncertainty was also evident in the analyte signals with HCl–Ar, pointing to the possibility that the mechanism of introducing HCl into the Ar stream by sparging is the primary contributing noise factor.

Although in many cases it is difficult to make a truly objective comparison of ETV–ICP–OES detection limits in light of the potential number of variables involved

(*e.g.*, sample size, use of matrix modifiers, wavelength monitored, type of optical arrangement and detection), the LOD values obtained in this study for IH–ETV sample introduction do fall somewhat towards the high end of the expected ranges[27], a fact that is slightly surprising in light of the rather favorable transport efficiencies recorded, especially when a halogenating atmosphere was used (Table 4-4). A somewhat objective comparison can be made between the LODs reported here and those reported by Goltz *et al.*[8] previously for ICP–OES, although the comparison should be qualified by the fact that not all elements were common to both studies, and in some cases, different wavelengths were monitored. When the detection limits obtained here are compared with those reported in the previous IH–ETV–ICP–OES study, in which an ICP–OES with a Rowland circle-type polychromator with photomultiplier tube (PMT) detection was used, a dichotomous picture exists: the IH–ETV detection limit values obtained for analytes vaporized under an HCl–Ar atmosphere were typically an order of magnitude better than those obtained for elements common to the present study under the same vaporization conditions, yet the solution nebulization detection limits reported in the current study were on average an order of magnitude better than those reported by Goltz *et al.*.[8] The disparity observed in these values points to a photon-sensitivity shortcoming encountered with the ICP–OES (echelle/CID detector) used in the present study when obtaining rapidly evolving transient signals *versus* steady-state signals and can be explained using signal-to-noise ratio (SNR) arguments. Low concentration, steady-state (*i.e.*, solution nebulization) signals from ICP–OES systems are in most cases limited by background flicker noise, and a CID–based system will integrate the signal simultaneously over the portions of the spectrum being monitored, meaning that when a background subtraction is

made, the flicker component present in both the background signal and the (background + analyte) signal is significantly reduced. This is especially beneficial with an echelle optical arrangement, as its highly dispersive nature (*i.e.*, separating light into many consecutively monitored, highly-resolved orders) results in relatively weak spectral lines when compared to those generated from a Rowland circle arrangement. Simultaneous measurement is not possible with the previously used PMT-based system where the background and (background + analyte) signals are measured sequentially[28]. With transient signals, such as those recorded here with IH–ETV sample introduction, the photon flux being integrated is small and finite, meaning that no appreciable SNR improvement is garnered by an increased integration period. As a result, the relatively weaker photon fluxes resulting from the highly-dispersive echelle optical arrangement, paired with factors such as quantum efficiency and detector noise (which is usually higher in CIDs *vs.* PMTs) will now prove to be influential or limiting factors. Unfortunately, few studies exist where ETV sample introduction has been coupled with charge transfer device (CTD)-based ICP–OES systems with echelle optics, and comparative ETV studies with PMT systems currently do not exist. If the performance of the echelle–CID arrangement does bear a direct consequence on the detection limits observed above, the detection limits reported by Goltz *et al.*[8] point to optimal IH–ETV–ICP–OES absolute detection limits with SF_6–Ar being of the order of 1–100 pg.

4.5 Conclusion

With demonstrated characteristics such as high vaporization surface temperatures, rapid heating response, linear temperature control, reproducible analyte volatilization, high

analyte transport efficiency and pg–ng range detection limits when interfaced with ICP–OES, it is clear that an induction heating-based ETV arrangement certainly has potential as a thermal sample introduction technique. For any thermal sample introduction technique to gain truly ubiquitous acceptance though, it must be capable of reaching vaporization surface temperatures of 2500–3000 °C, and with a maximum vaporization temperature of 1860 °C, the prototypical IH–ETV system described here is somewhat lacking in this regard. It is crucial to recognize though, that this temperature limit is an attribute inherent of the induction furnace/sample probe arrangement used in this study and is not an intrinsic limitation of induction heating. Fig. 4-3(a) clearly shows that the IH–ETV device was quite easily capable of heating a 3/8" (9.53 mm) o.d. graphite cup to temperatures in excess of 2200 °C, but that this could only be done by increasing the plate voltage on the oscillator tube above its recommended maximum operating potential of 2500 V. Even without applying voltages in excess of the maximum rating to the plate, the maximum vaporization surface temperature can be increased simply by changing to a sample probe with a wider diameter cup that will couple more efficiently with the induction field. The coupling of cups with diameters larger than 3/8" was found to draw grid and plate currents exceeding the maximum ratings of the oscillator tube. With induction furnaces of similar design possessing nominal forward power ratings upwards of 2.5 kW (as compared to 1.5 kW of the IH–ETV furnace) the next generation of IH–ETV instrument should be able to provide temperatures of 2500–3000 °C.

It has been demonstrated that the use of mixed-gas carriers as vaporization atmospheres, particularly halogenous mixtures such as HCl–Ar and SF_6–Ar, can impart favorable effects on transport efficiency and analyte sensitivity in IH–ETV sample

introduction. While the application of binary *x*–Ar mixtures in this IH–ETV study was concertedly motivated by the need to prevent electrical discharging in the RF field, the vaporization/transport phenomena observed with their use here is certainly applicable, and should be of interest to conventional ETV studies. Due to certain experimental instances, however, such as those often found in ICP–MS where species of atmospheric origin result in pervasive and irreconcilable spectral interferences or impart physical damage to the sampler/skimmer cones, the ability to conduct thermal vaporization events in an Ar-only atmosphere will certainly be needed. This is not currently possible with the existing IH–ETV prototype, however, with the origins of the electrical discharging elucidated, solutions do appear forthcoming. Thermionic electron emission from the sample probe can be reduced by moving to conductive materials that have higher work functions and by incorporating coatings and films that are electron affinitive. The electrical discharging encountered in IH–ETV is also somewhat reminiscent of that encountered in ICP–MS due to potential differences between the load coil, plasma, and elements of the interface region, and the solutions used in ICP–MS may prove to be applicable.[29] For instance, by establishing either a virtual or a physical ground on the center turn of the load coil, a balanced RF signal with an average potential about ground is established, and in turn, by grounding the sample probe, the average potential difference between the two elements would be minimized.

4.6 Acknowledgements

Sincere thanks are extended Jean-Pierre Farant of the Department of Occupational Health and Safety of McGill University for the generous loan of the infrared thermocouple used

in this study, to Simon Aubin for assistance with the calibration and operation of the device, and to Hai Ying for his assistance in developing a software routine for the conversion of ThermoSPEC/CID timescan files into other formats. Scholarship support provided by the province of Québec through Fonds pour la Formation de Chercheurs et l'Aide à la Recherche (FCAR) is gratefully acknowledged. This research was supported through funding from the Natural Sciences and Engineering Council of Canada (NSERC) by means of an NSERC Operating Grant.

4.7 References

1. Browner, R.F. and Boorn, A.W., *Anal. Chem.*, 1984, **56**, 786-798A.

2. Gunn, A.M., Millard, D.L., and Kirkbright, G.F., *Analyst*, 1978, **103**, 1066.

3. Matusiewicz, H., *Adv. At. Spectrosc.*, 1995, **2**, 63.

4. Salin, E.D. and Horlick, G., *Anal. Chem.*, 1979, **51**, 2284.

5. Sing, R., *Spectrochim. Acta, Part B*, 1999, **54**, 411.

6. Sturgeon, R. E. and Lam, J. W., *J. Anal. At. Spectrom.*, 1999, **14**, 785.

7. Goltz, D.M. and Salin, E.D., *J. Anal. At. Spectrom.*, 1997, **12**, 1175.

8. Goltz, D.M., Skinner, C.D. and Salin, E.D., *Spectrochim. Acta B*, 1998, **53**, 1139.

9. Bauer, C.F. and Natusch, F.S., *Anal. Chem.*, 1981, **53**, 2020.

10. Rattray, R., and Salin, E.D., *J. Anal. At. Spectrom.*, 1995, **10**, 829.

11. Skinner, C.D., and Salin, E.D., *J. Anal. At. Spectrom.*, 1997, **12**, 725.

12. Kirkbright, G.F., and Snook, R.D., *Anal. Chem.*, 1979, **51**, 1938.

13. Ren, J.M., and Salin,.E.D. *Spectrochim. Acta B*, 1994, **49**, 555.

14. Ren, J.M., and Salin, E.D., *Spectrochim. Acta B*, 1994, **49**, 557.

15. Rybak, M.E., and Salin, E.D., submitted to *J. Anal. At. Spectrom.*, 2000.

16. Sturgeon, R. E., Berman, S. S., and Kashyap, S., *Can. Anal. Chem.*, 1980, **52**, 1049.

17. Chu, F.Y., *IEEE Trans. Electr. Insul.*, 1986, **EI-25**, 693.

18. Karanassios, V.; and Wood, T.J., *Appl. Spectrosc.*, 1999, **53**, 197.

19. Fonseca, R.W.; Miller-Ihli, N.J.; Sparks, C.; Holcombe, J.A.; and Shaver, B., *Appl. Spectrosc.* 1997, **51**, 1800.

20. Fonseca, R. W.; and Miller-Ihli, N. J., *Appl. Spectrosc.* 1995, **49**, 1403.

21. Kántor, T., *Spectrochim. Acta B*, 1988, **43**, 1299.

22. Ruff, O., Braida, A., Bretshneider, O., and Plaut, H., *Z. anorg. allgem. Chem.*, 1932, **206**, 59.

23. Clevenger, W.L.; Smith, B.W.; and Winefordner, J.D., *Crit. Rev. Anal. Chem.*, 1997, **27**, 1.

24. Nakahara, T. *Adv. At. Spectrosc.*, 1995, **2**, 139.

25. Sesi, N.N., MacKenzie, A., Shanks, K.E., Yang, P., Hieftje, G.M., *Spectrochim. Acta B*, 1994, **49**, 1259.

26. Montaser, A., and Zhang, H., "Mass Spectrometry with Mixed-Gas and Helium ICPs", in Montaser, A. (ed.) *Inductively Coupled Plasma Mass Spectrometry*, Wiley-VCH, 1998, p.827.

27. Carey, J.M., and Caruso, J.A., *Crit. Rev. Anal. Chem.*, 1992, **23**, 397.

28. Pennebaker, F.M., Williams, R.H., Norris, J.A., and Denton, M.B., *Adv. At. Spectrosc.*, 1999, **5**, 145.

29. Douglas, D.J. and French, J.B., *Spectrochim. Acta, Part B.*, 1986, **41**, 197.

Chapter 5

Direct determination of metals in soils and sediments by induction heating–electrothermal vaporization (IH–ETV) inductively coupled plasma–optical emission spectrometry (ICP–OES)

Having now completed a thorough study of the performance attributes of the IH–ETV system, the next logical step was to develop an application to further demonstrate its capabilities as a sample introduction technique. The presence of SF_6 in the Ar carrier flow yielded the best overall performance in terms of analyte transport and detection limits, thus it was decided to incorporate its use in the ensuing application. At first, the analysis of the wood pulps already studied by DSI–ICP–OES (Chapter 2) was considered, as this would effectively enable a direct comparison of the two techniques. This was eventually dropped in favor of analyzing samples that were more homogeneous and better characterized, so as to acquire a more accurate picture of the true capabilities of the IH–ETV technique. Furthermore, one of the key elements of interest in the pulp sample, Mg, proved difficult to volatilize in preliminary experiments with SF_6, most likely due to the formation of highly refractory MgF_2. Consequentially, the analysis of homogeneous, well-characterized soil and marine sediment certified reference materials was selected as an interesting application to demonstrate the abilities of IH–ETV. This chapter describes the sampling and calibration strategies used, as well as the analytical performance of the IH–ETV–ICP–OES determination.

5.1 Abstract

The application of an induction heating (IH) electrothermal vaporization (ETV) sample introduction arrangement for the determination of As, Cd, Cu, Mn, Pb and Zn in soils and sediments by inductively coupled plasma–optical emission spectrometry (ICP–OES) is presented. Samples were deposited either directly as a solid or by means of slurry sampling into graphite cups which were then positioned in a radio-frequency (RF)-field and vaporized in a carrier flow of 15% (v/v) SF_6–Ar. Four certified reference materials (CRMs) were examined: two soil samples —SRM 2710 and SRM 2711 (NIST); and two marine sediments—MESS-2 and PACS-2 (NRC Canada). In general, sample delivery was simpler and observed signal precision was better with slurry sampling with RSDs from 4–16%. Plots of intensity *versus* certified concentration for the four CRMs were linear with log-log slopes of 0.98–1.02 and r^2 values ≥ 0.995 for As, Cu, Pb and Zn. Recoveries of 80–105% were achieved for the above elements in SRM 2711 using an external standards curve constructed from the 3 remaining CRMs. Aqueous standard solutions were used for the analysis of all 4 CRMs by standard additions, resulting in an average recovery of (101±15)% across all six determined elements in all four samples.

5.2 Introduction

The release of metals from various human activities inevitably results in their distribution throughout the environment, with soils and sediments functioning as an important sink for their accumulation. Common examples of anthropogenic activities that introduce trace elements into soils include soil-application practices (e.g., the application of fertilizers, agrochemicals, sewage sludges and effluents, and manures) as well as irrigation activities and general atmospheric deposition.[1] Increased frequency and magnitude of these

activities naturally increases the trace-element circulation in the environment and results not only in an increased accumulation of trace elements in soils, but ultimately a build-up of metals in the human food chain. With the effects on human health from the consumption of these elements often being vague and retrospective, the monitoring of soils serves as a prospective indicator of trace element consumption, as well as a retrospective indicator of anthropogenic activity.[1] Since the chemical form of a trace element often bears a direct consequence on its bioavailability and toxicity, analytical methodologies that are capable of speciation, *i.e.*, isolating and identifying the chemical form of an analyte are of considerable importance in the determination of metals in environmental samples. Nonetheless, the determination of the total trace element concentration of soils and sediments is still quite valuable in an absolute sense for establishing background levels and identifying occurrences of metal contamination.[2]

With the existence of well-established instrumental technologies such as atomic absorption spectrometry (AAS), x-ray fluoresence (XRF), inductively coupled plasma–optical emission spectrometry (ICP–OES), ICP–mass spectrometry (ICP–MS), glow discharge–MS (GD–MS) and neutron activation analysis (NAA), there is certainly no shortage of techniques that are capable of determining the total concentration of metals in samples such as soils and sediments. What often precludes their routine application are shortcomings in terms of methodological requirements. Examples of these include: simultaneous multi-element analysis capabilities (AAS); analyte sensitivity (XRF); user prevalence (GD–MS, NAA); and/or operating costs (NAA). These issues considered, with the ability to perform simultaneous or rapid sequential multi-element analyses at low ppb range detection limits with relatively few interferences, and moderate capital and

operating costs, ICP–OES presents itself as a well-suited candidate for the routine analysis of many sample types including soils and sediments.

The most common technique for introducing samples in ICP–OES is solution nebulization (SN), and though the SN interface is convenient for samples than can be presented in either an existing or an easily generated liquid form, solid samples must typically be subjected to a sample dissolution/digestion step[3] to facilitate their introduction. Although these digestion techniques are well-characterized, widely-used, and recognized by environmental agencies,[4] and the advent of microwave-assisted digestion methods[5,6] has improved the ease and reliability with which they can be conducted and reduced concerns regarding contamination, the conversion to liquid format does present an inconvenience, provides the potential for error and inevitably result in sample dilution. As an alternative approach, a thermal sample introduction method such as direct sample insertion (DSI)[7] or electrothermal vaporization (ETV)[8] can be used as a means of analyzing samples such as soils or sediments directly with no or minimal prior sample treatment. With these approaches, a solid sample can be placed on a surface that is subsequently heated, allowing the vaporized analytes to be swept into the plasma as a vapor or a dry aerosol, resulting in a transient emission signal that is integrated. Granted, the analysis of a relatively small amount (of the order of mg) of a solid sample does raise concerns in terms of sample homogeneity, however, judicious sampling practices and rigorous processing (*i.e.*, pulverizing, mixing) procedures can effectively mitigate these concerns. Furthermore, the development and application of slurry sampling, in which a solid is prepared simply as a fine, uniform particulate suspension in liquid media and can be volumetrically procured and delivered, has presented a means by which solid samples

can be systematically and reproducibly delivered into thermal sample introduction systems.[9]

There exist several examples where soils and sediments have been analyzed directly using ETV.[10,11,12] Recently, a variant of ETV was described in which a radio-frequency (RF) field-induced current was used to heat an electrically conductive vaporization surface[13,14,15] rather than an applied direct current (DC) as is commonly the case in conventional ETV systems. This inductively heated–ETV (IH–ETV) arrangement[13] is interesting in that it melds a highly controllable, *ex situ* thermal vaporization event analogous to that achieved in conventional ETV with an interchangeable graphite cup sample holder in a contact-free heating environment not unlike that encountered in DSI. This type of arrangement lends itself well to processes that would benefit from batch sample processing and high sample throughput, as samples can be prepared in individual probes, subjected to pretreatment off-line, and then be vaporized in rapid succession. Another characteristic of IH–ETV sample introduction is the routine use of mixed carrier gases, such as SF_6–Ar, as a means improving analyte volatilization and transport while at the same time preventing electrical discharging in the RF-field due to thermionic electron emission from the graphite sample probe.

The objective of this study was to evaluate the utility of IH–ETV sample introduction with ICP–OES as a general survey technique for metals in soil and sediment samples. Design aspects and operational considerations that are unique to IH–ETV sample introduction were examined in terms of their bearing on overall experimental design and implementation, as well as overall analytical performance using different calibration methodologies.

5.3 Experimental

5.3.1 IH–ETV and ICP–OES Instruments

The IH–ETV arrangement used in this study was a system designed and constructed in-house and has been described previously.[13] The system is depicted schematically in Fig. 4-1(a) of the previous chapter. In brief, a long, undercut graphite cup sample probe is positioned axially in a quartz cylinder partially encircled by a RF-generator load coil such that the cup-portion of the probe is centered in the coil. Application of forward power to the load coil will cause the cup portion to heat inductively with the temperature achieved being proportional to the power applied. The heating of the surface permits the vaporization of analytes from the cup, and a carrier-gas flow from the lower end of the cylinder sweeps the vaporized analyte plume through a transport-tubing network into the injector of the ICP torch. The vaporized analyte cloud is passed through the center channel of the plasma discharge where element-specific transient emission signals are generated, optically isolated and recorded by an ICP–OES instrument. In this study, the IH–ETV was operated with a carrier gas mixture of 15% (v/v) SF_6–Ar.

Samples in this study were vaporized from probes machined from cylindrical (2" (508 mm) length × 3/8" (9.525 mm) diameter) high-density graphite rod stock (HLM grade, SGL Carbon Group, Speer Canada Inc., St.-Laurent, QC, Canada) to the dimensions appearing in the cutaway diagram in Fig. 4-1(c) of the previous chapter. A bench-top lathe (Emco Compact 5, Emco Maier, Columbus, OH, USA) and high-speed stainless-steel tools were used for the machining process (described in detail elsewhere).[16] Vaporized samples were introduced into a radially-viewed ICP–OES with Echelle optics and charge induction device (CID) detection (TJA IRIS, TJA Solutions, Franklin, MA,

USA). Transient analyte emission signals were processed using the IRIS operating software (ThermoSPEC/CID v2.10, TJA Solutions). Details regarding the vaporization sequence and instrumental settings for both the IH–ETV and ICP–OES appear in Table 5-1.

5.3.2 Samples, standards and reagents

For the preparation of samples and standards, distilled deionized water (DDW) (Milli-Q Water System, Millipore Corp., Bedford MA, USA) and trace metal grade acids (Instra-Analyzed, JT Baker, Phillipsburg, NJ, USA) were used throughout, with ACS reagent grade acids (Baker-Analyzed, JT Baker) and DDW being used for the cleaning and conditioning of sample containers. Four certified reference materials (CRMs) were used: two soil samples (SRM 2710 (Montana Soil – Highly Elevated Traces) and SRM 2711 (Montana Soil – Moderately Elevated Traces), National Institute of Standards and Technology (NIST), Gaithersburg, MD, USA); and two marine sediment samples (MESS-2 (Beaufort Sea Marine Sediment) and PACS-2 (Esquimalt, BC (harbor) Marine Sediment), Institute for National Measurement Standards, National Research Council of Canada (NRC), Ottawa, ON, Canada). Slurries were prepared by mixing an accurately (gravimetrically) determined amount of CRM with an accurately known amount of DDW. The proportion of CRM to DDW in the slurries ranged from 1:10 to 1:100 (m/m) and were prepared in volumes of DDW of at least 30 ml. Slurries were stored in polypropylene containers (Nalgene) that had been preconditioned for 24 hours with 1:1 (v/v) HNO_3 in DDW and rinsed thoroughly with DDW. To ensure the homogeneity of the sample being drawn, slurries were actively stirred during the sampling step using a cleaned and preconditioned Teflon™ stirring bar and a magnetic stirrer. Slurries were sampled using a 10–100 µl micropipette with trace-metal grade disposable tips (Fisher

Table 5-1 Instrumental settings

Sample vaporization step (IH-ETV)-	
Carrier gas	15% (v/v) SF_6-Ar
Carrier gas flow rate	0.50 l min^{-1} [a]
Drying step	*Ex situ*
Pre-vaporization flush time	30 s
Vaporization temperature	ca. 1900°C
Vaporization time	60 s
ICP-OES (TJA IRIS – radial view, Echelle spectrometer, CID detection)	
Plasma forward power	1150 W
Ar plasma gas flow rate	15.0 l min^{-1}
Ar auxiliary flow rate	1.0 l min^{-1}
Ar injector flow rate	0.50 l min^{-1} [a]
Wavelengths monitored (nm)	As: 189.042, Cd: 214.438, Cu: 324.754, Mn 257.610, Pb: 220.353, Zn: 213.856
Signal increment (% full well capacity)	75%
Number of time slices	300
Time per slice	0.2 s

[a] Total flow rate of SF_6–Ar mixture.

Scientific, Nepean, ON, Canada). Weighed multi-element standard solutions were prepared by mixture and serial dilution of 1000 ppm single-element standards (SCP Science, Baie-d'Urfé, QC, Canada) into a final volume of DDW containing 0.5% trace metal grade HNO_3. Standard solutions were also stored in preconditioned polypropylene containers.

5.4 Results and Discussion

5.4.1 General observations

The temporal signal behavior observed with IH–ETV sample introduction is identical to that observed with conventional ETV, in that a transient peak results. Fig. 5-1 shows the elemental emission signals typically observed for the vaporization of a soil or sediment sample, using SRM 2711 as an example. Notwithstanding differences in peak appearance (*i.e.*, height, half-width, area) that are directly related to the amount of analyte being

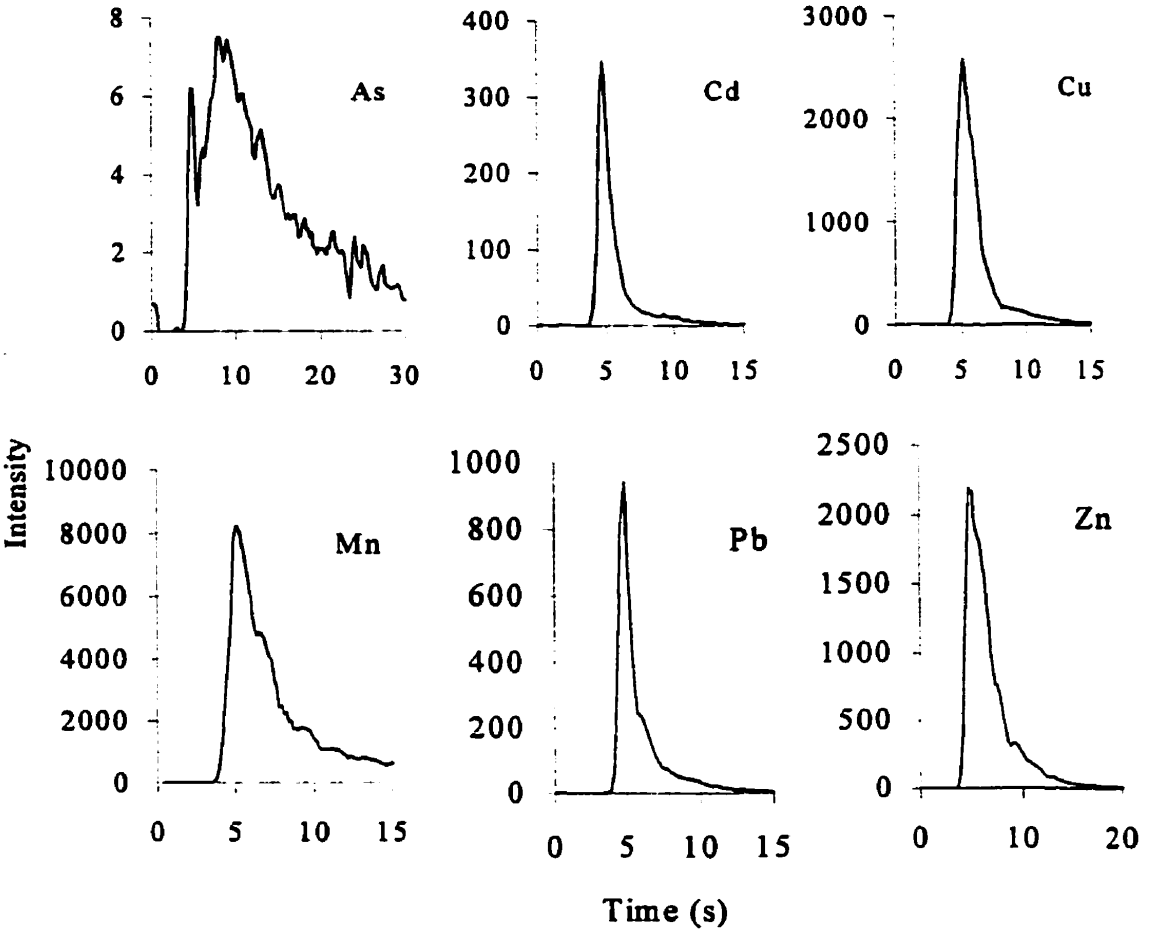

Figure 5-1 Typical IH–ETV–ICP–OES analyte emission signals for a soil sample (SRM 2711, approximately 1 mg of sample).

vaporized, analogous temporal signal behavior was observed for all elements except arsenic. The broader, tailing signals observed with As were a consequence of increased analyte diffusion resulting from the formation of volatile AsF_5 due to fluorination by the SF_6–Ar carrier.[13] In ETV, analyte is usually transported to the plasma as a fine aerosol of solid particles that form soon after vaporization. Presuming that this mechanism of transport was taking place for the remaining elements, one can assume that the larger and heavier aerosol particles were unlikely to diffuse as rapidly during transport in the carrier gas as smaller, lighter gas molecules. While this may result in a broader transient signal,

the formation of a non-condensing AsF_5 species does impart some benefits, such as high transport efficiency and low detection limits.[13]

Although element- and sample-specific trends in the observed precision values were not easily discernible, the peak area repeatability did appear to generally improve when either the amount of analyte deposited approached 1 μg or the amount of CRM deposited approached 5 mg, after which no significant improvement in precision was observed. The addition of an aliquot (50 μl) of concentrated HCl to the sample prior to vaporization was found to generally improve the reproducibility of the transient emission signals, although no significant increase in signal intensity was observed. Under these conditions and slurry sampling (100 μl of sample containing 10–100 mg ml^{-1} of sample), the precision of the transient emission signals ranged from 4% to 15% RSD (n=6) depending on the element and the CRM being analyzed. In terms of general sampling strategies, both the analysis of the solid directly and as an aqueous slurry were attempted. It was immediately apparent, however, that analyzing the solid directly was quite labor-intensive and prone to errors, as it involved the practice of having to accurately and reproducibly deposit a mass of solid sample on the order of 1–10 mg directly into the sample probe. This was reflected in the fact that the reproducibility of the transient signal peak areas was considerably poorer (7–37% RSD, n=6) when direct analysis of the solid was performed. By comparison, slurry sampling provided a simple and reproducible means by which such small quantities of sample could be transferred into the sample probe with no massing step involved, and the use of a relatively large amount of sample in preparing the slurry helped reduce sample homogeneity and massing errors.

5.4.2 Calibration and determination

For matters of convenience, calibration was first attempted using aqueous external standards. The relatively clean matrix of these standards, however, did not approximate well the complex composition of the soil and sediment samples and resulted in cases where equivalent standard and sample analyte concentrations would yield markedly different signal intensities, thus degrading the calibration method. As an alternative approach, an attempt was made at using the CRMs as matrix standards. Fig. 5-2 shows the log-log curve that results when peak intensity is plotted as a function of certified concentration for the CRMs studied. For As, Cu, Pb and Zn, linear curves with log-log slopes of 0.98–1.02 were achieved with r^2 values ≥ 0.99. The curves for Cd and Mn were also reproducible, however, their log-log slopes deviated noticeably from unity (0.93 and 0.81 respectively). The considerable deviation in the log-log slope for Cd is somewhat surprising, however, it should be noted that the Cd levels in the CRMs were the lowest amongst the elements studied in each case and the transient emission signals for Cd in some cases had the poorest repeatability amongst all of the elements and CRM studied, factors that together may have contributed to the deviation in the log-log slope observed.

To demonstrate the approach of using the CRMs as an external standards curve, a calibration was performed to determine the concentration of As, Cu, Pb and Zn in SRM 2711 using a linear regression based on the intensity *vs.* certified concentration values for MESS-2, PACS-2 and SRM2710. In each case, 100 µl of slurry and 50 µl of concentrated HCl were deposited in a sample probe, dried off-line, and then vaporized under full power in the IH–ETV. The gross amount of sample used in preparing the slurries for this calibration was adjusted such that the net amount deposited in 100 µl

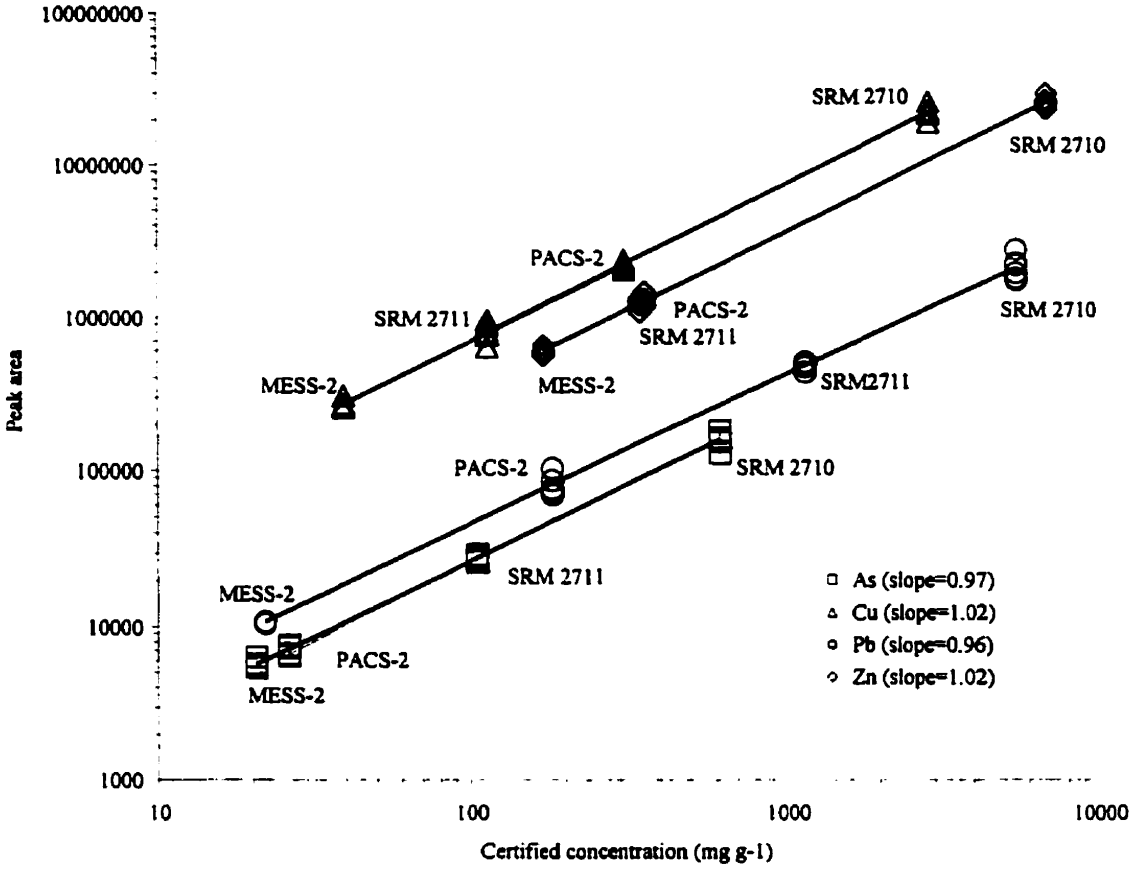

Figure 5-2 Log-log calibration plot for the CRMs studied

covered a concentration range of approximately one decade with the concentrations of the selected analytes in the unknown (SRM 2711) falling as close as possible to the median of this range. The results of this calibration appear in Table 5-2 reported at the 95% confidence level (c.l.), with the agreement between the determined and certified values appearing as % recovery (*i.e.*, the concentration determined for a given element expressed as a percent of its certified value). The practice of using CRMs as matrix-matched external standards appears to be a good approximation, with percent recoveries ranging from 80–105% for the elements determined in SRM 2711. The errors observed in the determination probably arose from differences in the matrices of the CRMs, and were

Table 5-2 Concentrations of metals determined in SRM 2711 (NIST) using CRMs[a] as external standards (slurry sampling).

Element	Concentration found /μg g^{-1} IH-ETV-ICP-OES	Certified value	% recovery
As	83.6 ± 6	105 ± 8	80
Cu	113 ± 18	114 ± 2	99
Pb	968 ± 44	1162 ± 31	83
Zn	368 ± 11	350.4 ± 4.8	105
% recovery (average)			92 ± 19

[a] SRM 2710, MESS-2 and PACS-2.

exacerbated by use of varying amounts of sample in preparing the slurries so as to offset the significantly different concentrations present in the CRMs.

For analysis by standard additions, two-point standard addition curves were constructed by vaporizing 50 μl of slurry and 50 μl of concentrated HCl with a 50 μl spike of a weighed aqueous standard for the spiked point, and with an equivalent aliquot of blank solution (0.5% HNO_3) for the point representing the sample alone. In this calibration, the gross amount of sample used in preparing the slurries was adjusted such that the net analyte concentrations were as close as possible to each other, using the certified concentration of As as a guide. The results of this analysis appear in Table 5-3, reported at 95% c.l. for 6 separate calibrations, with the agreement between the determined and certified values expressed as % recovery. Although the percent recoveries achieved did cover a considerable range [54–139%], the average recovery was 101% with half of the values reported being within 10% of their certified counterparts. Although the analytes present in both the sample and standard spike are co-volatilized with the sample matrix, differences in the chemical form of the analytes could still play a

Table 5-3 Concentrations of metals determined in CRMs using standard additions with aqueous standards (slurry sampling)

Sample	Element	Concentration found /μg g^{-1} IH-ETV-ICP-OES	Certified value	% recovery
MESS-2	As	22.6 ± 4.2	20.7 ± 0.24	109
	Cd	0.13 ± 0.05	0.24 ± 0.01	54
	Cu	31.1 ± 9.3	39.3 ± 2	79
	Mn	292 ± 14	365 ± 21	80
	Pb	24.6 ± 3.1	21.9 ± 1.2	112
	Zn	190 ± 16	172 ± 16	110
PACS-2	As	26.7 ± 8.1	26.2 ± 1.5	102
	Cd	2.2 ± 0.6	2.11 ± 0.15	104
	Cu	240 ± 40	310 ± 12	77
	Mn	354 ± 5	440 ± 19	80
	Pb	181 ± 45	183 ± 8	99
	Zn	391 ± 87	364 ± 23	107
SRM 2710	As	868 ± 73	626 ± 38	139
	Cd	27.2 ± 3.5	21.8 ± 0.2	125
	Cu	3020 ± 260	2950 ± 130	102
	Mn	10800 ± 1500	10100 ± 400	107
	Pb	5970 ± 520	5532 ± 80	108
	Zn	6860 ± 710	6952 ± 91	99
SRM 2711	As	136 ± 11	105 ± 8	130
	Cd	52 ± 7.3	41 ± 0.25	127
	Cu	95.3 ± 8.9	114 ± 2	84
	Mn	547 ± 82	638 ± 28	86
	Pb	1120 ± 190	1162 ± 31	96
	Zn	360 ± 37	350.4 ± 4.8	103
% recovery (average)				101 ± 15

role in terms of their volatilization and transport efficiency, and in turn will influence the accuracy of the determination. The addition of a second spike did not reveal any irregularities in the linearity of the standard additions curves, as r^2 values of at least 0.99 and as high as 0.9999 were obtained for the elements studied. Although not attempted here, the practice of spiking with a standard that closely matches the matrix forms of the

analytes being determined (*e.g.*, CRM), may further improve the accuracy of the results observed here. While the accuracy in the determination did not appear to have any dependence on the sample type, the precision in the determination was slightly better with the soil CRMs than the marine sediment CRMs (average of 11% *versus* 19%, respectively).

Table 5-4 lists the method detection limit (MDL) for each of the analytes determined. These values represent the absolute and relative (based on a 10 mg sample) concentrations necessary to generate a net signal three times (3×) the standard deviation of a low level analyte signal (using MESS-2 in this case). Comparison of these values with the determined concentrations in Tables 5-2 and 5-3 shows that the analyte levels present in the CRMs studied are at least an order of magnitude higher than their respective MDL, with the concentration of Cd in MESS-2 being the only possible exception.

5.5 Conclusion

By either using CRMs in an external standardization methodology or aqueous standards in a standard additions calibration, selected elements present in soil and sediment samples were determined with reasonable accuracy and precision by ICP–OES using IH–ETV sample introduction. These results are quite good in light of the fact that no matrix modifier was added to the sample, as is often the case with soil and sediment analyses using ETV sample introduction,[12] and that only an off-line drying step was incorporated into the vaporization sequence prior to the high-temperature volatilization step. Nonetheless, future IH–ETV studies should look to the use of matrix modifiers and temperature programming as means of improving overall performance. The

Table 5-4 Method detection limit (MDL) for soil/sediment analysis by ICP-OES using IH-ETV sample introduction (MESS-2, slurry sampling).

	MDL	
Element	Absolute /ng	Relative /μg g^{-1} [a]
As	20	2
Cd	1	0.1
Cu	5	0.5
Mn	8	0.8
Pb	12	1.2
Zn	5	0.5

[a] Based on the vaporization of 10 mg of sample.

interchangeable sample probe design of IH–ETV lent itself well to this type of analysis, facilitating the preparation of multiple samples off-line and their rapid introduction and removal from the induction field.

5.6 Acknowledgements

Sincere thanks are expressed to Hai Ying for his assistance in developing software for the conversion of time scan files. Scholarship support provided by the province of Québec through Fonds pour la Formation des Chercheurs et l'Aide à la Recherche (FCAR) is gratefully acknowledged by the author. This research was also supported through funding from the Natural Sciences and Engineering Council of Canada (NSERC) through an NSERC Operating Grant.

5.7 References

1. Senesi, G.S., Baldassarre, G., Senesi, N., and Radina, B., *Chemosphere*, 1999, **39**, 343.

2. Frink, C.R., *J. Soil Contam.*, 1996, **5**, 329.

3. Novozamsky, I.; van der Lee, H.J.; and Houba, V.J. G., *Mikrochim. Acta*, 1995, **119**, 183.

4. Method 3050B, United States Environmental Protection Agency (EPA).

5. Lamble, K.J., and Hill, S.J., *Analyst*, 1998, **123**, 103R.

6. Method 3051, United States Environmental Protection Agency (EPA).

7. Sing, R., *Spectrochim. Acta Part B*, 1999, **54**, 411.

8. Gunn, A.M., Millard, D.L., and Kirkbright, G.F., *Analyst*, 1978, **103**, 1066.

9. Darke, S.A., and Tyson, J.F., *Microchem. J.*, 1994, **50**, 310.

10. Schron, W., Liebmann, A., and Nimmerfall, G., *Fresenius' J. Anal. Chem.*, 2000, **366**, 79.

11. Florian, K., Hassler, J., Pliesovska, N., and Schroen, W., *Microchem. J.*, 1996, **54**, 375.

12. Záray, G., and Kántor, T., *Spectrochim. Acta Part B*, 1995, **50**, 489.

13. Rybak, M.E., and Salin, E.D., *Spectrochim. Acta Part B*, 2000, submitted.

14. Goltz, D.M., Skinner, C.D. and Salin, E.D., *Spectrochim. Acta B*, 1998, **53**, 1139.

15. Goltz, D.M. and Salin, E.D., *J. Anal. At. Spectrom.*, 1997, **12**, 1175.

16. Skinner, C.D., and Salin, E.D., *J. Anal. At. Spectrom.*, 1997, **12**, 725.

Chapter 6

Closed-system trapping method for the direct determination of transport efficiency in electrothermal vaporization sample introduction

It has been said that necessity is the mother of all invention, and this chapter deals with a technique for determining transport efficiency that was, at first, developed strictly out of necessity. The determination of the transport efficiency figures in the IH–ETV performance study (Chapter 4) presented a particular challenge whenever SF_6 was used, as one of the thermal decomposition products of SF_6, namely SF_4, will form hydrofluoric acid upon contact with water. The possibility of generating HF in a solution trapping device used for determining transport efficiency meant that no glass components could be used, effectively eliminating the use of available solution trapping devices, such as glass impingers (*i.e.* bubblers). Through the course of searching for solution trapping devices made of HF-resistant materials, the existence of gas-sampling bags made of inert fluoropolymers emerged. The possibility was then envisioned of connecting one of these bags to the exhaust of the IH–ETV system as a means of trapping the vaporized analyte for the determination of transport efficiency. This chapter describes the method developed using gas-sampling bags and its validation against an established method that uses solution impingers.

6.1 Abstract

A novel closed-system for the direct determination of analyte transport efficiency in electrothermal vaporization (ETV) sample introduction is described. A commercially available gas-sampling bag filled with 100 ml of 10% HNO_3 was connected to the exhaust of an ETV system and used to collect and seal the product of an electrothermal vaporization event. The bag was then manually agitated, and its liquid contents decanted and analyzed by solution nebulization ICP–MS. Analyte transport efficiency values were found to be in statistical agreement with those determined by a reference method on the same ETV system for a variety of volatile (As, Cd, Mn, Pb), involatile (Cu, Ni), and refractory carbide forming (V) elements. This simple experimental setup captures all of the analyte in a single solution, with the closed-system element of its design ensuring that this is done quantitatively. Absolute detection limits for most elements were of the order of 0.1–10 ng absolute for the technique, making it well suited for analyte masses typically vaporized in ETV–ICP–OES. The relative merits of using this type of setup for the determination of analyte transport efficiency in ETV sample introduction, along with experimental considerations, are described.

6.2 Introduction

The use of electrothermal vaporization (ETV) as a means of introducing samples as a dry aerosol into various atomization–excitation–ionization energy sources for atomic spectroscopy has been popularized due to its technical merits; these ranging from miniscule sample requirements to improved detection limits. With proliferation, however, undeniably comes variation, and the use of wide and varied instrumental designs and operational conditions in ETV sample introduction has necessitated the

reporting of analytical performance benchmarks, such as transport efficiency, in order to assist in the objective comparison of these devices. Analyte transport efficiency, in its simplest terms, refers to the amount of a specified analyte, usually expressed as a percentage, that successfully reaches the atom cell (*e.g.*, plasma) subsequent to the initial thermal vaporization event. One of the most robust benchmarks of analytical performance—transport efficiency—was first discussed by Millard *et al.*[1] for an ETV unit coupled to an inductively coupled plasma–optical emission spectrometry (ICP–OES) system. In this study, analyte losses were found to occur on many of the components of the ETV transport system ranging from the walls of the glass dome enclosing the ETV furnace to the walls of the transport tubing. It is then self-evident that differences in the ETV transport system design will result in differences in analyte losses along the system, and ultimately differences in analytical performance.

Along with the variety of ETV systems used for sample introduction comes an equally diverse selection of methods for determining transport efficiency. One of the most common methods found in transport efficiency studies[1,2,3] has been generalized as an "indirect" method.[2] An indirect method involves the dissolution (typically with an acid solution) and collection of the analyte adhering to the transport elements of the ETV system downstream from the vaporization element, followed by quantitation of the analyte in the collected sample. This technique has the inherent advantage of being able to pinpoint the location, as well as the magnitude of analyte losses simply by treating the ETV transport components, such as tubing, valves and connectors, separately. It remains, however, an indirect method of quantifying the amount of analyte actually leaving the ETV transport arrangement, and, when using an indirect method for this purpose, the possibility of overlooking other sites of analyte loss always exists. Consequently, indirect

methods are usually paired with the determination of transport efficiency by a "direct" method.

A direct method of determining transport efficiency usually entails placing a trap or collection vessel at the exit of the ETV transport system, where connection to the atom cell would normally be made, and then quantifying the amount of analyte collected.[2] The intuitive benefit of this method is the certainty that the amount of analyte actually reaching the source is being quantified. Numerous types of trapping apparatuses have been used for the direct determination of transport efficiency, some examples of which are solid substrates such as cotton wool,[1,4] filters,[5] and solution traps such as gas bubblers[5] or condensation setups.[2] A system has also recently been described where a second ETV furnace containing a corona-like discharge was used to electrostatically precipitate the aerosol transported from a primary ETV furnace upstream.[6,7] Not only do these methods give a truer representation of the transport efficiency value, but the use of size-discriminating media, such as filters, facilitates the speciation of the sample aerosol in terms of its particulate dimensions. Particle size distribution inferences, as well as transport efficiency determinations have also been made using laser scattering techniques.[8] With the exception of measurements made using laser scattering, which is a unique category unto itself, the aforementioned methods all have one potential drawback, in that they are all flow-through systems. Although flow-through systems have the advantage of being able to collect countless sample vaporization events in series as a means of overcoming detection limit and experimental precision concerns, the flow-through aspect of their design necessitates the use of not one, but rather a series of trapping devices.[1,4,5] The use of a series of traps is a precautionary measure to ensure that any analyte that "breaks through" one of the initial collection vessels in the series is

eventually captured. This ultimately results in the need to analyze multiple samples with increasingly low analyte concentrations, and may contribute to experimental uncertainty.

An ideal solution for the direct determination of analyte transport efficiency in ETV sample introduction would be the use of a closed system for analyte trapping. This could be achieved by connecting a vessel with non-rigid walls and a shut-off valve at the end of the ETV transport tube. Provided that the vessel expands easily enough, such that it does not create significant back-pressure throughout the ETV system, the analyte collected in the vessel should be representative of what reaches the atomization–excitation–ionization source. The collected analyte can then be dissolved in solution by either having a quantified amount of solution already present in the collection vessel and agitating the sealed vessel, or by introducing a known amount of solution into the vessel after collection of the vaporized sample and doing the same. The benefits of this kind of system are immediately apparent; all the analyte is unquestionably captured in one vessel and only one solution need be analyzed. Depending on the volume of the collection vessel, a number (albeit finite) of sample vaporizations may also be collected to overcome inadequacies in detection limits and experimental uncertainty.

A suitable example of a collection vessel for this type of application would be a gas-sampling bag not unlike those used for the collection of gaseous samples in environmental analysis. These bags are usually made of lightweight, chemically inert materials such as Teflon or Tedlar (Trade Marks of Dupont Corp.) making them ideally suited for this type of application. Gas-sampling bags have been used in the past in ICP spectroscopy applications, but usually in a capacity that is more representative of their traditional role in environmental analysis, a recent example of this being the determination of organometallic carbonyl complexes in sewage fermentation.[9] In this

study, fermentation gases were collected with sampling bags, with the organometallic complexes being extracted by cryotrapping, and analyzed by GC–ICP–MS. Examples also exist where sampling bags were used for the collection of an experimentally generated sample, rather than a naturally occurring one. An example of this being the determination of sulfur in high-purity iron, where sulfur in the form of H_2S was extracted from iron samples, collected in gas-sampling bags and then directly introduced into an ICP–MS for analysis.[10]

The objective of this study was to evaluate the utility of gas-sampling bags for the collection and dissolution of analyte in a closed-system arrangement for the direct determination of ETV sample introduction transport efficiency. Although the transport of analyte amounts typically encountered in ETV–ICP–OES was specifically studied in this investigation, the scope of the discussion addresses the applicability of closed-system trapping for the determination of analyte transport efficiency in both ETV–ICP–OES and ETV–ICP–MS.

6.3 Experimental

6.3.1 Instrumentation, samples and reagents

All samples described herein were prepared in distilled deionized water (DDW) (Milli-Q water system, Millipore Corp., Bedford, MA, USA) by sequentially diluting multi-element standards (High Purity Standards, Charleston, SC, USA) and trace metal grade acids (Baker Instra-Analyzed, J.T. Baker, Phillipsburg, NJ, USA). Solutions used for dissolving the analyte collected in trapping vessels were prepared with DDW and trace metal grade acids. Solutions used for the purposes of cleaning and conditioning experimental components were prepared from DDW and ACS reagent grade acids (Baker

Analyzed, J.T. Baker). All standards and solutions were stored in polypropylene containers (Nalgene) preconditioned with 1:1 DDW and concentrated nitric acid for 24 hours and rinsed with DDW.

The sample introduction device used in this study was an inductively heated electrothermal vaporization (IH–ETV) device based on a design originally described by Goltz and co-workers.[11,12] The main difference between an IH–ETV system and a conventional graphite furnace– (GF–)ETV arrangement is the manner in which the vaporization surface is heated: IH–ETV uses a free standing, long, undercut graphite cup sample probe that is heated inductively in a radio-frequency field; whereas GF–ETV uses a graphite cup or tube that undergoes ohmic (resistive) heating in a closed direct current circuit. In this study, the IH–ETV was operated with a vaporization atmosphere of argon doped with HCl (entrained in the carrier by sparging the argon through a flask of concentrated HCl) as a means of enhancing the volatility of refractory carbide-forming analytes and preventing arcing in the IH–ETV due to thermionic electron emission from the sample probe.

Samples collected in the trapping vessels were analyzed by solution nebulization ICP–MS (Elan 6000, PE-SCIEX, Concord, ON, Canada) with a cross-flow nebulizer and Scott-type spray chamber, and the method of standard additions was used for calibration and quantitation. Details regarding instrumental setup and acquisition settings for the ICP–MS analysis step appear in Table 6-1.

Table 6-1 Instrumental settings

Sample vaporization step (IH-ETV)—	
Carrier gas	Ar ($HCl_{(l)}$ sparged)
Carrier gas flow rate	0.65 l min^{-1}
Sample	25 ppm (nominal) in each of As, Cd, Cr, Cu, Fe, Mn, Ni, Pb and Zn; 5% (v/v) HNO_3 matrix
Sample volume	100 µl
Drying step	*Ex situ*
Pre-vaporization flush time	30 s
Vaporization temperature	2000°C
Vaporization time	60 s
Post-vaporization flush time	30 s
ICP-MS analysis (PE-Sciex Elan 6000)—	
Plasma forward power	1.0 kW
Ar plasma gas flow rate	16.0 l min^{-1}
Ar auxiliary flow rate	0.8 l min^{-1}
Ar injector flow rate	0.8 l min^{-1}[a]
Signals monitored	^{51}V, ^{52}Cr, ^{55}Mn, ^{59}Ni, ^{63}Cu, ^{66}Zn, ^{75}As, ^{111}Cd, ^{204}Pb
Mass dwell time	500 ms
Number of readings / replicate	1
Number of replicates	25

[a] Optimal setting determined following standard instrumental operating procedure.

6.3.2 Closed-system trapping

Gas sample bags made of Tedlar (SKC 232-03, SKC Inc., Eighty-Four, PA, USA) were used for collection of the vaporization plume. These bags have a capacity of 3 l and an airtight polypropylene valve with a Teflon-coated silicon rubber septum. Prior to their use for analyte vapor trapping, the gas sample bags were first subjected to a rigorous cleaning procedure. The gas sample bags were first repeatedly filled with and evacuated of prepurified argon, and then evacuated and closed under vacuum. The bags were then conditioned with 300 ml of a 1:1 mixture of HNO_3 and DDW for at least 24 h and then emptied of their contents and closed under vacuum. After this, the bags were then conditioned with 300 ml of DDW for 24 h, and then repeatedly filled with and emptied of

DDW until stable ICP–MS blank readings for the DDW were obtained (usually 3 times). Finally, the bags were emptied of their contents under vacuum and closed.

For the collection of a sample, an accurately determined 100 ml volume of a 10% (v/v) solution of HNO_3 in DDW was quantitatively transferred into a preconditioned, rinsed and evacuated sample bag. This was done gravimetrically, either using a peristaltic pump, or by decanting the solution into the bag through a clean polyethylene funnel. The sample bag was then carefully evacuated of any entrained air and closed.

One hundred (100) µl of a 25 ppm multielement (As, Cd, Cr, Cu, Mn, Ni, Pb, V, Zn) sample in 5% HNO_3 was pipetted into an IH–ETV sample probe that had been preconditioned by several sample firings and dried on a hot plate. The sample probe was then mounted in the IH–ETV device and the system was purged with the carrier gas flow for at least 1 min. A sampling bag was then attached to the vaporization device transport tube where the connection to the ICP torch injection tube would normally be made [Fig. 6-1(a)], the shut-off valve was opened and the carrier gas flow was initiated. After 30 s, the IH-ETV unit was fired at 2000 °C for 60 s, followed by a cooling flush time of 30 s. After completion of this 120 s cycle, the carrier gas flow was stopped, the valve on the sampling bag closed and the bag was removed from the transport line. With a carrier flow of 0.65 l min^{-1}, the 3 l gas-sampling bag then contained 1.3 l of carrier gas. The sampling bag was then manually agitated for 1–2 min, and the acid solution was then decanted through the valve into a polypropylene container to be analyzed. Only one sample firing was collected in each gas-sampling bag, and this was repeated eight times. Eight firings of an equivalent volume of a matrix-matched blank solution were also collected in an identical manner.

6.3.3 *Impinger solution trapping*

In order to validate the closed-system method, transport efficiency experiments were also conducted in parallel using an experimental arrangement schematically identical to that described by Grégoire and Sturgeon[5] to determine analyte transport efficiency in ETV–ICP–MS. The setup used in the present study, illustrated in Fig. 6-1(b), consisted of three 250 ml glass impingers with a coarse porosity 90° frit (Ace Glass, Vineland, NJ, USA) each connected in series with 6 cm of ¼ inch (0.635 cm) i.d. tubing. A diaphragm pump (Aircheck 50, SKC Inc.) calibrated to an Ar flow rate of 0.65 l min^{-1} was attached to the exhaust of the impinger series to ensure ambient flow of the vaporization carrier throughout the system. Unless stated otherwise, the first two impingers in the series were filled with an accurately determined 200 ml volume of 10% HNO_3 in DDW, and the third impinger was filled with an equivalent volume of DDW, to prevent any acid vapor from reaching and possibly contaminating and/or damaging the backing pump. This setup was also connected to the vaporization device transport tubing where the connection to the ICP torch injection tube would normally be made. The identical sample, sample volume and sequence and duration of vaporization steps were used in these experiments as in the previous section. Sample- and blank-firing collection experiments were also repeated 8 times.

6.4 Results and discussion

As stated earlier, flow-through systems for trapping analyte in transport efficiency studies usually consists of a series of trapping devices. Fig. 6-2 demonstrates precisely why this is done, using the recovery of Cu as an example. The first impinger in the series

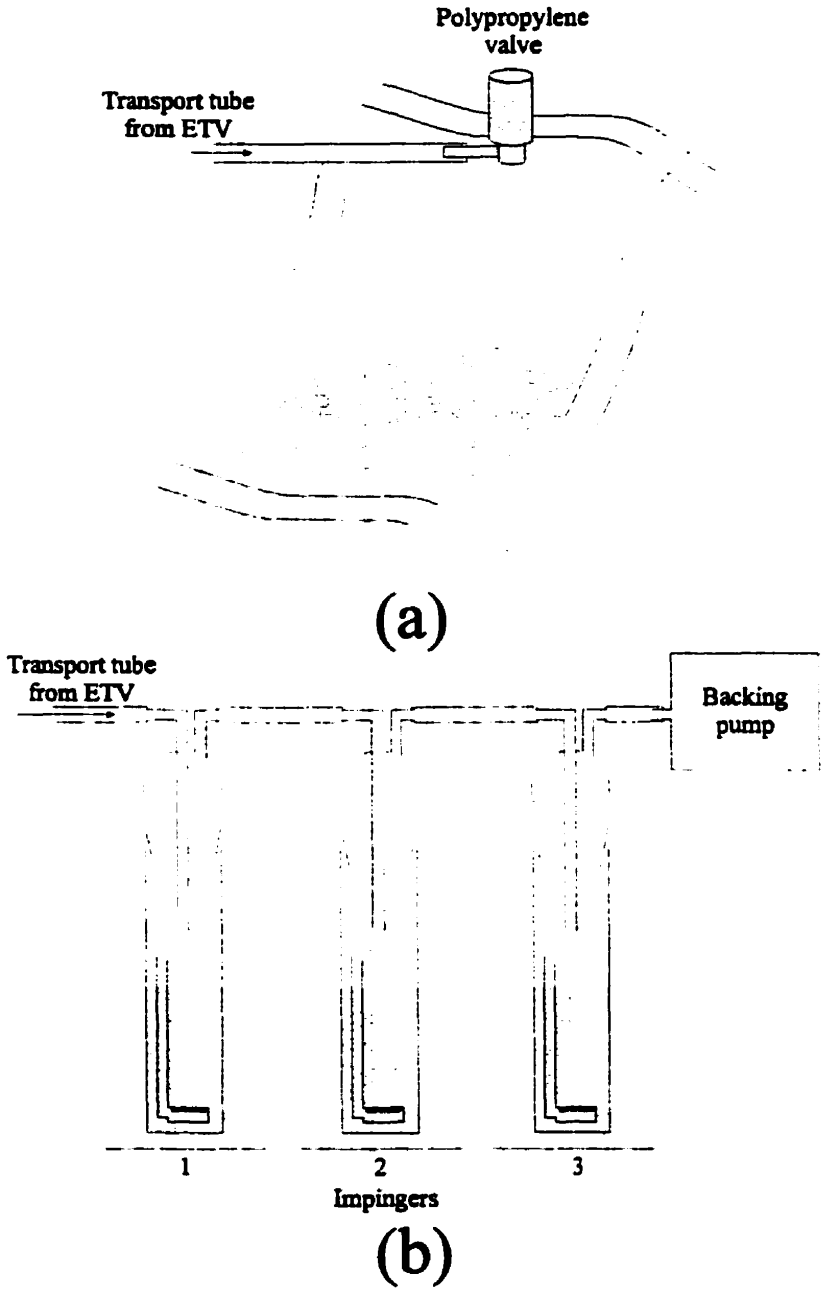

Figure 6-1 Schematic diagrams of the (a) closed-system trapping and the (b) flow-through impinger arrangements used for the direct determination of analyte transport efficiency (not to scale). In (a), the sampling bag (3 l capacity) contains 100 ml of 10% HNO_3. In (b), impingers 1 and 2 contain 200 ml of HNO_3; impinger 3 contains 200 ml of DDW.

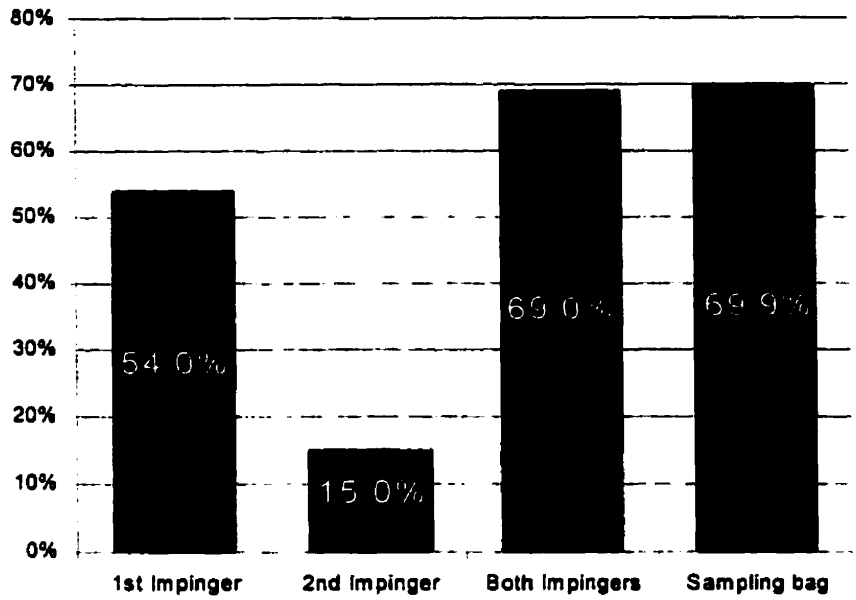

Figure 2 Comparison of the distribution and recovery of analyte (Cu) observed with the flow-through impinger and the closed-system sampling-bag arrangements.

used to recover analyte captures only about 80% of the total amount of Cu transported, with the remaining portion, around 20%, being captured in the second vessel. Experiments were conducted where the third impinger in a series of four was also filled with 200 ml of 10% HNO_3 and analyzed, but no significant amount of analyte was detected for any of the elements studied. This approximate 80:20 distribution of the recovered analyte in the first and second impingers, respectively, was true for most analytes studied, with As being the only notable exception, where an approximate distribution of 99:1 was observed. In contrast, Grégoire and Sturgeon[5] reported that for 30 sequential vaporizations of 20 µl of a 20 ng ml^{-1} (Mo, In, Tl, Bi) sample that 90% of the total recovered analyte was found in the first impinger, 9% in the second and undetectable amounts in the third. The difference in observed analyte distribution in

these studies may be due to any number of factors, the most influential being differences in the surface area and porosity of the frits used in the impingers.

A summary of the results obtained with the proposed closed-system method for determining transport efficiency and the method used for validation purposes appears in Table 6-2. Inspection of these results reveals no statistical difference at the 95% confidence interval between the two methods for elements ranging from the volatile (Cd, Mn, Pb) to the involatile (Cu, Ni) and refractory carbide-forming (V) (upper portion of Table 6-2). Of particular interest is the good agreement and relatively low uncertainty for the As values, considering the elevated ICP-MS background encountered at the monitored nominal charge-to-mass (*m/z*) ratio of 75, due to a molecular adduct interference ($^{40}Ar^{35}Cl^{+}$) arising from the HCl trapped in solution by both methods. Of the values reported in the upper portion of Table 6-2, the results for V appear to have the poorest statistical agreement, with a relatively high level of uncertainty in both methods. It is important to recognize, however, that several spectral interferences appear at *m/z* 51 monitored for the ICP–MS determination of V. These include: $^{37}Ar^{14}N^{+}$ and $^{36}Ar^{14}NH^{+}$, arising from the 10% HNO_3 used as a trapping solution in both methods; and $^{37}Cl^{14}N^{+}$ and $^{35}Cl^{16}O^{+}$ due to HCl from the carrier gas being captured by both methods. This results in an elevated background level count due to several compounding interferences, unlike the previously mentioned case for As where only HCl was a contributing factor, and could account for the higher degree of uncertainty in the values reported.

As for the precision associated with the analyte transport efficiencies reported in the upper portion of Table 6-2, isolated cases occur where either the impinger method is considerably more precise than the sampling bag method (Ni, V) or *vice versa* (Pb). Notwithstanding these anomalies, the precision observed for the remaining analytes

Table 6-2 Comparison of transport efficiency methods

	Analyte transport efficiency (%)[a]	
Element	Closed-system method (bags)	Reference method (impingers)
As	27.8 ± 7.2	26.9 ± 6.5
Cd	69.9 ± 4.8	72.2 ± 3.2
Cu	70.0 ± 4.6	69.0 ± 3.6
Mn	73.5 ± 5.7	76.5 ± 4.1
Ni	75 ± 12	66.7 ± 3.9
Pb	75.1 ± 4.7	78.3 ± 8.6
V	46 ± 15	30.9 ± 9.3
Cr	72 ± 18	40.0 ± 1.0
Zn	78 ± 110	60.9 ± 2.9

[a] Values represent the mean % analyte transport efficiency (n=8)± uncertainty at the 95% confidence interval

proved to be quite similar for both methods, although the precision observed with the impinger arrangement consistently performed approximately 1% better. Since the closed-system arrangement did not possess any sort of compensatory measure for back-pressure, such as the diaphragm pump used with the impingers, the possibilty of an increasing pressure gradient existing during the collection of a vaporization event with the closed system trapping technique was suspected as a factor contributing towards the slightly poorer precision. Pressure measurements performed on the contents of a sampling bag, however, revealed that the accumulation of vaporization products after a complete sample firing sequence augmented the pressure in the sampling bag by only 20 Pa over ambient air pressure. This was obviously an insignificant increase compared with both ambient air pressure (ca. 100 kPa) and the 275 kPa (40 psi) head pressure encountered in the carrier gas flow. In the light of this observation, it is suspected that the slightly higher imprecision observed with the closed-system trapping method arose simply from random errors in quantitatively transferring the trapping solution into the sampling bags. Whereas

the trapping solution for the impinger arrangement could be freely decanted directly into the solution vessels. The trapping solution for the closed-system arrangement had to be introduced through a line of tubing connected to the shut-off valve of the sampling bag. Also, the total volume of trapping solution introduced into the sampling bags was four times less than that used in the impingers (100 ml *vs.* 400 ml), meaning that any absolute error encountered during the transferring of solution would result in a greater relative error in the closed-system arrangement.

Results for Cr and Zn, however, were not in statistical agreement with each other for the two methods (lower portion of Table 6-2). The values for analyte transport efficiency obtained with the impinger apparatus [(40.0 ± 1.0)% for Cr, (60.9 + 2.9)% for Zn] were considerably more precise than those obtained using the sampling bags [(72 ± 18)% and (78 ± 110)% respectively], suggesting that some source of contamination from the sample bags must be taking place. Although the materials comprising the bag walls (Tedlar) and the shut-off fitting (polypropylene) do not present themselves as likely sources of Cr and/or Zn contamination, two parts of the fitting, namely the Teflon coated silicone rubber septum and the acrylonitrile–butadiene rubber O-ring seals in the valve, could be sources of contamination. The septum was suspected as the source of Cr contamination, and when it was removed and replaced with a cleaned and conditioned Teflon disk of equivalent dimensions, a Cr transport value of (36.8 ± 4.2)% for the gas-sampling bags was reported, now in statistical agreement with the impinger value of (40.0 ± 1.0)%. Replacement of the septum with a Teflon disk did not, however, improve the values observed for Zn transport. The source of Zn contamination was the two acrylonitrile–butadiene rubber O-rings in the polypropylene fitting. The vulcanization

process for acrylonitrile-butadiene rubbers involves the use of ZnO as an initiator, and zinc-containing dithiocarbamates such as bis(diethyldithiocarbamato)zinc are frequently used as vulcanization accelerators.[13] As a result, Zn will be leached with time from acrylonitrile–butadiene rubber that is in contact with aqueous solution (especially if the solution is acidic), a fact that has been observed with rubber stoppers used in biological samples.[14] Although not performed in this study, substituting these O-rings with replacements free of Zn contamination should solve this problem.

An important factor to consider when using this closed-system for determining transport efficiency is whether or not the detection limit capabilities of the technique are consistent with the absolute amount of analyte typically vaporized in the ETV–ICP–OES/MS system being studied. A logical means of evaluating this would be to compare the detection limits from the analysis step of the closed-system trapping technique with the instrumental detection limits of the ETV–ICP–OES/MS system being studied. Table 6-3 reports the limits of detection (LODs) obtained with the closed-system method of determining transport efficiency expressed in terms of the absolute amount of analyte collected in the sampling bag solution. Values appear only for elements that are not subject to an elevated ICP–MS background level due to spectral interferences from HCl, as the use of an HCl-sparged carrier gas, such as in this study, is not a typical operational condition for most ETV systems. The absolute detection limits are on a par with what are realized operationally with the current IH–ETV system when paired with ICP–OES,[11] as well as those achieved with typical ETV–ICP–OES arrangements,[15] making the closed-system method well suited for transport studies with analyte masses commonly vaporized in these systems. The detection limits do fall short of those typical of ETV–ICP–MS[15], meaning that analysis of the raw solution from the sampling vessel would be insufficient

Table 6-3 Limit of detection (LOD) for sampling bag method on current IH-ETV system

Element	LOD[a] /ng of vaporized element
Cd	0.6
Cr	10
Cu	2.1
Mn	1.7
Ni	5.8
Pb	3.8

[a] LOD defined as 3× the standard deviation of the blank firing samples collected (n=8) divided by the slope of the calibration curve.

if a mass of analyte of the order of a few pg was vaporized. This can be resolved by simply incorporating a preconcentration step into the closed-system trapping method prior to analysis. For example, the impinger method used by Grégoire and Sturgeon[5] called for the contents of each vessel to be evaporated down to dryness in a quartz crucible, brought up to a final volume of 1 ml, and analyzed by SN–ICP–MS using a microconcentric nebulizer. Samples collected could also be preconcentrated and analyzed subequently by ETV–ICP–MS in a similar way to enable the determination of transport efficiency from masses of analyte typically encountered with the same technique. Alternatively, one could simply deflate the sampling bag after each sample collection/dissolution and run the ETV system again. This type of approach would also have the theoretical advantage of improving precision by averaging, as well as improving detection limits towards those typical of ETV–ICP–MS.

An interesting aspect to consider with this closed-system arrangement is its potential application as a means of foregoing laborious digestion procedures in the preparation of aqueous samples. In the closed-system arrangement described above, the

vaporization product of an ETV event, notwithstanding that which is lost in transport, is captured in a single vessel and eventually dissolved in a single solution. If a closed-system trapping arrangement could be realized where sample transport losses were negligible, *e.g.*, if the gas-sampling bag was situated as close as possible to the ETV furnace, the solution generated would effectively be an aqueous sample similar to one prepared by conventional digestion/dissolution procedures. This could be advantageous especially in the digestion of organic samples, where organic matter could be vented in a pyrolysis step, with the remaining analytes being collected in a final vaporization step. The capacities of the ETV furnace and the trapping vessel could be adjusted such that samples suited to the detection limits of the SN–ICP–OES/MS technique being used are achieved. In order to evaluate the pragmatism of using closed-system trapping for sample dissolution, however, issues such as sample homogeneity and the precision/accuracy associated with sample preparation would not only have to be examined, but would also need to be objectively compared against existing techniques for analyzing solids and slurries.

6.5 Conclusion

Analyte transport efficiency in ETV sample introduction was determined in a direct, accurate and simple manner using commercially available gas-sampling bags in a closed-system arrangement for As, Cd, Cu, Mn, Ni, Pb and V. By replacing the silicone rubber septum and the acrylonitrile–butadiene rubber O-rings in the shut-off valve of the bag with trace-metal free components, the technique can be extended to the determination of Cr and Zn. The analytical performance of this method makes it immediately suited for analyte concentration ranges typically found in ETV–ICP–OES systems, and with the

incorporation of a preconcentration step, can be extended to the concentration range encountered in ETV–ICP–MS. Furthermore, this type of closed-system combined with a vaporization system may be applicable as a sample preparation technique.

6.6 Acknowledgements

Sincere thanks are extended to Dr. Jean-Pierre Farant of the Department of Occupational Health and Safety of McGill University for the generous loan of the impingers and backing pump used in this study, and Alan Rossner of Clarkson University for collegial discussions regarding the utility of gas-sampling bags. The author gratefully acknowledges scholarship support provided by the province of Québec through Fonds pour la Formation des Chercheurs et l'Aide à la Recherche (FCAR). This research was also made possible through funding from the Natural Sciences and Engineering Council of Canada (NSERC) by means of an NSERC Operating Grant.

6.7 References

1. Millard, D.L, Shan, G.F., and Kirkbright, G.F., *Analyst*, 1980, **105**, 502.

2. Kántor, T., and Güçer, S., *Spectrochim. Acta, Part B*, 1999. **54**, 763.

3. Sparks, C.M., Holcombe, J.A., and Pinkston, T.L., *Appl. Spectrosc.*, 1996, **50**, 86.

4. Park, C.J., Van Loon, J.C., Arrowsmith, P., and French, J.B., *Can. J. Spectrosc.*, 1987, **32**, 29.

5. Grégoire, D.C., and Sturgeon, R.E., *Spectrochim. Acta, Part B*, 1999, **54**, 773.

6. Bernhardt, J., Buchkamp, T.; Hermann, G., and Lasnitschka, G., *Spectrochim. Acta, Part B*, 1999, **54**, 1821.

7. Buchkamp, T., Hermann, G., *Spectrochim. Acta, Part B*, 1999, **54**, 657.

8. Sparks, C.M., Holcombe, J., and Pinkston, T.L., *Spectrochim. Acta, Part B*, 1993, **48**, 1607.

9. Feldmann, J., *J. Environ. Monit.*, 1999, **1**, 33.

10. Naka, H., Kurayasu, H., Ma, L., and Nakahara, T., *Bunseki Kagaku*, 1998, **47**, 203.

11. Goltz, D.M., Skinner, C.D., and Salin, E.D., *Spectrochim.Acta, Part B*, 1998, **53**, 1139.

12. Goltz, D.M., and Salin, E.D., *J. Anal. At. Spectrom.*, 1997, 12, 1175.

13. Hofmann, W., *Rubber Technology Handbook*, 1989, 1st ed. (English ver. of *Kautschuk-Technologie*, transl. by Bauer, R., and Meinecke, E.A.) Munich, Hanser Publishers, pp. 67, 71-72, 233-236.

14. Kennedy, B.W., and Beal, T.S., *Lab. Animal Sci.*, 1991, **41**, 233.

15. Carey, J.M., and Caruso, J.A., *Crit. Rev. Anal. Chem.*, 1992, **23**, 397.

Chapter 7

General conclusions and future work

There are certainly advantages to thermal vaporization sample introduction systems that have demountable, interchangeable sample supports. Throughout this study, the ability to remove and replace the sample probe in the technique being used permitted the preparation and pretreatment of multiple samples at a time, each in their own separate sample support. Consider for a moment the impact that this type of arrangement could have on the duration of a conventional electrothermal vaporization (ETV) cycle, which, complete with drying, ashing, vaporization, cleaning, and cooling stages, is usually of the order of several minutes. By using a system in which the sample supports are interchangeable and all sample pretreatment is performed off-line, the complete vaporization cycle would be appreciably shorter, as it would now consist only of a vaporization stage (which is usually a few seconds) and a stage for probe changeover. Automation of the changeover and vaporization processes, which already has been accomplished with DSI (see Section 1.5.2.1.1 of Chapter 1), would result in a sample introduction system capable of throughput surpassing that of many existing techniques.

The use of a contact-free heating environment is probably the best way to facilitate this sort of sample support interchange in a thermal vaporization system. Both direct sample insertion (DSI) and induction heating–electrothermal vaporization (IH–

ETV) use this approach—but which method is better? The literature review on DSI and ETV paints a picture of two techniques that, despite their markedly different vaporization arrangements are strikingly similar in both their features and performance. In fact, the use of a pyrolytically coated vaporization surface in DSI (Chapters 2 and 3) was probably one of the few remaining features that had yet to be implemented in both techniques. The pyrolytically coated sample probe developed in this study was found to greatly enhance the appearance and reproducibility of the DSI signals observed and could be used for routine determination of metals in solid samples such as wood pulps. Other types of coatings (such as carbides) which have been used to improve the performance characteristics of ETV systems could also be used in the future with DSI. While innovations such as these will undoubtedly expand and improve the analysis possibilities of DSI, it is highly unlikely that these enhancements would result in DSI supplanting the widespread-use of ETV.

The interfacing of an ETV sample introduction system with an ICP source is a straightforward task and is probably a principal contributing factor towards its current prevalence over DSI. With ETV, interfacing is accomplished by simply connecting the exhaust of the ETV transport tube to the injector tube of the ICP torch, whereas DSI requires the physical mounting of a complex insertion device to an ICP system with a customized torch. One should also consider the fact that most ETV work at present is being done with ICP–MS, as the better sensitivity of the MS technique, the freedom from oxide and hydroxide interferences that results from a "dry" vaporization event, and the ability to perform isotopic analyses presents the analyst with a wealth of analysis possibilites. Interfacing ETV to the horizontal torch environment of ICP–MS does not

present any additional difficulties, but the interfacing of DSI in a horizontal arrangement requires special design and experimental considerations (see Section 1.5.2.1.1 of Chapter 1). Based on these realities, the use of an ETV arrangement is probably the better approach for a thermal vaporization system with an interchangeable sample probe.

Another aspect where ETV surpasses DSI is temperature control. The ability to generate and reproducibly execute detailed temperature programs with ETV is certainly an advantage in terms of optimizing the analyte vaporization process, as well as permitting unique applications such as thermal speciation studies. The question remained, however, whether or not this kind of temperature control could be realized in an ETV system with a demountable probe in a contact-free heating environment. The temperature studies carried out on the IH–ETV arrangement (Chapter 4) demonstrated that rapid heating rates and reproducible temperature control were indeed possible using a graphite probe in an induction field. The current IH–ETV system was found to be somewhat lacking, however, in its high-temperature capabilities as it was only capable of heating the vaporization surface of the sample probe used to a maximum temperature around 1900 °C, whereas most conventional ETV instruments are capable of reaching temperatures of 2500–3000 °C. This shortfall, however, is an attribute of the induction furnace currently used with the IH–ETV system, and by using a more powerful furnace in the future, the next generation of IH–ETV instrument should be capable of reaching higher vaporization surface temperatures. Monitoring of the vaporization surface was possible with an infrared thermocouple, but the use of an optical transducer required frequent realignment whenever the sample support was changed. Future studies should look more closely at the possibility of using indicators which have been demonstrated as

varying linearly with temperature (such as grid and/or plate current) as means of temperature feedback.

The electrical discharging that occurs in the IH–ETV cell with an Ar atmosphere admittedly is a hindrance to its development as a sample introduction technique, although its origins and methods of prevention are now better understood (Chapter 4). The use of various *x*–Ar gas mixtures with electron scavenging qualities proved to be a very simple yet effective means of suppressing electrical discharging in the IH–ETV cell. By having to rely on additives to the carrier gas flow, however, one constantly runs the risk of introducing spectral interferences to an IH–ETV analysis. Although no spectral interferences were encountered in the IH–ETV–ICP–OES studies (Chapters 4 and 5), some of the *x*–Ar mixtures used would certainly present problems in quadrupole ICP–MS. For example, the use of HCl–Ar would eliminate the possibility of determining As (monoisotopic at *m/z* 75) due to an interference from $^{40}Ar^{35}Cl^{+}$, and the use of SF_6–Ar would present a similar interference from $^{40}Ar^{19}F^{+}$ for Co (monoisotopic at *m/z* of 59). Although the use of collision cells in ICP–MS may reduce or eliminate some of these interferences, future studies should look to the use of different probe materials, coatings and induction coil circuits as alternative means of preventing electrical discharging in the furnace.

In spite of the possibility of introducing additional interferences, the use of certain *x*–Ar combinations, particularly SF_6–Ar, were found to significantly enhance the volatilization, transport and sensitivity observed for most analytes introduced by IH–ETV, and could be used in routine analyses such as the determination of metals in soils and sediments by ICP–OES (Chapter 5). The improvements seen here with SF_6 are not

exclusive to IH–ETV, and future studies should examine its use as a chemical modifier in conventional ETV arrangements. The formation of a highly transportable form of arsenic (most likely gaseous AsF_5) when vaporized in the presence of SF_6 presents an interesting means of enhancing its introduction by ETV and should be studied further, along with other analytes that may form metal–fluorides that are volatile at ambient temperature (such as Ge and Se).

The closed sampling-bag system developed for trapping and dissoluting analyte vaporized from the IH–ETV system proved to be a simple and accurate means of determining ETV–ICP–OES transport efficiency (Chapter 6). Future studies should evaluate its performance in ETV–ICP–MS transport efficiency studies, where the collection of multiple vaporization events may be required.

In conclusion, the results presented here from the fundamental and applied study of DSI and IH–ETV sample introduction demonstrate that a demountable, raplidly interchangeable sample support can serve a valuable role in ICP spectroscopy by improving both the processing and introduction throughput of samples. Of the two systems studied, the IH–ETV approach shows the most promise, as it is a more flexible, versatile design that at the same time has all of the functional attributes of conventional ETV. Future studies should certainly be pursued in the design, automation, and application of advanced IH–ETV instrumentation with the long-term goal of developing an equally capable, versatile, high-throughput alternative to conventional ETV systems.

Appendix A

Software for extracting time scan data from the TJA *IRIS* ICP–OES

The following files, written in C++, allow the time scan files from the IRIS to be converted from their binary format (*.dts) to ASCII format. "try.cpp" is the main program, "try.h" is a function for producing target file names, and "tsfile.h" is a definition of the file structure, obtained from TJA Solutions (Franklin, MA, USA). All 3 of the following files were originally written or modified by Hai Ying, to whom full credit and sincere thanks are due.

A1.1 "try.cpp"

```
#include "try.h"

typedef int bool;

#include "tsfile.h"

typedef struct
                {
                long    left;                   /* average left background value */
                long    center;                 /* average signal value */
                long    right;                  /* average right background value */
                float   time;       /* time at which data point was taken in seconds */
//                   bool   ts_knockdown;   /* subarray knockdown occurred after read */
                } time_study_pt;

int main()
{
        long i,j,n;
        TSFileHdrtyp tsfilehdr;
        TSScanHdrtyp tsscanhdr;
        time_study_pt pt;
        FILE *in,*out;
        char dirname[100];
        char infile[80],outfile[80];
        DIR *dir;
        struct dirent *ent;

        printf("\n\nThis program is used for converting file from DTS format to TXT
format\n");
```

```
        printf("usage: 1. input the directory name where only DTS files are located.\n");
        printf("       2. input the directory name where the output files will be
put.\n");
        printf("These two directories should exist!\n\n\n");

        printf("path for DTS files : ");
        scanf("%s",dirname);
        printf("output path : ");
        scanf("%s",outdir);
        n=strlen(outdir)-1;
        if (outdir[n]!='\\')
                strcat(outdir,"\\");
        if ((dir = opendir(dirname)) == NULL) {
                perror("Unable to open directory");
                exit(1);
        }
        while ((ent = readdir(dir)) != NULL) {
                if (strcmpi(ent->d_name,".")==0 || strcmpi(ent->d_name,"..")==0)
                        continue;
                strcpy(infile,dirname);
                if (infile[strlen(infile)-1]!='\\')                    strcat(infile,"\\");
                strcat(infile,ent->d_name);
                filename_producer(ent->d_name,outfile);

                        in=fopen(infile,"rb");
                        if (in==NULL) {
                                printf("Error in opening file %s.\n",infile);
                                exit(1);
                        }
                        out=fopen(outfile,"w");
                        if (out==NULL) {
                                printf("Error in opening file %s.\n",outfile);
                                exit(1);
                        }
                        fread(&tsfilehdr,sizeof(TSFileHdrtyp),1,in);
                        fprintf(out,"version: %s. filedate: %s. method:
%s.\n",tsfilehdr.version,tsfilehdr.created,tsfilehdr.method);
                        fprintf(out,"number of lines: %d\n",tsfilehdr.num_lines);
                        fprintf(out,"gasflushT: %f. samflushT:
%f.\n",tsfilehdr.gasflushtime,tsfilehdr.sampflushtime);
                        for (i=0;i<tsfilehdr.num_lines;i++) {
                                fread(&tsscanhdr,sizeof(TSScanHdrtyp),1,in);
                                fprintf(out,"datapoints: %ld. element: %s. wavelength:
%s.\n",
                                        tsscanhdr.numpts,tsscanhdr.elsym,tsscanhdr.wl);
                                fprintf(out,"order: %d. wlsrc: %d. absindex: %d.\n",
                                        tsscanhdr.order,tsscanhdr.wlsrc,tsscanhdr.absindex);
                                fprintf(out,"center left right time\n");
                                for (j=0;j<tsscanhdr.numpts;j++) {
                                        fread(&pt,sizeof(time_study_pt),1,in);
                                        fprintf(out,"%ld %ld %ld
%f\n",pt.center,pt.left,pt.right,pt.time);
                                }
                        }
                        fclose(in);
                        fclose(out);
                        printf("%s DONE!\n",outfile);
        }
        if (closedir(dir)!=0)
                printf("Unable to close directory\n");
        return 1;
}
```

A1.2 "try.h"

```
#include <stdio.h>
#include <stdlib.h>
#include <conio.h>
#include <string.h>
#include <dirent.h>

char outdir[100];

void filename_producer(char *stemp,char *outfile)
{
        int i;
        char string_tmp[100];
        strcpy(string_tmp,stemp);
        i=0;
        while(i<strlen(string_tmp) && string_tmp[i]!='.')
                {i++;}
        if (i<strlen(string_tmp))
                i++;
        string_tmp[i]='t';i++;
        string_tmp[i]='x';i++;
        string_tmp[i]='t';i++;
        string_tmp[i]='\0';
        strcpy(outfile,outdir);
        strcat(outfile,string_tmp);
        return;
}
```

A1.3 "tsfile.h"

```
#define TS_VERS          "1.0"
/* include file for tsfile.c */
typedef char verstyp[6];
/* following lines are added by HY */
typedef char timestring[16];
typedef char tnametyp[10];
typedef char opertyp[10];
typedef char comntyp[62];
typedef char elsymtyp[4];
typedef char wltyp[8];

typedef struct
                {
                verstyp        version;          // version no. this scan was saved under
                timestring       created;       // date, time stamp when file was created
                tnametyp           ethod;     // name of mtd assoc. with this scan file
                unsigned int     num_lines;         // number of lines (scans) in file

                // parameters from Runtime_type

                opertyp                  operid;                 // operator id
                comntyp                  comment;              // comment for this scan file
                float                    gasflushtime;    // gas flush time
                float                    sampflushtime;  // sample flush time
                unsigned long    numslices;              // number of time slices
        float                        timeperslice;    // time per slice
                float                 ignalinc;          // signal inc to get signal data

                // remaining parameters are from time_study_param_type

//              bool                  remove_fp;       // removal of fixed pattern signal?
                int                   gain_param;             // CID camera gain parameter
                int                        source;                  // instrument source
                int               slit;                // slit to be used (on or off axis)
                int             resultantscans; // YES if scans are resultant (results of
```

```
        // subtraction of 2 scans), otherwise NO
                char                    anything[58];   // AVAILABLE FOR FUTURE USE
//              char                    anything[56];   // AVAILABLE FOR FUTURE USE
                } TSFileHdrtyp;

typedef struct
        {
        unsigned long   token;                  // token to indic. beginning of scan data
        unsigned long   numpts;                 // number of data pts saved for this line
        elsymtyp                elsym;                  // element symbol
        wltyp                   wl;                             // wavelength
        unsigned int    order;                  // order
        unsigned int    wlsrc;                  // wavelength source (instrument)
        unsigned int    absindex;               // absindex of this line in orig. method
        char                    anything[16];   // AVAILABLE FOR FUTURE USE
        } TSScanHdrtyp;

typedef struct
        {
        unsigned long   token;                  // token to indic. beginning of scan data
        unsigned long   numpts;                 // number of data pts saved for this line
        } TSScanInfotyp;


//extern FAR int ts_filelist(HWND hWnd, int Ctrl);
//extern int ts_SaveScan(char *filepath, Runtime_typ *Runtime, time_study_param_type
*ts_params);
//extern int ts_OpenScan(char *filepath, TSFileHdrtyp *TSFilehdr);
//extern int ts_GetScan(char *fname, TSFileHdrtyp *TSFilehdr);

//extern int TS_SubtractScans(LPSTR pfile, LPSTR sfile, LPSTR rfile, HWND hListbox, LPSTR
operid, LPSTR comment);
```

Appendix B

Cold junction compensator and matched amplifier circuit for thermocouple interfacing

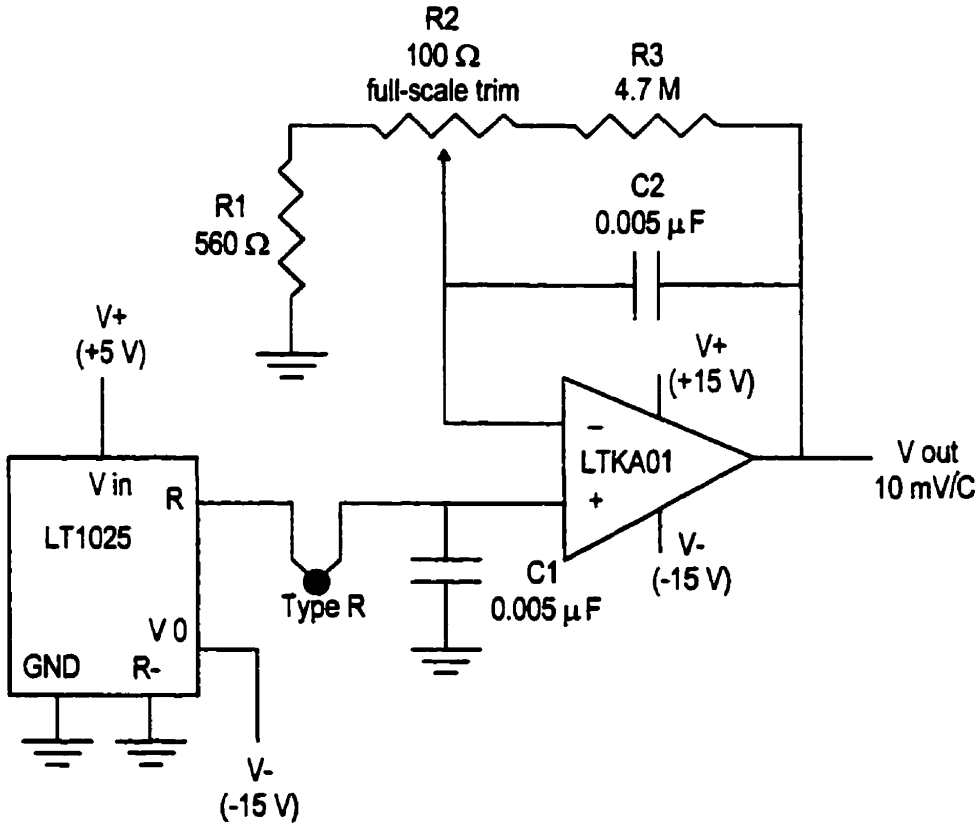

The above circuit was built for the purposes of interfacing the R-type infrared thermocouple used in Chapter 4 with either a strip chart recorder or an A/D board. It was built using a kit available from Linear Technology (Milpitas, CA, USA). It consists of two components: a thermocouple amplifier (LTK A01), and a matched cold junction

compensator (LT 1025). The gain of the amplifier circuit, *i.e.*, R3/R1, was set to approximately 8400 in order to yield a 50 mV $°C^{-1}$ output response (based on the 5.95 μV $°C^{-1}$ input response expected of an R-type thermocouple). R2, a 100k trim pot, was used for fine adjustments of the gain to suit the range of the A/D converter or the strip chart recorder. A capacitor (C2) was placed in parallel with R3 for the purposes of output signal smoothing; the RC time constant of the circuit, based on the values of R3 and C2, is approximately 25 ms. All resistors used in the above circuit are 1% tolerance rated (metal film).